SURFACE ACOUSTIC WAVE FILTERS IN ZnO-SiO_2-Si LAYERED STRUCTURES

Design, Technology, and Monolithic Integration with Electronic Circuitry

Jaco H. Visser

SURFACE ACOUSTIC WAVE FILTERS IN ZnO-SiO_2-Si LAYERED STRUCTURES

Design, Technology, and Monolithic Integration with Electronic Circuitry

SURFACE ACOUSTIC WAVE FILTERS IN ZnO-SiO_2-Si LAYERED STRUCTURES

Design, Technology, and Monolithic Integration with Electronic Circuitry

Akoestische oppervlaktegolf filters in ZnO-SiO_2-Si gelaagde structuren: ontwerp, technologie en monolithische integratie met elektronische schakelingen

PROEFSCHRIFT

ter verkrijging van de graad van doctor
aan de Technische Universiteit Delft,
op gezag van de Rector Magnificus,
prof. drs. P. A. Schenck,
in het openbaar te verdedigen
ten overstaan van een commissie
aangewezen door het College van Dekanen
op dinsdag 19 december 1989 te 16.00 uur

door

Jacobus Hendrik Visser

elektrotechnisch ingenieur
geboren te Hillegom, Nederland

Dit proefschrift is goedgekeurd door de promotor
prof. dr. ir. S. Middelhoek.

Dr. ir. A. Venema heeft als toegevoegd promotor
in hoge mate bijgedragen aan het
totstandkomen van het proefschrift.

Leden van de promotiecommissie:

Rector Magnificus prof. drs. P. A. Schenck	Technische Universiteit Delft
Promotor prof. dr. ir. S. Middelhoek	Technische Universiteit Delft
Toegevoegd promotor dr. ir. A. Venema	Technische Universiteit Delft
Prof. dipl.-ing. dr.techn. F. J. Seifert	Technische Universität Wien
Dipl.-ing. dr. G. F. Riha	Siemens AG, München
Prof. dr. P. Balk	DIMES, Delft
Prof. dr. ir. J. Davidse	Technische Universiteit Delft
Prof. dr. ir. P. M. van den Berg	Technische Universiteit Delft

Ter Nagedachtenis aan mijn Vader en Grootouders.
Opgedragen aan mijn Moeder, Bart en Caroline, en Hester.

PREFACE

This Ph.D. Thesis is the result of four years of research at the Department of Electrical Engineering of the Delft University of Technology. It deals with the design and technology of surface acoustic wave (SAW) filters in ZnO-SiO_2-Si layered structures. The monolithic integration of these SAW filters with electronic circuitry, into a complete electronic system on one chip, was part of the research and was successfully realized.

In Chapter 1 the reasons for conducting research in silicon-integrated SAW devices are discussed and a review of previous work in this field is given. In Chapter 2 propagation and transduction properties of Rayleigh waves in ZnO-SiO_2-Si layered structures are discussed. The conditions for surface acoustic wave amplification by the interaction of the acoustic wave with drifting charge carriers in the silicon substrate are examined in Chapter 3. A new and simple computational technique is used to determine the amplification. The technology to manufacture SAW devices is the subject of discussion in Chapter 4. Both the high-resolution technology to etch aluminum interdigital transducers and the monolithic integration of SAW devices with electronic circuitry on one chip are investigated in depth. Attention is paid to ZnO deposition and its passivation. Chapter 5 presents silicon-integrated SAW devices: the SAW delay line, the SAW transversal filter and the SAW resonator filter. Second order effects, especially those related to the use of a ZnO-SiO_2-Si layered structure, are discussed. A new layered structure to suppress electromagnetic feedthrough in silicon SAW devices is presented. The rest of this chapter is devoted to the electronic modeling of the SAW device and conclusions are drawn as to how to drive and load such a monolithically integrated device. In Chapter 6, the last chapter, potential applications of silicon-integrated SAW filters are discussed. Especially the research and development of an integrated FM upconversion radio receiver with on-chip SAW filters is described.

Many aspects of the subject discussed in this thesis have already been published and a number of papers are in preparation. A complete list of publications and presentations is listed at the end of this book.

During the past four years the Laboratory of Electronic Instrumentation, supervised by Professor S. Middelhoek, has been a stimulating environment in which to do research. I wish to thank all its members. Within this laboratory I have been working in the Microacoustics Group of Dr. A. Venema. His guidance, the valuable and intellectually stimulating discussions, and the fact that he always managed to make time for me, substantially contributed to the success of my research. I am also grateful to the other members of the Microacoustics Group: to my fellow Ph.D. students, J. C. Haartsen and M. J. Vellekoop, and to G. W. Lubking for the many fruitful discussions, helpful comments and their moral support. Moreover, M. J. Vellekoop is acknowledged for the competent fabrication of the piezoelectric ZnO layers. I am deeply indebted to my students: B. M. Blok, J. C. Groenendijk and A. J. M. van der Harg for their contributions to this thesis.

I would like to express my gratitude to Dr. C. C. W. Ruppel (Siemens AG, München) for the intellectually stimulating, helpful and pleasant discussions and demonstrations of SAW filter design. The numerical programs for the acoustoelectric field analysis of multilayered structures, developed by Dr. W. J. Ghijsen (Laboratory of Electromagnetic Research), have been of invaluable help in SAW propagation, transduction and amplification calculations. I am grateful to J. C. Haartsen for his help in adapting these programs for the purposes of this thesis. P. E. Platzbecker (Laboratory of Network Theory) is acknowledged for his assistance in the use of digital filter synthesis software.

The research was part of a project to develop a monolithically integrated FM upconversion radio receiver, with on-chip SAW filters. This project was carried out in cooperation with the Laboratory of Electronics and was supervised by Professor J. Davidse, Dr. E. H. Nordholt and Dr. A. Venema. My colleague P. T. M. van Zeijl took care of the system and electronic circuitry design, as described in his Ph.D. Thesis "Fundamental Aspects and Design of an Integrated FM Upconversion Receiver Front-End with On-Chip SAW Filters." His perspective on SAW devices from an electronic circuit and system point of view was refreshing and I have appreciated his useful suggestions and cooperation. I would like to thank the other members of the Laboratory of Electronics' Radio Group, especially Dr. J. W. Th. Eikenbroek for his work on SAW resonators on quartz.

All experimental results in this thesis have been obtained from devices manufactured at the Delft Institute for MicroElectronics and Submicron Technology (DIMES). I thank all its members for their expertise and dedication so crucial to this thesis, in particular Dr. E. van der Drift (high-resolution aluminum etch technology), Dr. L. K. Nanver (Delft BIFET process) and Dr. P. M. Sarro (special processes). Further acknowledgment goes to A. H. de Vreede (Laboratory of Telecommunications and Teleobservatory Technology) for the fabrication of sputtered SiO_2 layers. I am very grateful to D. P. Nelemans (Department of Applied Physics), N. M. van der Pers and W. G. Sloof (Department of Materials Science) for the X-ray microanalysis of samples and their interpretation.

Thanks are also due to W. G. M. M. Straver and J. Tóth for making the photographs and scanning electron micrographs, respectively. The skillful improvement of my English in this thesis by J. B. Zaat-Jones, and the final review by W. A. Visser-Benschop and M. Indrajadi have been indispensable.

The research for this Ph.D. Thesis has been financially supported by the Netherlands Technology Foundation (Stichting voor Technische Wetenschappen – STW) under contract DEL 44/47.0592. This organization has also financed scientific visits to universities and industries, paid for several engineering courses in the SAW field and made it possible to present papers at a number of conferences and symposia in the USA. Royal Dutch Shell is acknowledged for paying the traveling expenses of a trip to the USA in May/June 1989.

I thank all my friends and my family, for their support made it easier for me to finish this work. Finally, I wish to thank all those not mentioned but not forgotten!

J. H. Visser

Delft, The Netherlands
October 1989

CONTENTS

Chapter 1

INTRODUCTION

1.1 SURFACE ACOUSTIC WAVE FILTERS

Although the earliest investigations in acoustics can be traced back to Pythagoras in the sixth century B.C., the science of ultrasonics originated in the nineteenth century [1]. By the close of that century piezoelectricity had been discovered by the brothers Jacques-Paul and Pierre Curie (1880) [2] and the first scientific paper on the subject of acoustic wave propagation along the stress-free surface of a homogeneous solid had been published by the third Lord Rayleigh (1885) [3]. Since the development of submarine detection systems during World War I, ultrasonics has been applied in science, industry, medicine, communication systems and the military. Mortley [4] has invented the InterDigital Transducer (IDT) in 1962 and has employed this transducer in bulk acoustic wave devices. This same transducer can be used to generate and detect Surface Acoustic Waves (SAW), as demonstrated by Rowen in 1963 [5], [6] and by White and Voltmer [7] in 1965. The use of surface acoustic wave devices in electronic signal processing systems has steadily been growing since 1965 [8]–[12], which has resulted in an annual estimated world wide market of approximately $100 million. New applications and new SAW device generations

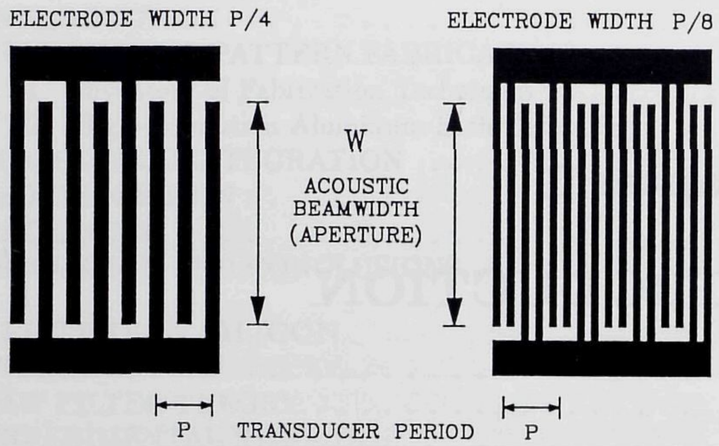

Figure 1.1: *Top view of uniform interdigital transducers with single and double electrodes.*

will fuel a further market growth.

Figure 1.1 shows a uniform interdigital pattern, i.e. with thin, equidistant, plane and parallel, metal electrodes all of the same length and width. This pattern becomes an electric-to-acoustic (and vice versa) energy transducer when it is placed on the (polished) surface of a piezoelectric substrate and a Radio Frequent (RF) electrical signal is applied to it. Between the electrodes of opposite polarity an RF electric field is produced. As a result of the piezoelectricity, surface acoustic waves travel away from the transducer in both directions. Unwanted reflections at the edges of the electrodes in the IDT as a result of the discontinuity in acoustic wave impedance can be canceled out by using a double-electrode structure [13] (Fig. 1.1). In a SAW delay line, the most simple SAW device, the propagating surface acoustic wave is reconverted into an electrical signal at a second, uniform output interdigital transducer, as shown in Fig. 1.2. It is clear that frequencies for which the acoustic wavelength corresponds to the period p of the interdigital pattern are maximally converted into an acoustic signal. The synchronous or center frequency f_0 is related to the (frequency independent) phase velocity v_{ph} of the acoustic wave, the period p of the IDT and the corresponding acoustic wavelength λ_0 according to

$$f_0 = v_{ph}/\lambda_0 = v_{ph}/p \tag{1.1}$$

The propagating acoustic wave is in first order a plane wave when the acoustic beamwidth W is much larger than the acoustic wavelength λ_0.

Because surface acoustic wave velocities are five orders of magnitude slower than the velocity of light, delays of 3 μs/cm are obtained and used, for example, in radar systems. Coquin and Tiersten were, in 1966, among the first with a theoretical analysis of the excitation and detection of surface acoustic waves in piezoelectric quartz [14].

Reproducible production in large quantities at low cost of such a metal interdigital pattern on a piezoelectric crystal is made possible by using silicon planar technology, originally developed for manufacturing integrated circuits in electronics. Using the piezoelectric transduction mechanism, the IDT is by far the most efficient transducer for signal processing devices. Using, for example, a wedge transducer [15] (mounted on the surface) results in lower efficiency and is, in general, not suited for application in a microacoustic device for signal processing.

Surface acoustic wave generation (and detection) on nonpiezoelectric substrates are achieved through the use of the magnetostrictive [16], [17], the electromagnetic-acoustic [17] and the thermoelastic [18] transduction mechanisms. Devices employing magnetostatic surface waves are potentially promising for carrying out signal processing, especially at microwave frequencies [19], [20]. ElectroMagnetic-Acoustic Transducers (EMATs) are based on the (weak) Lorentz force mechanism in a meander line structure. In this work only the piezoelectric transduction mechanism is considered.

On a piezoelectric (and thus anisotropic) crystal the particle displacements u_1, u_2, u_3 (in the x_1, x_2, x_3 directions, respectively, Fig. 1.2) of the surface acoustic wave, are coupled with the electrical potential ϕ, caused by the piezoelectricity. In SAW devices with the substrate thickness much larger than the acoustic wavelength, two types of surface waves are often used: Rayleigh waves and Surface Transverse Waves (STW). The type of wave propagation depends on the crystal properties, cut and direction of propagation [21]. The mechanical displacement normal to the surface is much smaller than the acoustic wavelength. The frequency independent phase velocities range from 10^3 to 10^4 m/s. Operating frequencies thus range from approximately 10 MHz to above 10 GHz. The upper frequency is limited by the current limitations in lithography and the etching of the interdigital metal pattern. Other types of acoustic waves which can travel from input to output transducer do exist but are not considered here.

Pure Rayleigh-wave modes can propagate along the stress-free surface of a crystal in which the sagittal plane (the x_1x_3-plane) is a plane of mirror symmetry, causing a decoupling between (u_1, u_3, ϕ) and (u_2). A Rayleigh wave is thus a composition (in the sagittal plane) of a transverse and a longitudinal wave, with a retrograde elliptic polarization at the

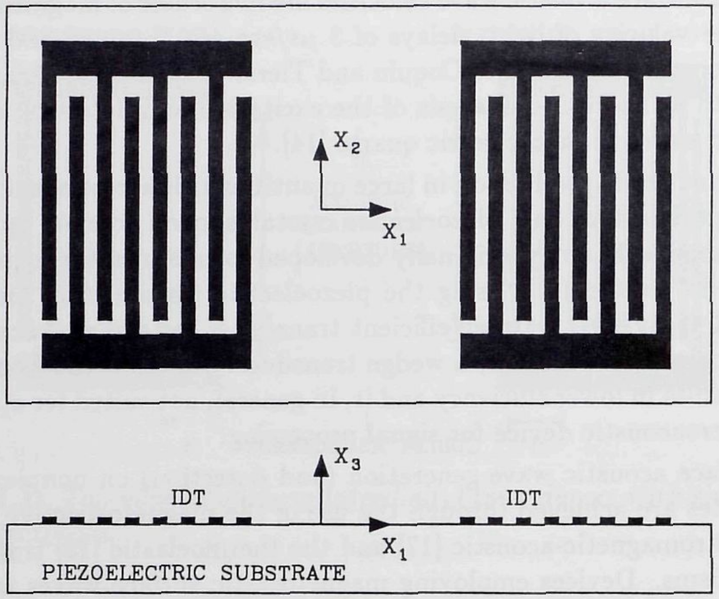

Figure 1.2: *Top view and cross section of a SAW delay line with input and output (metal) InterDigital Transducers (IDTs) on top of a piezoelectric substrate.*

crystal surface. Since the piezoelectric coupling increases the acoustic wave velocity, these waves are also called "(piezoelectrically) stiffened" Rayleigh waves. The penetration depth is in the order of one acoustic wavelength.

STW waves exist when the sagittal plane in the crystal is perpendicular to an axis of two-fold rotation, resulting in a decoupling of (u_1, u_3) and (u_2, ϕ). These waves are also called "Bleustein-Gulyaev" waves. The penetration depth of this type of surface wave is smaller, the greater the piezoelectricity. However, in general, the penetration depth is larger than that of Rayleigh waves.

The efficiency of the electric-to-acoustic energy conversion in the interdigital transducer is of great importance in the application of surface acoustic wave devices in electronic systems. It is expressed by the piezoelectric coupling coefficient κ^2 and depends on the type of crystal, its cut and the direction of wave propagation. The piezoelectric coupling coefficient κ^2 can be approximated (numerically and experimentally) with

$$\kappa^2 \approx 2\frac{\Delta v}{v} = 2\frac{v_{ph} - v_m}{v_{ph}} \tag{1.2}$$

as suggested by Campbell and Jones in 1968 [22]. The acoustic wave phase velocity v_{ph} is reduced to v_m when the piezoelectric fields at the surface are shorted by a metal layer.

An equivalent circuit model of the interdigital transducer has been developed by Smith et al. [23]. It consists of a static capacitance parallel to an acoustic (frequency dependent) admittance. The real part of this admittance can be interpreted as a radiation conductance representing the electric-to-acoustic energy conversion. The conductance G_0 at f_0 and the capacitance C are approximately related to each other, according to

$$G_0 = 8 f_0 \kappa^2 C N \tag{1.3}$$

The static capacitance is determined by the interdigital pattern layout and the equivalent dielectric constant ϵ given by

$$\epsilon = \sqrt{\epsilon_{11}\epsilon_{33} - \epsilon_{13}^2} = \epsilon_0 \epsilon_r \tag{1.4}$$

with $\epsilon_{11}, \epsilon_{33}$ and ϵ_{13} the dielectric constants of the anisotropic substrate and ϵ_0 the permittivity of vacuum. The relative equivalent dielectric constants ϵ_r are listed in Table 1.1. The aperture W of the transducer can be chosen to optimally match the IDT with the electronic circuitry driving and loading these IDTs.

One of the longest known, although weak, piezoelectric materials is (natural) quartz (SiO_2) and it is still widely used because of its excellent temperature stability (ST-X quartz has a zero first-order temperature coefficient of delay at room temperature). High "piezoelectric" materials, but with worse temperature behavior, are the poled ferroelectric ceramics, like PZT, lithium niobate ($LiNbO_3$) and lithium tantalate ($LiTaO_3$) [24]. The application of electrostrictive ceramic materials enables a variation in induced "piezoelectric" coupling [26], [27]. For lithium niobate, lithium tantalate and quartz the basic surface acoustic wave propagation and transduction parameters are summarized in Table 1.1 and are discussed in more detail in the next paragraphs.

In high-quality (scratch-free) polished piezoelectric substrates, the room-temperature propagation loss A of a surface acoustic wave as a function of the frequency f (in GHz), can be approximated by [24]

$$A = vac \cdot f^2 + air \cdot f \qquad [\mathrm{dB}/\mu\mathrm{s}] \tag{1.5}$$

Air loading causes an attenuation proportional to the frequency. The f^2 term is caused by attenuation of the wave where the substrate is in

Table 1.1: *Basic surface acoustic wave propagation and transduction parameters for lithium niobate, lithium tantalate and quartz piezoelectric substrates* [24], [25].

Material	Orient.	v_{ph} [m/s]	κ^2 [%]	ϵ_r	$\frac{1}{v}\frac{\partial v}{\partial T}$ [ppm/K]	$\frac{1}{\tau}\frac{\partial \tau}{\partial T}$ [ppm/K]	vac [A]=[dB/μs]	air [A]=[dB/μs]
$LiNbO_3$	Y,Z	3488	4.5	50.2	-87	94	0.88	0.19
	41.5,X	4000	5.7	67.2	-57	72	0.75	0.30
$LiTaO_3$	Z,Y	3329	0.93	47.9	-52	69	0.77	0.23
	Y,Z	3230	0.74	47.9	-31	35	0.94	0.20
Quartz	Y,X	3159	0.23	4.52	38	-24	2.15	0.45
	ST,X	3158	0.16	4.55	14	0	2.62	0.47

vacuum. Numerical values for the constants *vac* and *air* can be found in Table 1.1.

The frequency f is temperature dependent since the propagation velocity v_{ph} and the transducer period p depend on substrate temperature. A linear Taylor expansion (sufficient for a 100 K temperature range) yields

$$f(T) \approx f(T_0)[1 + \frac{1}{f(T_0)}\frac{\partial f}{\partial T}(T - T_0)] \tag{1.6}$$

with the first-order temperature coefficient of frequency related to the first-order temperature coefficients of the delay τ (τ=l/v_{ph}, l an arbitrary length), phase velocity and thermal expansion α, according to

$$\frac{1}{f}\frac{\partial f}{\partial T} = -\frac{1}{\tau}\frac{\partial \tau}{\partial T} = \frac{1}{v_{ph}}\frac{\partial v_{ph}}{\partial T} - \frac{1}{l}\frac{\partial l}{\partial T} = \frac{1}{v_{ph}}\frac{\partial v_{ph}}{\partial T} - \alpha \tag{1.7}$$

The temperature coefficients of delay and velocity for the three substrate materials are shown in Table 1.1.

A uniform interdigital transducer produces a rectangular impulse response, which results (through Fourier transform) in a $\sin x/x$ shaped amplitude response in the frequency domain with a linear phase response. The (−4 dB) bandwidth B depends on the length L of the uniform transducer according to

$$B = v_{ph}/L = v_{ph}/N\lambda_0 = 1/T_\delta \tag{1.8}$$

with N the length of the transducer in wavelengths and T_δ the duration of the impulse response in seconds. This results in a constant Time-Bandwidth product $T_\delta B$

$$T_\delta B = 1 \tag{1.9}$$

In a SAW delay line the total transfer function is determined by the product of the transfer functions of the IDTs and the delay in between. Two basic types of SAW bandpass filters are: the SAW transversal filter and the SAW resonator filter. Both types are introduced below.

The theoretical transversal filter concept, as introduced by Kallmann [28], is a Finite Impulse Response (FIR) filter. It can be approximated and physically implemented in a microacoustic device with the (typical) layout of the transducers as shown in Fig. 1.3. The overall frequency characteristic of this device is in first order determined by the narrow-band transfer characteristic of the apodized (i.e. variable electrode overlap) IDT. The sketched truncated $\sin x/x$ apodization results in an approximately rectangularly shaped amplitude response in the frequency domain and a linear phase. However, in this type of filter amplitude and phase response can be independently and (to a great extent) arbitrarily designed. This advantage and the before-mentioned superior fabrication technology and filter size has resulted in the replacement of LC and ceramic filters by SAW transversal filters. To prevent differences in the velocity of propagation (and thus variations in group delay), the areas (in the apodized transducer) with no electrodes present (Fig. 1.3) are filled with dummy electrodes [29]. SAW transversal filters, with as a special case the SAW delay line with uniform transducers, have a constant Time-Bandwidth product in the range

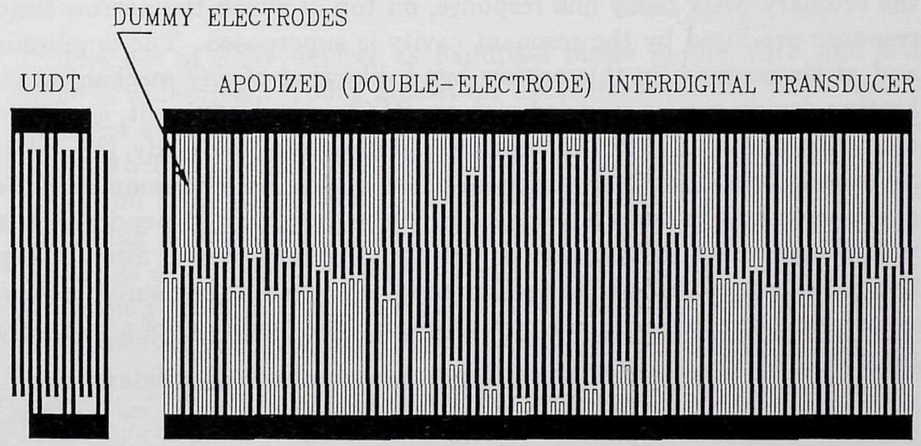

Figure 1.3: *Typical layout of the interdigital transducers in a SAW linear-phase transversal filter configuration.*

$$1 \leq T_\delta B < \infty \tag{1.10}$$

The shortest impulse response required to obtain a prescribed bandwidth is obtained in the SAW delay line. Putting stronger demands on passband ripple, stopband rejection and the shape factor results in a longer impulse response T_δ. In general, the narrower the bandwidth or lower the shape factor, the larger the device; infinitely long in the case of realizing an ideal passband. The physical length of a transversal filter, for a given bandwidth, ripple, stopband rejection and transition bandwidth, is therefore proportional to (only) the phase velocity. In the case of a layered structure with dispersive acoustic wave propagation properties, as discussed in the coming chapters of this thesis, the length is proportional to the group velocity.

To limit the size of the microacoustic device, narrow bandwidths can be realized with SAW resonator filters, first presented by Ash in 1970 [30]. This type of filter has (at least in theory) an Infinite Impulse Response (IIR). Figure 1.4 shows a typical layout of a two-port resonator. Two reflector arrays, each consisting of strips at distances of $\lambda_0/2$, at both ends of the acoustic wave path form the resonant cavity, analog to the Fabry-Perot type of cavity in optics. The amplitude characteristic consists of the ordinary SAW delay line response, on top of which the narrow band response produced by the resonant cavity is superposed. The amplitude and phase response in this narrow band, like that of any mechanical vibrating device, can be modeled with an RLC equivalent circuit, as proved by Butterworth in 1915 [31] and later rediscovered by Cady [32]. The SAW resonator filter is a minimum-phase filter. As a consequence, the amplitude and phase characteristic cannot be designed independently and with less freedom, in comparison with the SAW transversal filter. When the SAW resonator is used as the frequency determining element in a (low-noise) oscillator this need not be a problem. The quality Q of a resonator filter is given by

$$Q = \frac{f_0}{B} = \frac{2\pi}{\lambda_0} L_{eff} \frac{1}{1-\Gamma_0^2} \tag{1.11}$$

In Eq. 1.11 B is the -3 dB bandwidth. As shown by Collin [33], this expression is only valid where $\Gamma_0 \approx 1$. The length of the cavity is, as a result of the distributed surface wave reflections at the strips, given by the effective length L_{eff}. The reflection factor Γ_0 (where $\Gamma_0 \approx 1$) is given by

$$\Gamma_0 = tanh(Mr) \tag{1.12}$$

with M the number of strips in the reflector and r the absolute value of the reflection per strip. The device length, for a given Q, is in first order determined by the product Mr. As a consequence, a low phase velocity

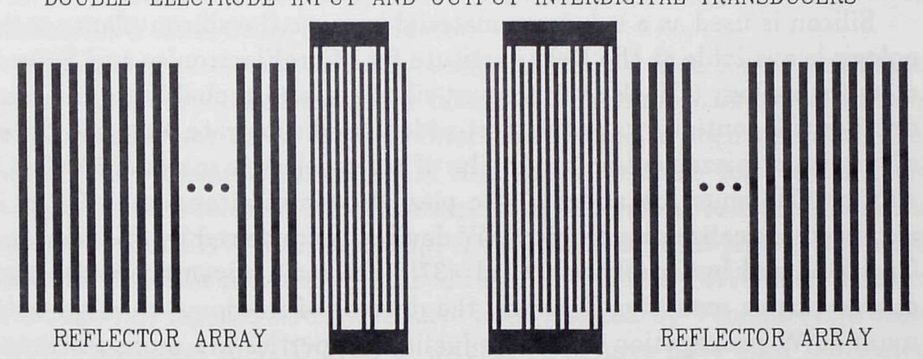

Figure 1.4: *Typical layout of the metal pattern in a two-port SAW resonator filter configuration.*

and a high reflection per strip minimizes for a given center frequency f_0 the overall length of the device. In a layered structure with dispersion, the length is also determined by the phase velocity and not by the group velocity as has been found in SAW transversal filters.

The use of SAW devices as bandpass filters in the VHF and UHF range is widespread. Today almost all television receivers, video cassette recorders and cable television converters contain one or more SAW filters, as do other telecommunication systems. In measuring equipment SAW filters and SAW based oscillators are key components, while SAW signal processing is pervasive in radar systems. Despite progress [34], conventional LC or ceramic filters have a two to three orders of magnitude lower fabrication precision, are much larger and require complex and expensive adjustments. Moreover, SAW filters have proven their inherent reliability and durability in consumer electronics products and in space applications [35].

1.2 STATEMENT OF THE PROBLEM

One of the research topics of the Microacoustics Group at Delft University of Technology is the realization of silicon-integrated SAW devices. The reasons for interest in this area are basically twofold: the possibility of monolithic integration of SAW devices with electronic circuitry and the development of new generations of SAW devices which use the acousto-electric interaction between the surface acoustic wave and the (majority or minority) charge carriers in the silicon substrate. A combination of

both types of devices is possible as well.

Silicon is used as a substrate material because the silicon-planar technology is available at the Delft Institute for MicroElectronics and Submicron Technology (DIMES). Moreover, silicon is, and probably for the next decades will continue to be the most widely used substrate material. Since silicon is not piezoelectric, a thin film of a piezoelectric material like ZnO, AlN or CdS must be added. The piezoelectric semiconductor GaAs is also used to realize monolithic SAW devices, as reviewed by Webster and Carr [36], and by Grudkowski et al. [37]. The main advantage is the high charge carrier mobility. However, the degrees of freedom to design optimum SAW propagation and transduction properties are more restricted than for layered structures on a silicon substrate. The piezoelectric coupling of GaAs is very low ($\kappa^2 < 0.1\%$) and its temperature coefficient of delay cannot be made zero without additional layers.

In the next paragraphs the reasons for conducting research in the above-mentioned two main areas are given in more detail and some of the work already done is shortly reviewed. The realization of silicon-integrated SAW devices, especially the materials to obtain a thin piezoelectric film are also discussed.

Monolithic integration of SAW devices

In thirty years of continuing development in chip processing technology the number of transistors in one chip has at least doubled every two years, caused by further miniaturization and by the increase of the chip size. During the same period the price per elementary electronic function has fallen sharply. This development is driven by price/performance calculations and will continue some time before there is a leveling off due to fundamental scientific or technological limitations. Because of these developments the tendency in microelectronic engineering is towards the integration of an increasing number of signal processing functions and even complete electronic systems in one single chip.

In the last decade analog and digital circuitry are combined by fabricating bipolar and MOS transistors in one single chip [38]. A next step, being developed, is the integration of non-electronic circuitry on that same chip. Examples are integrated optics [39] and sensors for the measurement of non-electrical quantities. Integrating sensors and signal-processing circuitry in one chip leads to versatile, high-quality "smart sensors" at low cost. A number of such sensors have been described by Middelhoek and Audet [40]. An on-chip SAW physical-electronic system for sensors has been realized, as described by Vellekoop et al. [41]. In this application

the SAW delay-line frequency selectivity is sufficient for proper operation of the SAW dual delay-line oscillator.

In analog electronic circuitry design there is a need for on-chip band pass filters. Switched-capacitor filters or continuous-time active filters can be used, but these types of filters are limited in their operating frequency and dynamic range. SAW filters are low noise devices and have a high intermodulation-free dynamic range. Therefore, it is advantageous to implement SAW filters on chip. This is the main subject of this work and discussed in more detail in Sections 1.3 and 1.4. SAW delay lines in CdS-SiO_2-Si layered structures have been realized by Venema [42], while SAW resonators in ZnO-SiO_2-Si layered structures have been fabricated by Martin et al. [43].

Acoustoelectric interaction

When SAW devices are fabricated on silicon substrates, the interaction of the surface acoustic wave with the charge carriers in this substrate can be employed to manufacture a new generation of SAW components, such as SAW (acoustoelectric) convolvers, acoustic transport devices, SAW programmable filters and SAW amplifiers. The convolvers have been described in detail by Khuri-Yakub and Kino [44], and by Motamedi et al. [45]. Acoustic transfer devices in silicon have been discussed by Augustine et al. [46]. Programmable filters have been developed by Hickernell et al. [47] and Green et al. [48]. In these filters interdigital transducers are used for generation of the surface acoustic wave and piezoresistive NMOS FET taps are employed for detection of the acoustic wave. A new SAW detection method, the Barrier Modulated Tap (BMT), has been introduced by Haartsen [49]. SAW amplification is examined in Chapter 3 of this thesis.

Realization of silicon-integrated SAW devices

To obtain the piezoelectric thin film in silicon-integrated SAW devices a low temperature process is required to enable a monolithic integration with electronic circuitry. Further, it is often desirable to have the (aluminum) interdigital transducer underneath the piezoelectric layer, as shown in Chapter 2. Sputtering of materials like ZnO, AlN, CdS or ferroelectric materials has become one of the most reliable technologies. A review has been given by Shiosaki and Kawabata [50]. High-quality and reproducible CdS layers are difficult to obtain. For this reason CdS is not considered anymore. Sputtering of ZnO or AlN is well understood and gives good results. The properties of acoustic propagation and transduc-

tion in a ZnO-SiO_2-Si layered structure are better than in a AlN-SiO_2-Si layered structure, as is shown in Chapter 2. New piezoelectric materials are being developed. One promising group of materials are the piezoplastic polymers, which can be deposited by spinning as has been demonstrated by Fiorillo et al. [51]. A problem with this technology is the poling of the layer after deposition.

With the current technology the piezoelectric thin film is the limiting factor in performance of silicon-integrated SAW devices. This situation, however, is very similar to the situation in the fifties and the early sixties when the first silicon transistors were compared with the superior germanium transistors and somewhat later when the transistors on an IC were not yet as good as discrete transistors. In three decades the technology has been improved to the degree that 10^6 transistors can be integrated on a single chip. In addition, the characteristics of these transistors have greatly been improved. Research by Yamazaki et al. [52] at Matsushita has shown the applicability of sputtered ZnO on glass substrates for TV-IF filters. Such filters replace the expensive lithium niobate substrates and are manufactured by Murata Mfg., as reported by Shiosaki [53]. The next step in this development, described in this thesis, is the realization of SAW filters in ZnO-SiO_2-Si layered structures and the monolithic integration of these filters with electronic circuitry in the same silicon substrate.

1.3 OBJECTIVES OF THIS WORK

This thesis deals with the design and fabrication of SAW filters in ZnO-SiO_2-Si layered structures. The basic SAW filter structures, i.e. the SAW delay line, the SAW transversal filter and the SAW resonator filter, are realized. The layered structure with the aluminum interdigital patterns at the ZnO-SiO_2 interface is depicted in Fig. 1.5. The monolithic integration of these SAW filters with electronic circuitry in one chip is part of the problem, investigated in depth and realized. Important for application of SAW filters in an electronic system are its contribution of noise and intermodulation to the complete system. Therefore, these aspects and the driving and loading of the SAW device are examined. In addition, the SAW amplification mechanism is examined and its application in silicon-integrated SAW filters is considered. This amplification mechanism is based on the acoustoelectric interaction of the traveling acoustic wave with the (drifting) charge carriers in the silicon substrate.

This thesis attempts to cover the entire above-mentioned field, which is accomplished by using existing numerical programs and first-order approximations for analysis and synthesis. Only bidirectional transducers and no multistrip couplers have been employed. The emphasis lies on problems directly related to the use of a ZnO-SiO_2-Si layered structure, since SAW filter design itself (in particular the first-order modeling) is well known. In this context higher-order Rayleigh-wave modes are examined and attention is paid to triple transit echo and electromagnetic feedthrough suppression.

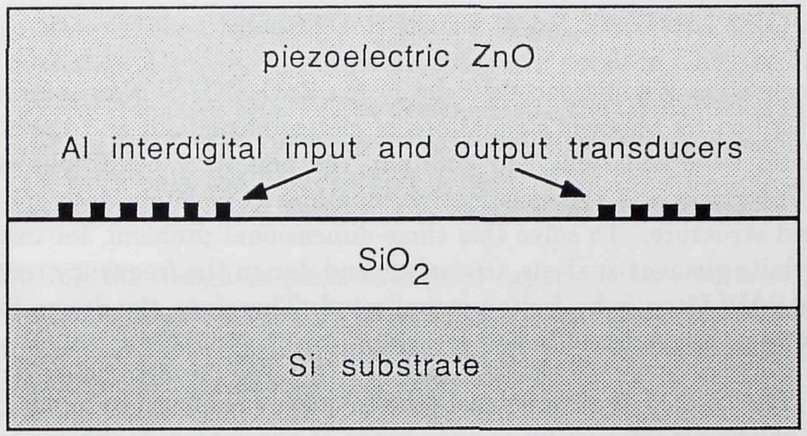

Figure 1.5: *ZnO-SiO_2-Si layered structure with the interdigital transducers at the ZnO-SiO_2 interface.*

In the SAW filter design used in this thesis a number of second-order effects (diffraction, nonzero electrode resistance, SAW propagation losses etc.) are neglected. It is assumed that only pure Rayleigh-wave modes are excited in the ZnO-SiO_2-Si layered structure. Acoustic beam misalignment from the silicon crystal axes is neglected. However, misalignment is inevitable because the transducer pattern cannot perfectly be aligned with the flat of the wafer, which itself is a cut with an imperfect alignment to the crystal axes.

Analysis of bulk wave generation is not carried out since the layered structure with its interdigital transducers is, too a large extent, already determined by the demands on SAW propagation and transduction, and on the desired frequency response of the SAW filter.

Since the feasibility of SAW filters in ZnO-SiO_2-Si layered structures and their monolithic integration with electronic circuitry in one single chip is demonstrated in this thesis, a more detailed analysis and design can be the subject of future research. In addition, the reproducibility and long-term stability of these silicon-integrated filters can be studied in more detail.

1.4 OUTLINE OF SAW FILTER DESIGN

The operation of a microacoustic device in a ZnO-SiO_2-Si layered structure is described by Maxwell's equations of electromagnetism and the elastodynamic wave equations. In addition, the boundary conditions at the layer interfaces and the constitutive equations completely determine the layered structure. To solve this three-dimensional problem, for example with finite element analysis, to analyze and design the frequency response of the SAW filter, is by far too complicated. Therefore, the design is split into two parts, as listed below

- The layered structure causes the frequency response to be no longer solely determined by the geometry of the interdigital transducers. The layered structure must, therefore, be analyzed with respect to SAW propagation and transduction properties. A high piezoelectric coupling and a small temperature coefficient of delay are desired. Further, small phase and group velocities result in a small length of the SAW resonator filter and SAW transversal filter, respectively. Finally, the variations in phase velocity and group velocity must be minimal when the layer thicknesses vary (as a result of the fabrication tolerances). In Chapter 2 these demands will be examined in more detail for the ZnO-SiO_2-Si and AlN-SiO_2-Si layered structures.

- When the layered structure with the location of the interdigital transducer have been determined the layout of the aluminum interdigital patterns and reflector arrays (in the case of a SAW resonator) must be designed.

  In a SAW transversal filter the geometry of the apodized interdigital transducer corresponds in first order to a spatially sampled version of the impulse response of the SAW filter. By using the "delta-function" model, sampling and design concepts used in digital signal processing for FIR digital filters can be extended to SAW filters. This delta-function model was first introduced by Tancrell and Holland [54], and is closely related to the "impulse model" described later by Hartmann et al. [55]. The design is now a mathematical problem, no longer connected to the complicated physics of the layered structure. To improve the design an analysis of the complete design can be carried out, taking second order effects into account as much as possible. The results of this analysis can be used to improve the design in an iterative manner. As already described this latter step in SAW filter design is not carried out in this work. The design

  is accomplished by using the delta-function model and the Remez Exchange Algorithm, as described in more detail in Chapter 5.

  A SAW resonator filter can be designed with the transmission matrix formulation or with the more versatile coupling-of-modes method. In this work only the first method is used. This transmission matrix formulation has been described in detail by Datta [56].

By splitting the design in parts successful experimental results of SAW filters in ZnO-SiO_2-Si layered structures have been obtained. In addition, this approach enables future improvement of the SAW filter design by including second-order effects.

Chapter 2

SAW PROPAGATION AND TRANSDUCTION

2.1 INTRODUCTION

In this chapter layered structures for silicon-integrated SAW filters are investigated. The layered structure must have a high piezoelectric coupling and preferably a frequency and temperature independent group velocity v_g (variation in group velocity $\Delta v_g(\omega, T) = 0$). When the dispersion can be neglected standard SAW filter design techniques can be used to obtain a desired amplitude and phase response. Furthermore, the reproducibility in center frequency of the SAW filter must be guaranteed and the device length should be minimal to make a monolithic integration with electronic circuitry attractive. Hence, v_{ph} and v_g must be as small as possible for SAW resonator and SAW transversal filter applications, respectively. In addition, $\Delta v_{ph}(kh, T) = 0$ (with kh the normalized layer thickness).

The piezoelectric coupling for the second- and higher-order Rayleigh-wave modes must be small in comparison with the coupling of the fundamental mode.

Whether the above-mentioned demands on the SAW filter performance can be met in the case of a realization in a layered structure depends on the materials chosen, the design and the fabrication procedure. The materials (especially the question of whether to use ZnO or AlN as a piezoelectric thin film) and part of the design (namely the determination of the layer thicknesses and the choice of the location for the interdigital transducer) are discussed in this chapter. The fabrication of the silicon-integrated SAW filter and the design of the interdigital pattern are discussed in Chapters 4 and 5 respectively. To determine the best choice of materials and to find the optimum device configuration, Rayleigh wave propagation and transduction (as the key parameters in SAW filter design) are studied as a function of frequency, layer thicknesses and temperature. Kino and Wagers [57] were among the first to examine the excitation of SAW on a nonpiezoelectric substrate by the use of an interdigital transducer overlaid with a piezoelectric layer. The theory and some experimental results of Rayleigh wave propagation and transduction in three-layered structures have been published by Venema [58], Venema and Dekkers [59], Ghijsen [60] and Ono et al. [62], but a complete overview and a discussion of SAW filter design integrated with electronic circuitry in one single chip are given here. Second-order effects such as reflections, diffraction, nonlinear phenomena, bulk waves etc., have not been investigated. The interdigital metal pattern is considered ideal, i.e. perfectly conducting and infinitely thin. Interaction of the surface acoustic wave with the charge carriers in the silicon substrate does not result in losses, since the silicon conductivity can be considered infinitely. Chapter 3 deals with the acoustoelectric interaction (in the case of noninfinite and nonzero silicon conductivity) and its influence on SAW propagation.

Section 2.2 deals with the theory of Rayleigh wave propagation and transduction. In Section 2.3 an inventory of material constants is given. Numerical and experimental data of Rayleigh wave propagation and transduction are presented for the ZnO-SiO_2-Si and the AlN-SiO_2-Si layered structures in Sections 2.4 and 2.5, respectively. In Section 2.6 the different configurations are discussed and conclusions as to their applicability as layered structures for silicon-integrated SAW filters are drawn.

2.2 THEORY OF PROPAGATION AND TRANSDUCTION

2.2.1 Choice of Materials

The aim is a monolithic integration of the SAW filter with electronic circuitry on one single silicon substrate. A piezoelectric thin film is required since silicon is not a piezoelectric material. A maximum enhancement in piezoelectric coupling is obtained when the interdigital tranducer is located at the bottom of the piezoelectric layer compelling the insertion of an extra, dielectric layer. As discussed in Section 1.2, ZnO and AlN are the most promising piezoelectric thin film materials at the moment. SiO_2 is chosen as an IC compatible, high-quality dielectric layer. The possible configurations are sketched in Fig. 2.1. The application of a silicon

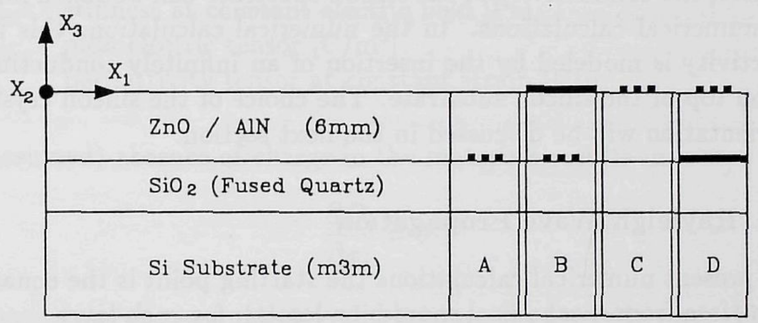

Figure 2.1: *Layered structure for silicon-integrated SAW filters with the investigated materials and the four different transducer configurations.*

nitride dielectric layer would be very attractive from a fabrication point of view (as discussed in Chapter 4), but an extensive literature search failed to provide the necessary material constants (and their temperature dependencies) to numerically evaluate the application of this material. Values for permittivity, density and thermal expansion coefficients can be found, but the stiffness constants are not known since only information on Young's modulus for silicon nitride layers was found [63], [64]. Experimental results with a silicon nitride layer instead of an SiO_2 layer did not give much of an acoustic response, probably due to the non-optimum ZnO sputter conditions for this substrate material. Therefore, curve fitting with experimental results to obtain the relevant material constants has not yet been feasible. Another use of silicon nitride is the deposition of a nitride layer on top of the ZnO layer, as a passivation of the ZnO, to improve the stability of the frequency response of the SAW device. Since this layer is thin its influence on SAW propagation and transduction is

small as demonstrated by Vellekoop et al. [65].

The most simple implementation of the SAW filter with electronic circuitry can be realized when the silicon conductivity is determined by the IC process. In virtually all IC processes and with the 10 MHz – 1 GHz SAW device operating frequency range in mind, the following relation is obtained

$$\frac{\omega}{\omega_c} \ll 1 \tag{2.1}$$

with ω_c determined by the silicon conductivity and permittivity, according to

$$\omega_c = \frac{\sigma_{Si}}{\epsilon_{Si}} \tag{2.2}$$

Therefore, the conductivity of the silicon substrate can be taken infinitely in all numerical calculations. In the numerical calculations this infinite conductivity is modeled by the insertion of an infinitely conducting thin plate on top of the silicon substrate. The choice of the silicon crystal cut and orientation will be discussed in the next section.

2.2.2 Rayleigh Wave Propagation

In the present numerical calculations the starting point is the equation of motion (free from mechanical sources or losses), for each layer

$$\rho \frac{\partial^2 u_i}{\partial t^2} = \frac{\partial T_{ij}}{\partial x_j} \qquad i,j = 1,2,3 \tag{2.3}$$

with

ρ	mass density [kg/m^3]
u_i	particle displacement [m]
t	time [s]
T_{ij}	stress [Pa]
x_j	position in Cartesian coordinates [m] (Fig. 2.1)

together with the constitutive relations of linear, time-invariant and locally reacting materials

$$T_{ij} = c^E_{ijkl} S_{kl} - e_{ijk} E_k \tag{2.4}$$

$$D_i = e_{ikl} S_{kl} + \epsilon^S_{ik} E_k \tag{2.5}$$

with $i,j,k,l = 1,2,3$, and

$$S_{kl} = \frac{1}{2}\left(\frac{\partial u_k}{\partial x_l} + \frac{\partial u_l}{\partial x_k}\right) \tag{2.6}$$

The vectors and tensors of the field quantities are

S_{kl}	strain
E_k	electric field [V/m]
D_i	electric displacement [C/m^2]

and the material constants are

c^E_{ijkl}	stiffness at constant electric field [Pa]
e_{kij}	piezoelectric tensor [C/m^2]
ϵ^S_{ik}	permittivity tensor at constant strain [F/m].

The (assumed) absence of charge in the materials results in

$$\frac{\partial D_i}{\partial x_j} = 0 \tag{2.7}$$

The quasi-static approximation (valid because the acoustic wave velocities are five orders of magnitude lower than the velocity of light) results in

$$E_k = -\frac{\partial \phi}{\partial x_k} \tag{2.8}$$

where ϕ is the electrical potential associated with the surface acoustic wave. The problem of surface acoustic wave propagation is completely described by the equations above and can be solved by applying the boundary conditions at the layer interfaces. In general (u_1, u_2, u_3, ϕ) are coupled. For optimum device operation the direction of propagation must be colinear with the direction of the energy flow, the "pure modes." In addition the piezoelectric material has a 6mm (hexagonal) textured crystal orientation with a preferred c-axis normal to the surface. Venema [58] has shown that pure (stiffened) Rayleigh-wave modes can propagate in such a layered structure which results in a decoupling between (u_1, u_3, ϕ) and (u_2). The direction of propagation of the surface acoustic wave, with respect to the silicon crystal cut and orientation is important. Si (100) is widely used in IC processing. By taking the [010] or [001] directions for SAW propagation, pure Rayleigh-wave modes result, as shown by Venema. Since

all experimental devices have been realized in such a structure, the numerical calculations only consider the Si(100)[001] - SiO_2 (fused quartz) - ZnO/AlN (6mm, c-axis $\perp$ substrate surface) layered structures. The effect of a deviation between crystal cut, orientation and the wave propagation has not been subject to investigation. The pure Rayleigh-wave mode propagation will be assumed to have a particle displacement in the u_2-direction equal to zero at all times, resulting in a two-dimensional plane-wave solution for the potential ϕ and the particle displacements u_i of the form

$$u_i, \phi \sim e^{jkbx_3} e^{jk(x_1 - v_{ph}t)} \tag{2.9}$$

All solutions and boundary conditions can be expressed in one large system of equations. The related determinant is zero for the surface acoustic wave solutions. However, the problem is often ill-conditioned and the determinant cannot be forced to zero in a machine computation because of round-off errors. A more attractive way to solve the problem (of in fact a structure of arbitrarily number of layers) has been developed by Ghijsen [60], and Ghijsen and Van den Berg [61], who have reduced the problem to a dual-boundary-value problem for the potential and current density only. The number of equations is maximally equal to eight. The numerical results in this chapter have been obtained with the numerical programs developed by Ghijsen.

In the ZnO-SiO_2-Si and AlN-SiO_2-Si layered structures higher-order Rayleigh-wave modes can propagate, because the bulk shear wave phase velocities of the layers are lower than that of the silicon substrate.

Design parameters ωh and kh

The phase velocity can be determined as a function of ωh or kh. Both design parameters are important in the design of SAW filters as is now explained.

To estimate the influence of ZnO (or AlN) layer variations (inevitable due to the fabrication tolerances) the phase velocity must be determined as a function of the normalized piezoelectric layer thickness kh_{ZnO} (or kh_{AlN}). The wavenumber k is related to the period p of the transducer according to $k = 2\pi/p$ and can, therefore, be considered constant. The variations in the SiO_2 layer thickness are small when compared with the piezoelectric layer thickness variations. Hence, the normalized SiO_2 layer thickness is constant.

To determine the dispersion in surface acoustic wave propagation in the multilayered structure, the phase and group velocity must be calculated

as a function of ωh, where h_{SiO_2} and h_{ZnO} (or h_{AlN}) are constant. The group velocity v_g is then given by

$$\frac{1}{v_g} = \frac{\partial k}{\partial \omega} = \frac{1}{v_{ph}} - \frac{(\omega h)}{v_{ph}} \frac{\partial v_{ph}}{\partial (\omega h)} \tag{2.10}$$

Temperature coefficient of frequency

Both phase and group velocity depend on the temperature of the substrate. To obtain a temperature-stable center frequency of the SAW filter transfer function a number a measures can be taken, as reviewed by Lewis [66]. The definitions of the first-order temperature coefficients of frequency and delay are given in Chapter 1. An attractive solution is the combination of materials with an opposite sign in their temperature coefficient of frequency. This approach has been demonstrated by Nakagawa [67] and Defranould [68] for ZnO layers on pyrex glass.

Numerical calculations for the ZnO-SiO_2-Si layered structure have been presented by Ono et al. [62]. They proved that the first-order temperature coefficient of delay is mainly determined by the temperature dependence of the stiffness constants, the effect due to linear expansion being negligible by comparison. The thermal expansion coefficients are only used to calculate the temperature dependent mass density of the different layers. Also for the ZnO-SiO_2-Si layered structure, Martin [69] has realized temperature coefficients of delay of about -1 ppm/K for a normalized SiO_2 layer thickness of about 0.48. In the research presented in this thesis no attempts have been made to realize temperature-stable SAW devices. The SAW delay line, as presented in the next section and in Chapter 5, has a temperature coefficient of frequency of about 15 ppm/K in the -40°C to $+80$°C temperature range. This temperature coefficient is obtained for a normalized SiO_2 layer thickness of about 0.45 and is already better than for $LiNbO_3$.

For the AlN-SiO_2-Si layered structure, temperature stability should be feasible too. However, in this case both the AlN and the SiO_2 layer have a negative temperature coefficient of delay. Temperature stability on silicon and Al_2O_3 substrates have been realized by Tsubouchi et al. [77], [78].

Propagation losses

The attenuation of the propagating surface acoustic wave is neglected in this thesis. Attenuation is caused by acoustic beam misalignment, diffraction, reflections (caused by electrical and mechanical discontinuities), scattering from surface imperfections and grain boundaries, and by interaction

with thermal phonons. A review on the attenuation of surface waves is given by Dransfeld and Salzmann [70]. Hickernell [71] has obtained in his experiments data on the SAW attenuation in ZnO films. The losses in the sputtered ZnO film can be considered dominant in the ZnO-SiO$_2$-Si layered structure.

2.2.3 Rayleigh Wave Transduction

The efficiency of the electric-to-acoustic energy conversion in the interdigital transducer is expressed by κ^2. Ristic [72] and Kino [73] have shown that only κ^2 of the total input electrical energy is converted to elastic energy of the surface acoustic wave. This can easily be verified in the one-dimensional case.

In a one-dimensional model the stiffness constant c in Eq. 2.4 can be replaced by

$$c' = c\left(1 + \frac{e^2}{\epsilon c}\right) = c\left(1 + \kappa^2\right) \tag{2.11}$$

with κ^2 the piezoelectric coupling coefficient. The phase velocity v_{ph} of an acoustic wave is proportional to $\sqrt{c/\rho}$ and in the case of a piezoelectric medium $\sqrt{c'/\rho}$. The piezoelectricity causes an increase in phase velocity of approximately $\frac{1}{2}\kappa^2$. When the conductivity of the medium becomes infinite, all piezoelectric fields are shorted and the phase velocity v_m is related to v_{ph} as

$$\frac{\Delta v}{v} = \frac{v_{ph} - v_m}{v_{ph}} \approx \frac{1}{2}\kappa^2 \tag{2.12}$$

Equation 2.12 is also valid as an approximation for the piezoelectric coupling of surface acoustic waves in multilayered structures. The phase velocity v_m is now obtained by the insertion of a perfectly conducting, infinitesimally thin metal plane at the interface where the IDT is located. Ghijsen [60] has shown that the $\Delta v/v$ approximation of the piezoelectric coupling is within 10% of the exact value. When the inaccuracy in the material constants (as discussed in the next section) is taken into account, the accuracy of the $\Delta v/v$ approximation is sufficient. The piezoelectric coupling must be calculated for a constant radial frequency ω. The κ^2 dependence of the electric to acoustic energy conversion is not only valid for the interdigital transducer but also in the acoustoelectric interaction mechanism of the SAW amplifier, as discussed in the next chapter.

Table 2.1: *Material constants at $T = 300K$ of silicon, silicon dioxide (fused quartz), ZnO (monocrystalline bulk material constants* and experimentally obtained material constants for thin films**) and AlN.*

		Si	SiO_2	ZnO*	ZnO**	AlN
ρ	10^3 kg/m^3	2.33	2.20	5.68	5.72	3.26
c_{11}^E	10^{11} Pa	1.66	0.785	2.10	1.57	3.45
c_{13}^E		0.639	0.161	1.05	0.83	1.20
c_{33}^E		1.66	0.785	2.11	2.08	3.95
c_{44}^E		0.796	0.312	0.425	0.38	1.18
e_{31}	C/m^2			-0.61	-0.51	-0.58
e_{33}				1.14	1.22	1.55
e_{15}				-0.59	-0.45	-0.48
ϵ_{11}	10^{-10} F/m	1.03594	0.33468	0.737		0.8
ϵ_{33}		1.03594	0.33468	0.782		0.95
α_{11}	ppm/K	2.6	0.55	4.0		5.27
α_{33}		2.6	0.55	2.1		4.15
TC(c_{11}^E)	ppm/K	-68	239	-112		80
TC(c_{13}^E)		-100	584	-161		160
TC(c_{33}^E)		-68	239	-123		100
TC(c_{44}^E)		-44	151	-70		50
Ref.		[62], [80]	[62], [80]	[62], [80]	[76]	[77], [79]

2.3 MATERIAL CONSTANTS

To evaluate the different layered structures, sets of the material constants of amorphous, dielectric layers and polycrystalline (textured) piezoelectric layers are required. Where the monocrystalline material constants are used, the theoretical results do not match the experimentally obtained results, as will be shown in the next section. Efforts, based on theoretical models, to calculate these material constants from the monocrystalline material constants have not been very successful [74], [75]. A better approach is to accurately measure surface acoustic wave parameters, such as the wave velocities and piezoelectric coupling factors, and determine the matching material constants by curve fitting. This approach has been carried out by Carlotti et al. [76] in the case of ZnO layers, and by Tsubouchi et al. [79] for AlN layers.

Carlotti et al. have determined the ZnO material constants (with the exception of the dielectric permittivity) by measurements of the phase

velocity of RF magnetron sputtered ZnO on Al_2O_3 and Si substrates. Therefore, it is expected that the material constants do not completely match with the constants obtained in a DC magnetron sputtered ZnO layer on a SiO_2-Si substrate. Tsubouchi made a computer calculation of the material constants of a metal-organic chemical vapor deposited (single-crystal) AlN film. The epitaxial growth takes place at 1200°C, which is not very attractive in the case of a monolithic integration with electronic circuitry.

In comparison with the uncertainties in piezoelectric material constants, the silicon crystal material constants are very well known. The SiO_2 layer is taken equivalent to fused quartz since no better set of material constants for this layer is available. The material constants are tabulated in Table 2.1. The material constants are given in matrix notation. In Table 2.1 α_{11} and α_{33} are the (linear) thermal expansion coefficients and TC(c_{ij}^E) is the first-order temperature coefficient of c_{ij}^E.

2.4 THE ZnO-SiO$_2$-Si LAYERED STRUCTURE

In Figs. 2.2 and 2.3 the two different sets of material constants for the ZnO layer (as listed in Table 2.1) have been used to calculate the phase velocity and piezoelectric coupling. Compared to the monocrystalline approximation of the ZnO layer, the phase velocity can be up to 10% lower when the computer fit ZnO material constants from Carlotti et al. are

Table 2.2: *Measured (normalized) layer thicknesses and center frequencies. Phase velocities are calculated based on these measurements, based on a monocrystalline approximation of the ZnO layer* [80], *and based on a set of experimentally obtained material constants* [76].

	h_{SiO_2} [μm]	h_{ZnO} [μm]	λ_0 [μm]	kh_{SiO_2}	kh_{ZnO}
Delay L.	2.00±0.02	11.1±0.4	28.00	0.449±0.006	2.5±0.1
Transv.	1.53±0.02	5.6±0.2	9.333	1.03±0.02	3.8±0.2
Reson.	1.53±0.02	5.6±0.2	9.000	1.07±0.02	3.9±0.2

	f_0 [MHz]	$v_{ph} = \lambda_0 f_0$ [m/s]	v_{ph} [80] [m/s]	v_{ph} [76] [m/s]
Delay L.	100.4±0.2	2811±5	2891±15	2773±18
Transv.	283.0±0.5	2641±5	2743±5	2588±8
Reson.	292.2±0.2	2630±2	2742±4	2583±8

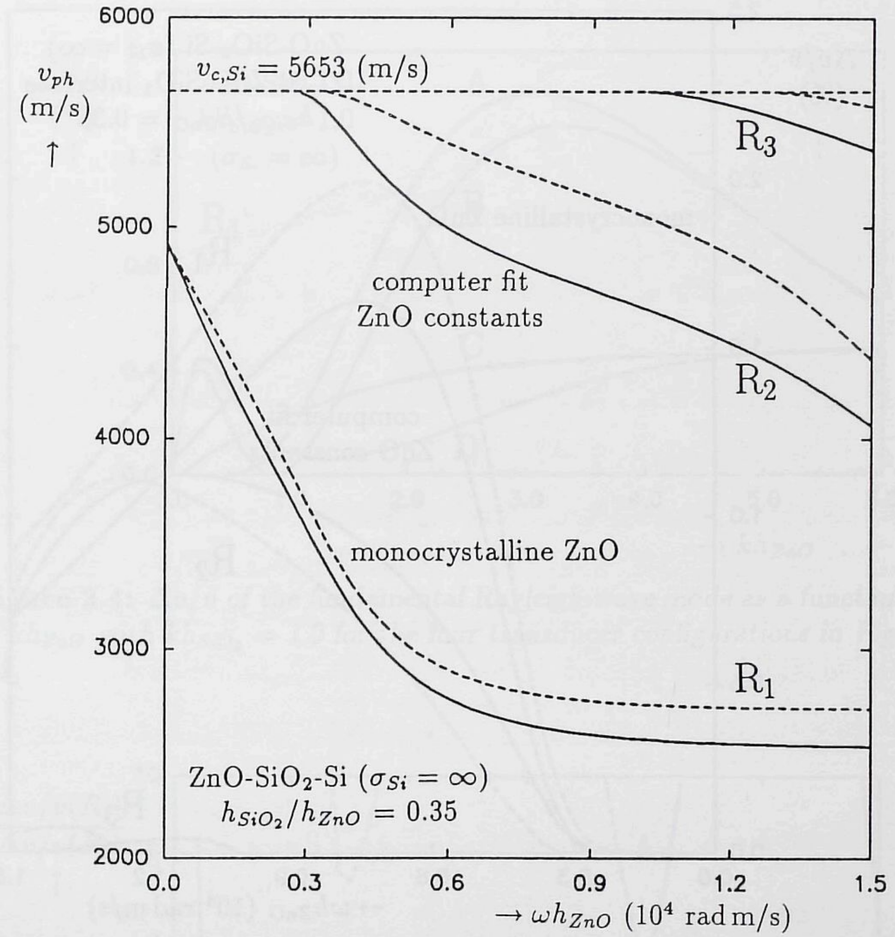

Figure 2.2: *Phase velocities of three Rayleigh-wave modes in the case of a monocrystalline approximation of the ZnO layer (dashed). The solid line is obtained when the computer fit ZnO material constants are used.*

used. The piezoelectric coupling can be up to 20% lower. Experimental data have been obtained from a SAW delay line (Delay L.), a SAW transversal filter (Transv.) and a SAW resonator filter (Reson.). The transfer functions of these SAW filters are presented in Chapter 5, here the propagation properties are discussed. The ZnO layer thickness has been determined with a Tencor alpha-step 200. Because a sputter mask has been used to fabricate the ZnO layer, the layer is not uniform. In Table 2.2 an average value and the variation across the acoustic beam are given. The silicon dioxide layer thicknesses are measured with an ellipsometer. SiO_2 layer variations are one order of magnitude smaller and

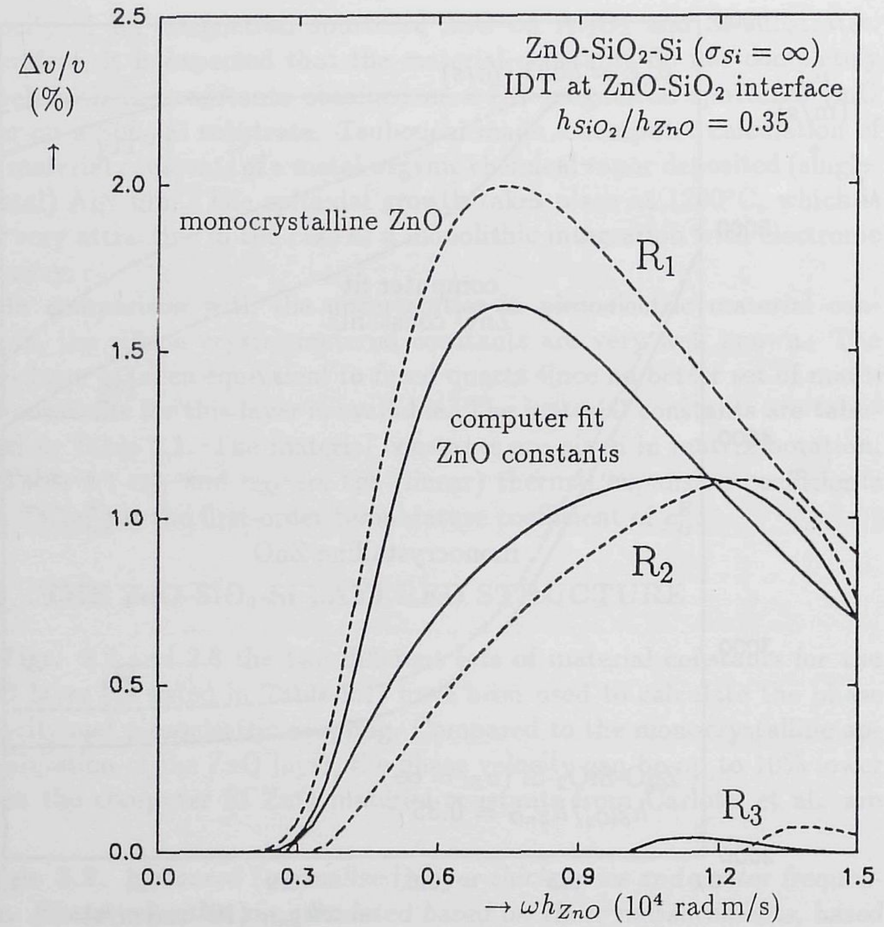

Figure 2.3: *$\Delta v/v$ of three Rayleigh-wave modes in the case of a monocrystalline approximation of the ZnO layer (dashed). The solid line is obtained when the computer fit ZnO material constants are used.*

are, therefore, neglected. For the same reason the inaccuracy in the fabrication of the transducer is neglected. The calculated phase velocities when a monocrystalline approximation of the ZnO layer is used, are about 4% higher than the measured velocities. Using the computer fit ZnO material constants of Carlotti et al., the calculated phase velocities are 1.5–2% too low. Errors is this case can be caused by the fused quartz approximation of the silicon dioxide layer and by the fact that a SiO$_2$-Si substrate is used. In the rest of this chapter the computer fit constants are used, since they are more accurate.

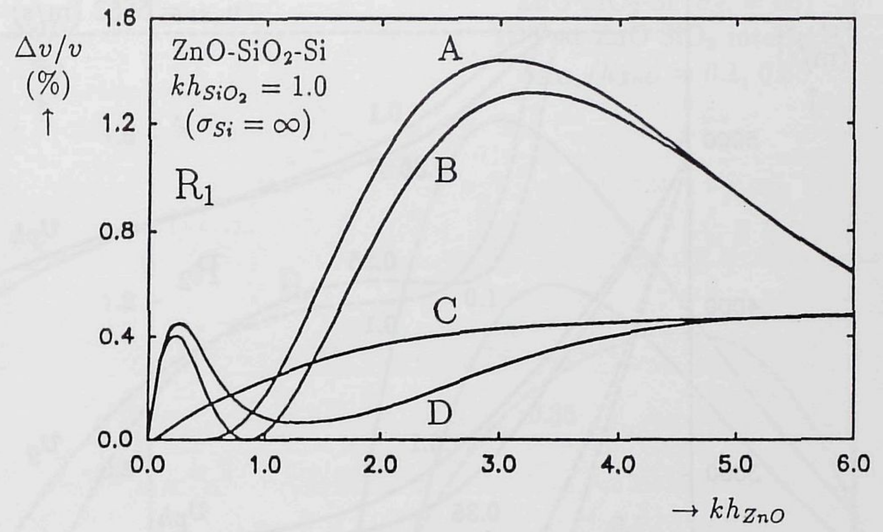

Figure 2.4: *$\Delta v/v$ of the fundamental Rayleigh-wave mode as a function of kh_{ZnO} with $kh_{SiO_2} = 1.0$ for the four transducer configurations in Fig. 2.1.*

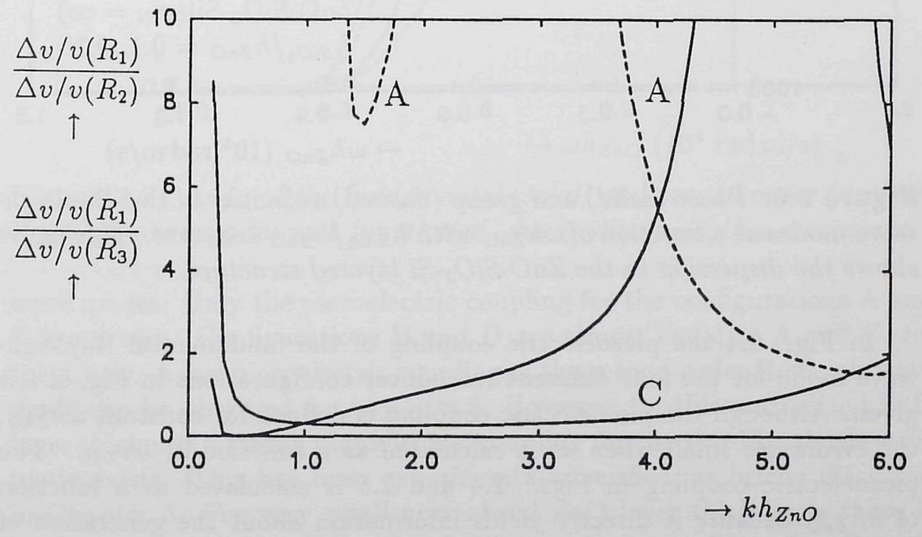

Figure 2.5: *$\Delta v/v$ of the fundamental Rayleigh-wave mode relative to the $\Delta v/v$ ratio of the second- (solid) and third-order (dashed) Rayleigh-wave modes for transducer configurations A and C (Fig. 2.1).*

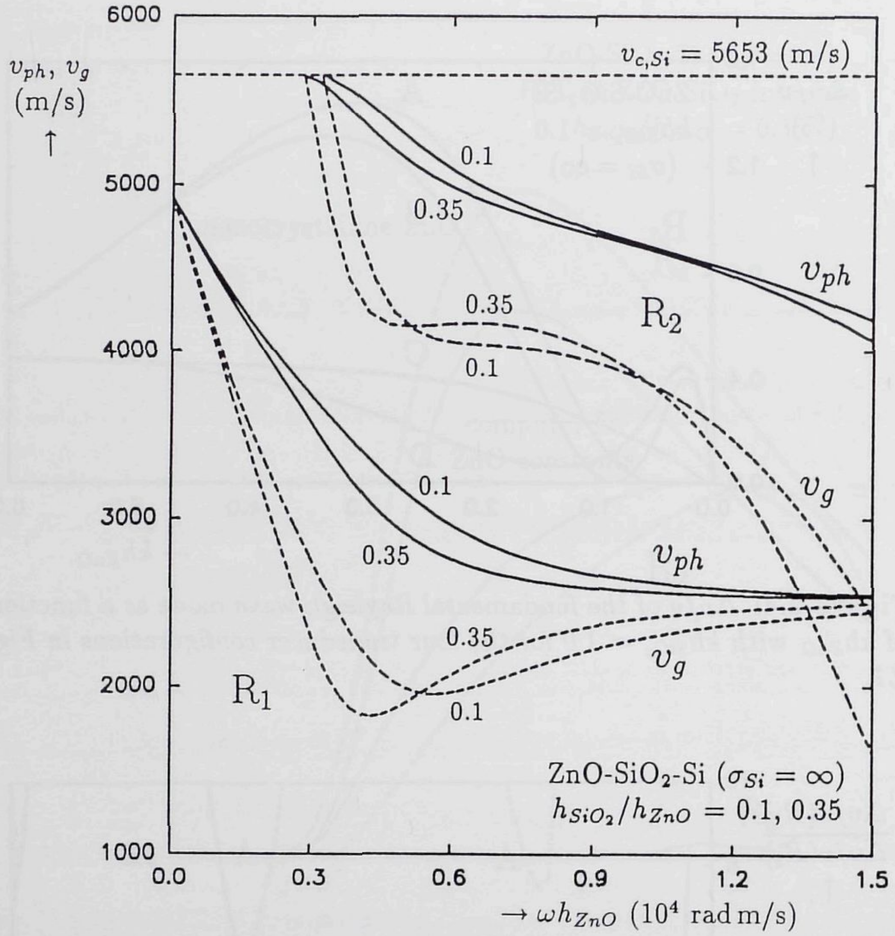

Figure 2.6: *Phase (solid) and group (dashed) velocities of two Rayleigh-wave modes as a function of ωh_{ZnO} with h_{SiO_2}/h_{ZnO} constant. This figure shows the dispersion in the ZnO-SiO$_2$-Si layered structure.*

In Fig. 2.4 the piezoelectric coupling of the fundamental Rayleigh-wave mode for the four different transducer configurations in Fig. 2.1 is given. Although the piezoelectric coupling is defined for constant ωh_{ZnO}, the errors are small when κ^2 is calculated as a function of kh_{ZnO}. The piezoelectric coupling in Figs. 2.4 and 2.5 is calculated as a function of kh_{ZnO} because it directly yields information about the generation of higher-order Rayleigh-wave modes in interdigital transducers.

Figure 2.5 shows the piezoelectric coupling of the fundamental Rayleigh-wave mode relative to coupling of the second- and third-order Rayleigh-

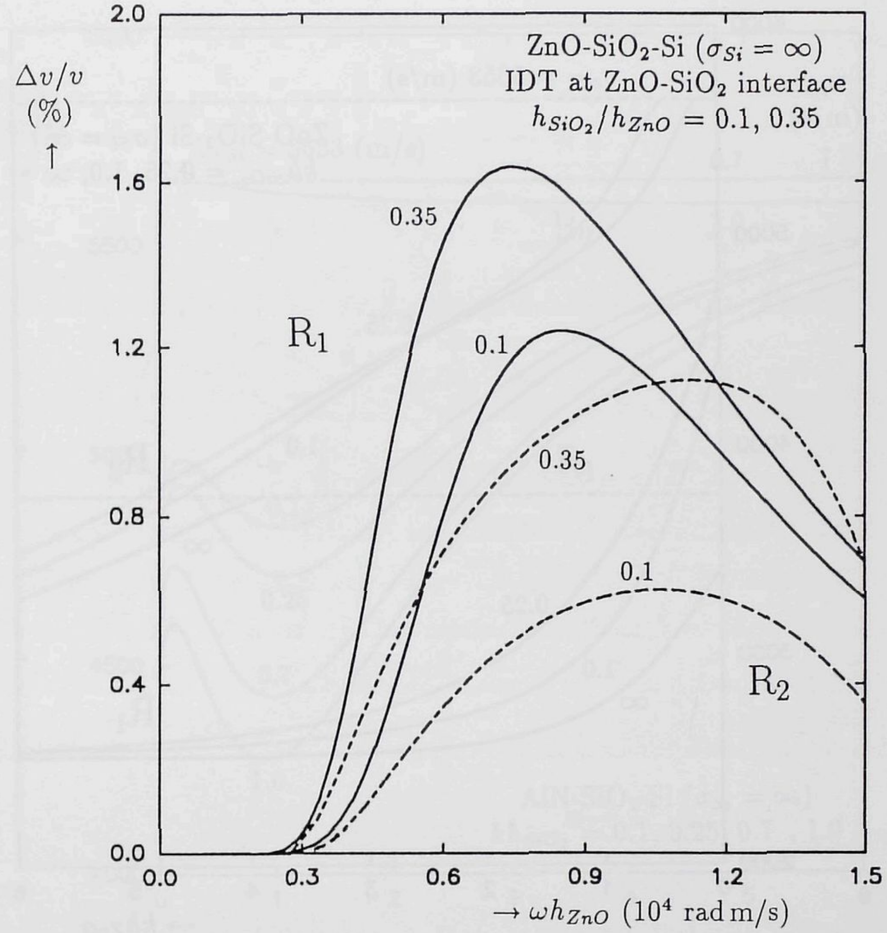

Figure 2.7: *$\Delta v/v$ of the fundamental (solid) and second-order (dashed) Rayleigh-wave modes as a function of ωh_{ZnO} with h_{SiO_2}/h_{ZnO} constant.*

wave modes. Only the piezoelectric coupling for the configurations A and C are drawn. Configurations B and D are almost equal to A and C, respectively. A low piezoelectric coupling of the second-order Rayleigh-wave mode can be obtained for $kh_{ZnO} \approx 5$. However, for this normalized ZnO layer thickness a strong piezoelectric coupling for the third Rayleigh-wave mode exists. This has been experimentally verified, as briefly discussed in Chapter 5. For very small normalized ZnO layer thicknesses there is no second Rayleigh-wave mode. In that case the configuration B or D must be used to obtain an acceptable piezoelectric coupling for the first Rayleigh-wave mode.

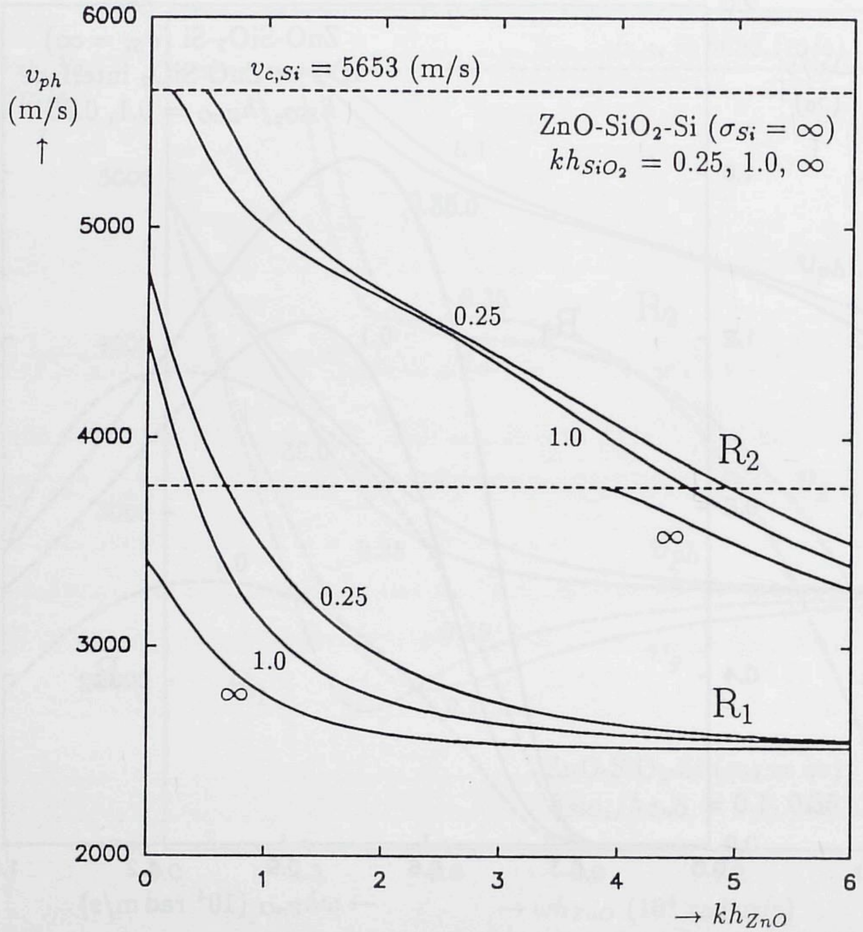

Figure 2.8: *Phase velocities of the fundamental and the second Rayleigh-wave modes as a function of kh_{ZnO}. This figure shows the influence of ZnO layer thickness variations.*

Figures 2.6 and 2.7 show the phase and group velocity, and the piezoelectric coupling as a function of ωh_{ZnO}. When $\omega h_{ZnO} \rightarrow 0$, then $\omega h_{SiO_2} \rightarrow 0$ and the Rayleigh wave phase velocity (equal to the group velocity) of the silicon substrate ($v_{R,Si}$ = 4921 m/s) results. Finally, Fig. 2.8 shows the variation in phase velocity (and thus in center frequency of the SAW filter) by variation of the ZnO layer thickness.

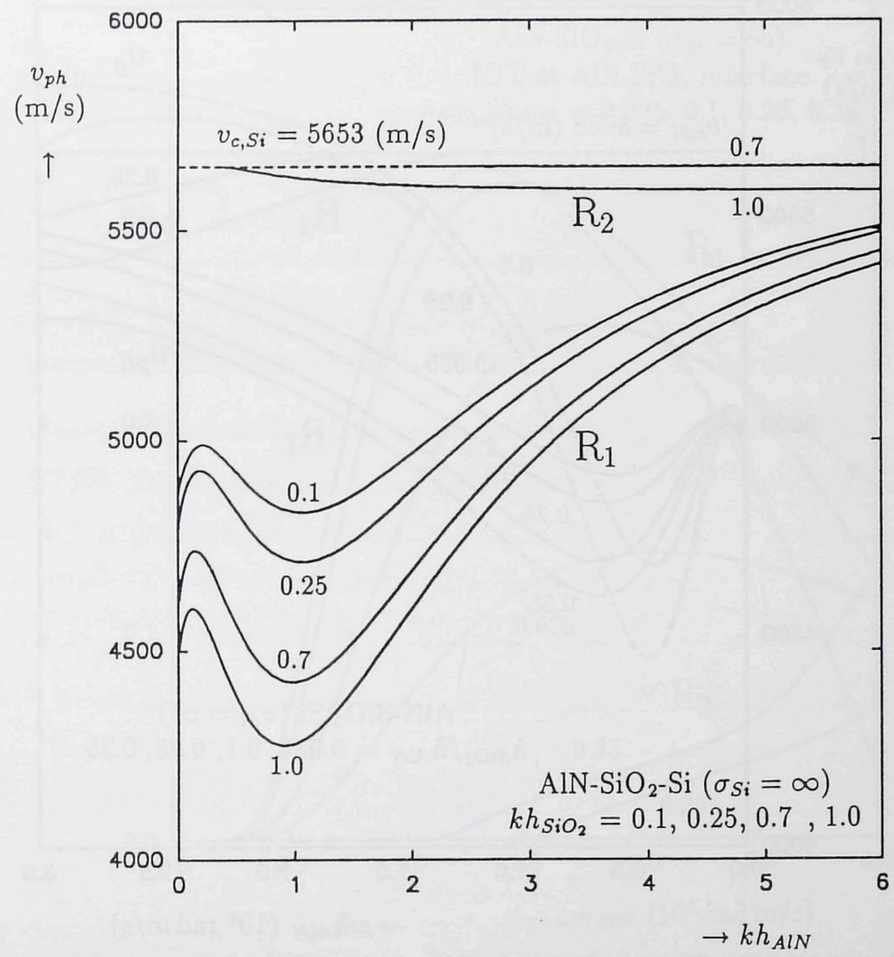

Figure 2.9: *Phase velocities of the fundamental and the second Rayleigh-wave modes as a function of kh_{AlN}. This figure shows the influence of AlN layer thickness variations.*

2.5 THE AlN-SiO$_2$-Si LAYERED STRUCTURE

Besides ZnO as a piezoelectric thin film, AlN seems a promising material. Therefore, the AlN-SiO$_2$-Si layered structure is subject to investigation in this section.

The variation in phase velocity (and thus in the center frequency of the SAW filter transfer function) when the AlN layer thickness varies (due to the fabrication tolerances) is shown in Fig. 2.9. For thin SiO$_2$ layer

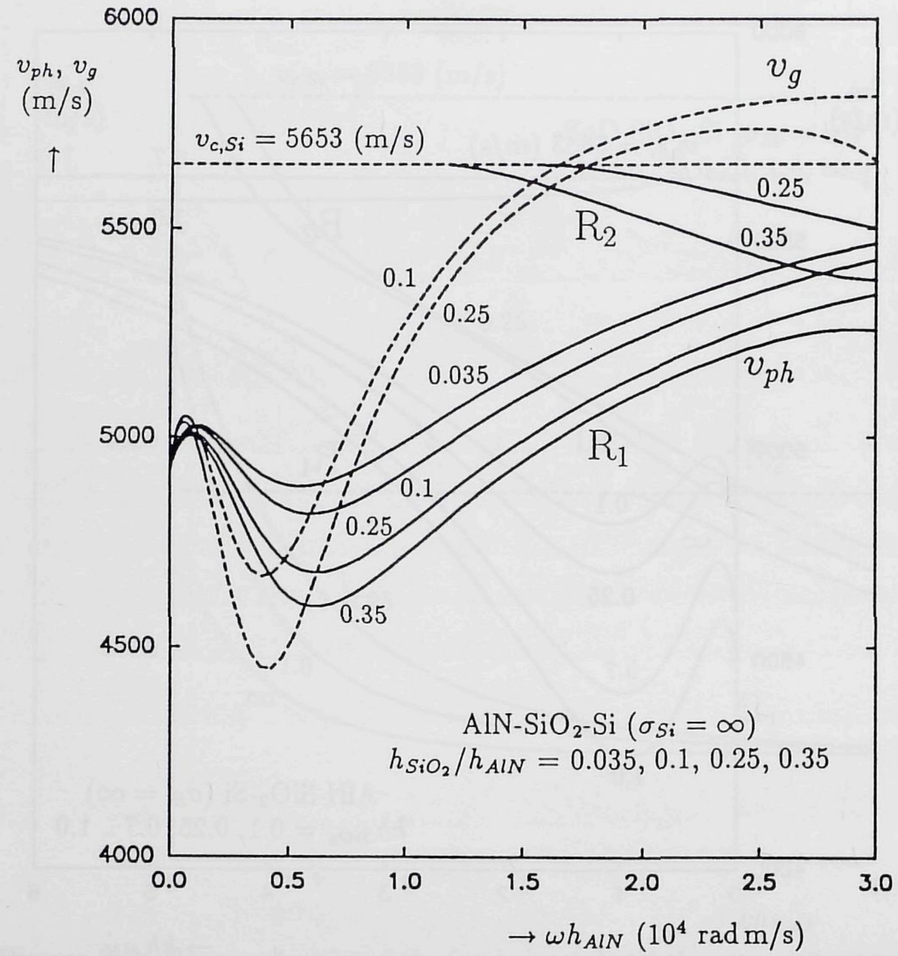

Figure 2.10: *Phase velocity (solid) of two Rayleigh-wave modes and group velocity (dashed) of the fundamental Rayleigh-wave mode as a function of ωh_{AlN} with h_{SiO_2}/h_{AlN} constant. This figure shows the dispersion in the AlN-SiO$_2$-Si layered structure.*

thicknesses no second- and higher-order Rayleigh-wave modes exist in the AlN-SiO$_2$-Si layered structure. Higher-order modes can exist, because the Rayleigh wave phase velocity in a bulk crystal of AlN ($v_{R,AlN} = 5607$ m/s) is less than the cut-off velocity of a semi-infinite silicon substrate ($v_{c,Si} = 5653$ m/s).

Figure 2.10 shows the dispersion in surface acoustic wave propagation in the AlN-SiO$_2$-Si layered structure.

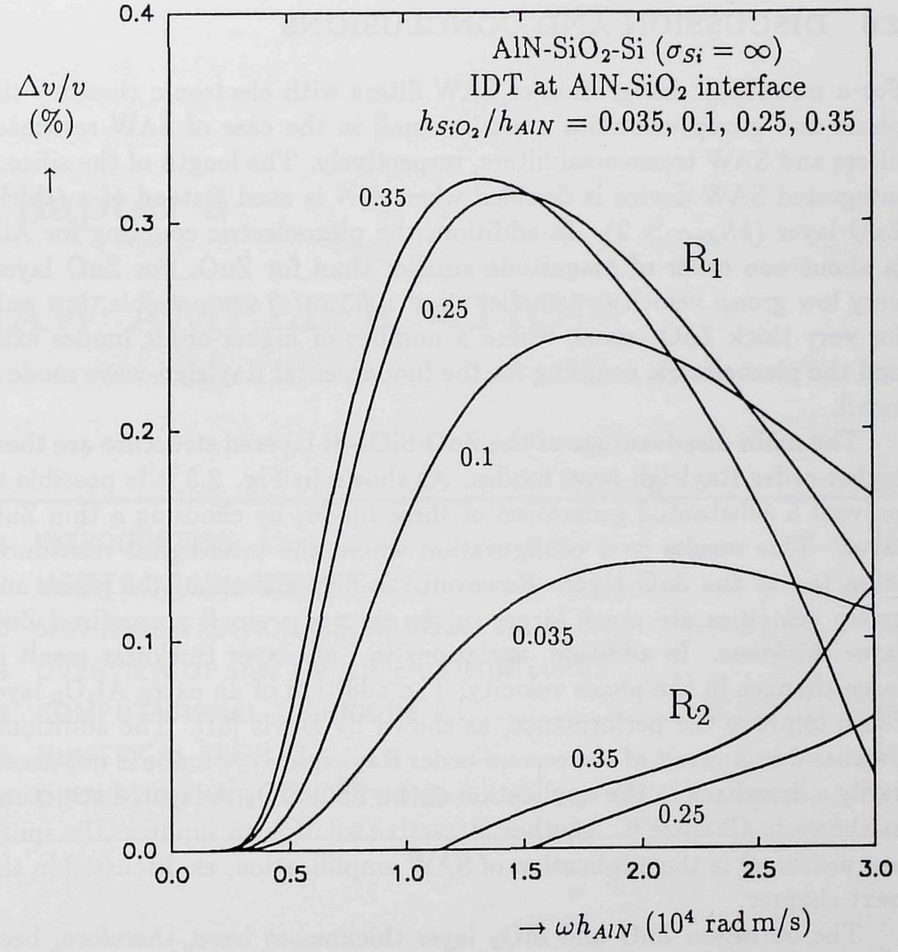

Figure 2.11: *$\Delta v/v$ of the fundamental and second-order Rayleigh-wave modes as a function of ωh_{ZnO} with h_{SiO_2}/h_{ZnO} constant.*

Figure 2.11 shows the corresponding piezoelectric coupling in the case of configuration A (see Fig.2.1). For configurations B, C and D results similar to those in Fig. 2.4 are obtained. An advantage of the AlN-SiO$_2$-Si layer is the absence of higher-order Rayleigh-wave modes when the normalized SiO$_2$ layer thickness is chosen smaller than 0.7 (and $kh_{AlN} < 3$). However, the piezoelectric coupling is almost one order of magnitude smaller than for the ZnO-SiO$_2$-Si layered structure.

2.6 DISCUSSION AND CONCLUSIONS

For a monolithic integration of SAW filters with electronic circuitry the phase and group velocities must be small in the case of SAW resonator filters and SAW transversal filters, respectively. The length of the silicon-integrated SAW device is doubled when AlN is used instead of a (thick) ZnO layer ($kh_{ZnO} > 2$). In addition, the piezoelectric coupling for AlN is about one order of magnitude smaller than for ZnO. For ZnO layers very low group velocities (smaller than 1000 m/s) are possible, but only for very thick ZnO layers, where a number of higher-order modes exist and the piezoelectric coupling for the fundamental Rayleigh-wave mode is small.

The main disadvantage of the ZnO-SiO_2-Si layered structure are these higher-order Rayleigh-wave modes. As shown in Fig. 2.5 it is possible to prevent a substantial generation of these modes by choosing a thin ZnO layer. This results in a configuration where the interdigital transducer is on top of the ZnO layer. However, the dispersion and the phase and group velocities are much larger in the case of a small normalized ZnO layer thickness. In addition, variations in ZnO layer thickness result in large changes in the phase velocity. The addition of an extra Al_2O_3 layer could improve the performance, as shown by Davis [81]. The additional passband as a result of the second-order Rayleigh-wave mode is not necessarily a drawback in the application of the ZnO-SiO_2-Si layered structure, as shown in Chapter 6. Another attractive solution to suppress the spurious passband is the application of SAW amplification, as discussed in the next chapter.

The optimum ZnO and SiO_2 layer thicknesses have, therefore, been chosen $kh_{ZnO} \approx 3$ and $kh_{SiO_2} > 1.0$. The interdigital transducer is located at the ZnO-SiO_2 interface and the ZnO deposition is the final process step in the case of a monolithic integration with electronic circuitry (as discussed in more detail in Chapter 4). For these layer thicknesses a constant group delay in SAW transversl filters can be obtained, as experimentally verified and shown in Chapter 5. For a good temperature stability of the center frequency a normalized SiO_2 layer thickness of approximately 0.5 must be chosen. This results in a small degradation of the dispersion and piezoelectric coupling properties.

Chapter 3

SAW AMPLIFICATION

3.1 INTRODUCTION

In this thesis the monolithic integration of SAW filters with electronic circuitry is the subject of investigation and has resulted in the use of a ZnO-SiO_2-Si layered structure. Here, the amplification of surface acoustic waves in silicon-integrated SAW filters is discussed. The used perturbational technique enables the accurate calculation of the amplification/attenuation and of the SAW phase velocity in the case of nonzero or noninfinite conductivity of the silicon substrate.

There are two principal mechanisms of amplifying the surface acoustic waves. The first mechanism, "traveling-wave type amplification," is by interaction of the acoustic wave with drifting charge carriers. The other, "parametric amplification," occurs due to the nonlinear interaction between acoustic waves. The nonlinearity is caused by the nonlinear space

charge distribution in the silicon substrate.

Parametric amplification of SAW was first reported in 1970 by Chao [82], where the parametric interaction occurs due to the nonlinearity in elastic properties of the $LiNbO_3$ substrate. A more efficient parametric amplifier is obtained when the above-mentioned nonlinearity in space charge distribution in the semiconductor is used, as described by Minagawa et al. [83], [84]. The convolver in a ZnO-SiO_2-Si layered structure, described by Khuri-Yakub and Kino [85], operates on the same principle.

SAW traveling-wave type amplifiers are basically the solid-state equivalent of the traveling-wave tube. The operation of the traveling-wave tube can be explained in terms of a coupling between a slow electromagnetic wave and a space-charge wave, as described by Pierce [86]. In the case of a SAW traveling-wave type amplifier the acoustic wave produces (as a result of the piezoelectricity of the ZnO layer) a slow moving electromagnetic wave which couples with the stream of drifting charge carriers in the silicon substrate. Amplification occurs when the carrier drift velocity exceeds the phase velocity of the acoustic wave. By choosing the layer thicknesses in the ZnO-SiO_2-Si layered structure as proposed in Chapter 2, a frequency independent phase-velocity is obtained which results in a broad bandwidth of the SAW amplifier.

To obtain not only amplification of the acoustic wave but a suppression of spurious acoustic waves as well, the traveling-wave type amplification mechanism is suited only. This is discussed in more detail in Section 3.2. For this reason no more attention is paid to parametric amplification and "SAW amplification" refers in the rest of this thesis to the traveling-wave type amplification mechanism. The SAW amplification mechanism is explained with a simple one-dimensional model in Section 3.3. A review of SAW amplifier structures is given in Section 3.4. Section 3.5 describes the macroscopic model, the approximations used, and the simple computational technique to determine the surface acoustic wave amplification (or attenuation) and the Rayleigh wave velocity in the case of a nonzero of noninfinite silicon conductivity. Numerical results are presented in Section 3.6 and compared with a rigorous analysis. A discussion on potential applications of SAW amplification and conclusions are given in Section 3.7.

3.2 MERITS OF SAW AMPLIFICATION

SAW amplification is possible when the drift velocity of the charge carriers exceeds the phase velocity of the surface acoustic wave. Otherwise, the

device acts as an attenuator. This distributed, nonreciprocal amplification mechanism has a number of advantages when compared with electronic amplification at the input or output of a SAW filter, or when compared with parametric amplification. It can be used for the suppression of undesired acoustic waves, which are generated by the interdigital transducer, and for increasing the output signal of the SAW filter. Both improvements in the SAW filter transfer function are discussed in the next paragraphs.

The SAW amplification mechanism can be used for suppression of higher-order Rayleigh wave modes by choosing a drift velocity higher than the first, but lower than the second- and higher-order Rayleigh wave modes. Since bulk waves have a phase velocity higher than the SAW phase velocity, the same kind of choice for the charge carrier velocity can be used to suppress bulk waves traveling near the substrate surface. This kind of bulk wave is difficult to suppress by other means because such measures will also influence the surface acoustic wave propagation. Choosing a layered structure with different layer thicknesses to suppress the bulk waves is often not possible because of the restrictions on center frequency reproducibility, phase linearity and on the technological limitations. In power matched SAW devices the Triple Transit Echo (TTE), as discussed in Chapter 5, is a serious problem, since it increases the ripple in amplitude and group delay response. To reduce the TTE the SAW amplification mechanism, or actually its potential to attenuate acoustic waves, can be used to suppress the backward moving surface acoustic wave.

The other advantage of the amplification mechanism is the enlargement of the SAW filter output signal. In this way a larger stopband rejection can be obtained, since it is usually limited by bulk wave propagation and by the (direct) electromagnetic feedthrough between the input and output transducer. In addition, the bidirectionality losses in the interdigital transducer and the acoustic wave propagation losses can be compensated. An increased output signal of the SAW filter also relieves the demands on the electronic circuitry driving and loading the device. Especially in front-end applications (as discussed in Chapter 6) a substantial improvement of the total system performance can be expected. The noise contribution of the SAW amplifier is important in this context. The noise of a SAW amplifier in a ZnO-SiO_2-Si layered structure must be the subject to further investigation, since it is not treated in this thesis. For SAW amplifiers in other (layered) structures, theoretical and experimental results show an adequate noise behavior of this type of amplifier. A noise figure calculation is given by Kino and Coldren [87].

The main disadvantage is the high power dissipation. Only a small part

of the supplied energy is actually used to amplify the surface acoustic wave. Measures to keep the dissipation within acceptable limits are discussed in Section 3.5.

3.3 SAW AMPLIFICATION MECHANISM

To understand the SAW amplification mechanism a simple one-dimensional model (based on the conservation of energy) is introduced. It is valid for longitudinal bulk waves, traveling in a (doped) semiconducting piezoelectric medium. Only the majority charge carriers are considered. For SAW amplification in a layered structure the model is too simple, a more detailed computational technique as given in Section 3.5 is necessary.

Consider a bulk acoustic wave traveling through a piezoelectric semiconductor. As a result of this piezoelectricity the particle displacements result in an electric field E_{pe} with amplitude E_0 of

$$E_{pe} = E_0 e^{j(kx-\omega t)} = E_0 e^{j\psi} \tag{3.1}$$

where x is the direction of propagation, t the time, ω the radial frequency and k the wave number according to

$$k = k_r + jk_i \tag{3.2}$$

For $k_i = 0$ a lossless acoustic wave propagation results. SAW amplification takes place for $k_i < 0$, attenuation for $k_i > 0$. The piezoelectrically induced field E_{pe} is affecting the charge carriers in the medium and v.v. Electric currents are generated to form charge bunches, which in turn generate an electric field E_{cb}. The piezoelectrically induced electric fields are so large that the creation of charge bunches is not hindered by electrostatic repulsion of the charge carriers. The charge bunches tend to screen out the piezoelectric field, which results in a total electric field E_{tot}

$$E_{tot} = E_{pe} + E_{cb} \tag{3.3}$$

The AC current density J, corresponding to the traveling wave of induced charge ρ, is given by

$$J = \sigma E_{tot} = \rho v_{ph} \tag{3.4}$$

with σ the electrical conductivity of the medium and v_{ph} the acoustic wave propagation (phase) velocity. The induced charge ρ is given by

$$\rho = \epsilon \frac{\partial E_{cb}}{\partial x} \tag{3.5}$$

with ϵ the dielectric permittivity of the medium. The time derivative of the mechanical work W on the charge carriers by the acoustic wave is given by

$$\partial_t W = E_{tot} J \tag{3.6}$$

The acoustic wave is attenuated when $E_{tot}J > 0$. It losses energy to the charge carriers. Amplification occurs when $E_{tot}J < 0$. No acoustoelectric interaction takes place when $E_{tot}J = 0$, which results in a lossless SAW propagation (acoustic losses are neglected in this model). In order to obtain an electric field E_{tot} in phase with the current density J the electric field generated by the charge bunches must be

$$E_{cb} = \alpha E_0 e^{j(\psi+\eta)} \tag{3.7}$$

where η is the phase difference between E_{pe} and E_{cb} and α is the relative amplitude factor. When E_{tot} and J are not in phase, regions of amplification and attenuation will exist within one wavelength, which is not possible. From Eq. 3.4 and using the Eqs. 3.1, 3.3, 3.5 and 3.7, it is found that

$$\alpha e^{j\eta} \left(j\frac{\omega}{\omega_c} - 1 \right) = 1 \tag{3.8}$$

with $\omega_c = \sigma/\epsilon$ the dielectric relaxation frequency.
In the case $\omega/\omega_c \gg 1$, $\alpha \to 0$ and $\eta \to \pi/2$. There is a minimum creation of charge bunches, which are lagging behind the traveling wave by half an acoustic wavelength. Since in this case $J \to 0$, no energy is transferred between the acoustic wave and the charge carriers. The semiconductor can be considered as an insulator.
In the case $\omega/\omega_c \ll 1$, $\alpha \to -1$ and $\eta \to 0$. There is a maximum creation of charge bunches, which are in phase with the piezoelectric field E_{pe}, resulting in an electric field $E_{tot} \to 0$. The charge carrier distribution can respond quickly enough to short the piezoelectric field E_{pe}. No energy is, therefore, transferred between the acoustic wave and the charge carriers. The semiconductor can be considered as a metal.

The energy lost by the acoustic wave is supplied to the charge carriers. Taking into account that only a κ^2 fraction of the acoustic wave energy is electric energy, the result after integration Eq. 3.6 over one acoustic wavelength is

$$\frac{k_i}{k_r} = \frac{1}{2}\kappa^2 \frac{\omega/\omega_c}{1+(\omega/\omega_c)^2} \tag{3.9}$$

To obtain the normalized attenuation k_i/k_r as given in Eq. 3.9 the weak

coupling approximation ($\kappa^2 \ll 1$) has been used, thus

$$\frac{k_i}{k_r} \ll 1 \tag{3.10}$$

A maximum normalized attenuation of the acoustic wave of $k_i/k_r = 1/4\kappa^2$ is obtained at $\omega/\omega_c = 1$. In that case $\alpha = -\frac{1}{2}\sqrt{2}$ and $\eta = \pi/4$. The charge bunches are lagging behind the acoustic wave by a quarter of a wavelength.

In the case of drifting charge carriers with a drift velocity v_d Eq. 3.4 must be replaced by

$$J = \rho(v_{ph} - v_d) \tag{3.11}$$

All equations are still valid, but relative to a frame of reference moving at the drift velocity v_d. For $v_d > v_{ph}$, $E_{tot}J < 0$, which results in an energy transfer from the drifting charge carriers to the acoustic wave. The acoustic wave radial frequency thus changes into the effective (Doppler-shifted) frequency $\delta\omega$, according to

$$\delta\omega = \left(1 - \frac{v_d}{v_{ph}}\right)\omega \tag{3.12}$$

A small attenuation or amplification is now obtained for

$$|\delta\omega/\omega_c| \ll 1 \tag{3.13}$$

and

$$|\delta\omega/\omega_c| \gg 1 \tag{3.14}$$

This includes the case when

$$v_d \approx v_{ph} \tag{3.15}$$

In this latter case the medium behaves like a perfect conductor. Conservation of energy now results in a normalized amplification of

$$\frac{k_i}{k_r} = \frac{1}{2}\kappa^2 \frac{\delta\omega/\omega_c}{1 + (\delta\omega/\omega_c)^2} \tag{3.16}$$

A result also obtained by Adler [88], who has used an *RC* equivalent circuit model as basis for his derivation. In the case of amplification the acoustic wave is lagging behind the charge bunches. A maximum amplification is obtained when $\delta\omega/\omega_c = -1$. The acoustic wave is lagging behind the charge bunches by a quarter of a wavelength. Diffusion of the charge carriers due to their thermal motion is neglected. Diffusion reduces

the charge bunches, thus reducing ρ and J. As a result the interaction between the charge carriers and the acoustic wave is diminished. A review article by McFee [89] describes in more detail the effect of diffusion on the amplification of bulk waves. In the SAW amplifier this diffusion and the layered structure must be taken into account. Therefore, both longitudinal and transverse components of the fields are important.

3.4 OVERVIEW OF SAW AMPLIFIER STRUCTURES

Acoustic wave amplification was first reported in bulk acoustic wave devices by Hutson et al. [90] in 1961 and theoretically investigated by Hutson and White [91], and White [92]. Reviews are given by McFee [89] and May [93]. Surface acoustic wave amplification was first demonstrated on a CdS bulk crystal by White and Voltmer [94] in 1966. Since then a number of SAW amplifier structures have been realized. A short review (with a few representative references) is given below.

The combined medium amplifier

The combined medium amplifier uses one semiconducting piezoelectric crystal such as GaAs, ZnO or CdS. The high mobility GaAs has a weak piezoelectric coupling which results in a low amplification. ZnO and CdS on the other hand have rather poor semiconductor properties. The poor reproducibility of CdS is another disadvantage. In general, it is difficult to obtain the optimum piezoelectric (i.e. high piezoelectric coupling) and semiconductor properties (i.e. high mobility and a wide range of available and reproducible conductivities) in one crystal.

The separated medium amplifier

The separated medium amplifier uses a piezoelectric substrate with a semiconducting layer, separated by a uniform air gap in order to maintain the traction-free boundary conditions required for Rayleigh wave propagation. Now it is possible to make an optimum choice for the piezoelectric and the semiconductor media. The suggestion that SAW amplification could be obtained in this structure was made by Tien [95], and by Gulyaev and Pustovoit [96] in 1964. The external electric fields diminish rapidly when moving away from the piezoelectric surface and results in the need of sophisticated and expensive technology for the construction of the uniform air gap. In experimental results for a lithium niobate piezoelectric substrate (with a thin silicon film deposited on sapphire and separated

from the lithium niobate with the help of silicon dioxide rails) a gain of 65 dB/cm at 108 MHz has been reported by Lakin and Shaw [97].

The monolithic amplifier with a piezoelectric substrate

Monolithic amplifiers have been constructed by using a thin semiconducting layer on top of a piezoelectric substrate, thus eliminating the critical air gap. The small layer thickness can and usually does severely reduce the charge carrier mobility. Another problem is the adjustment during fabrication of the desired conductivity of the semiconducting layers. Coldren and Kino [98] used InSb vacuum deposited on $LiNbO_3$. Electronic gains of 25 and 70 dB/cm at 220 and 660 MHz, respectively, have been observed. Hannebrekke and Ingebrigtsen [99] obtained 38 dB/mm (!) at 170 MHz in a structure of CdSe on $LiNbO_3$. In this last experiment the required conductivity of the photoconductive CdSe could be accurately adjusted for a maximum amplification by illumination from a halogen lamp.

The monolithic amplifier with a semiconductor substrate

Theoretical and experimental results of SAW amplification in ZnO-Si layered structures have been reported by Tarakci and White [100]. A maximum gain of 21 dB/cm was obtained at 440 MHz (which was not the optimum frequency for maximum gain).

SAW amplification in the ZnO-SiO_2-Si layered structure is of interest in this thesis. To reduce the Joule heating the charge carriers are thought to drift in an epitaxial layer, which can be more or less depleted. Because of its better electron mobility in silicon an n-type epitaxial layer is used. With the proposed structure, shown in Fig. 3.1, the proper conductivity for a maximum amplification can be accurately adjusted during the fabrication of the epitaxial layer. With former multilayer amplifier structures this was more difficult to achieve. With an epitaxial layer present it is also possible to control (together with the charge carrier drift velocity) the amplification. The next section gives a simple, but accurate computational method to analyze the ZnO-SiO_2-Si amplifier structure.

3.5 COMPUTATIONAL TECHNIQUE

3.5.1 Introduction

To calculate the SAW amplification a number of approximations and assumptions are made. The layers are assumed to be homogeneous with

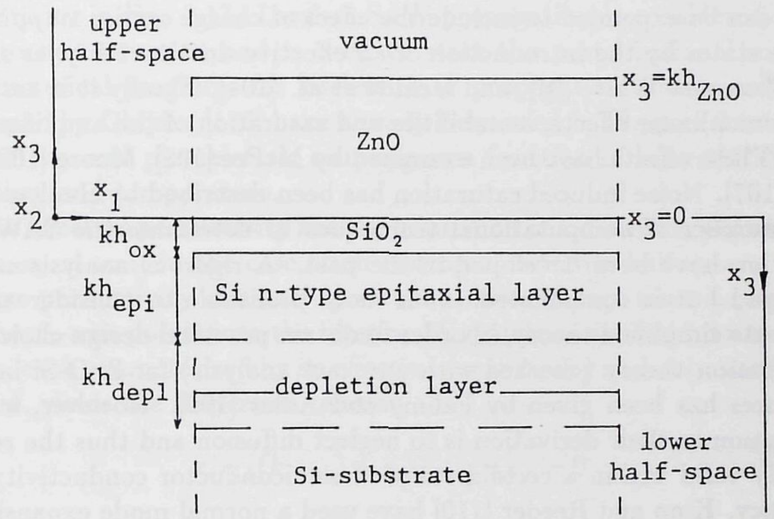

Figure 3.1: *ZnO-SiO_2-Si layered SAW amplifier structure separated into an upper and lower half-space. The upper half-space contains the ZnO layer, the lower half-space is built up of the silicon substrate, the epitaxial layer and the silicon dioxide layer.*

respect to thickness, acoustic properties and doping. Attenuation results from the acoustoelectric interaction only (acoustic attenuation is neglected). A linear, macroscopic theory is used, i.e. $kl \ll 1$ (k is the acoustic wave number and l is the mean free path of the charge carriers). The piezoacoustic wave is treated classically as an electric potential wave for charge carriers. Further, the distribution in the charge carrier drift velocity is neglected and the drift velocity is taken much smaller than the thermal velocity. In addition, only the majority charge carriers (i.e. electrons in the case of an n-type epitaxial layer) are considered and electron-hole recombination and generation are neglected. In general, a good agreement between theory and experiment for the different SAW amplifier structures has been obtained. It is, therefore, concluded that the SAW amplification depends only on the average properties of the drifting stream of charge carriers. The diffusion cannot be neglected in SAW amplification calculations and is fully taken into account. Also taken into account is the piezoelectricity of the ZnO layer. It is assumed that the passivation of the silicon substrate by the silicon dioxide layer reduces sufficiently the presence of surface states, as shown by Venema [101]. The effect of surface states on SAW amplification have been discussed by Ze-

mon and Conwell [102], and by Moore and Smith [103]. However, the model can be expanded to include the effect of charge carrier trapping by surface states by the introduction of an effective drift mobility, as shown by Hutson and White [91], and Uchida et al. [104]. Finally it is assumed that no nonlinear effects, instabilities and saturation of the amplifier take place. These effects have been examined by McFee [105], Moore [106] and Skeie [107]. Noise induced saturation has been described by Hanlon [108].

A number of computational techniques to determine the SAW amplification have been developed in the past. A rigorous analysis can be developed but is complicated. It is more profitable to consider an approximate simplified theory, in order to obtain practical design choices. A perturbation theory (checked with an exact analysis) for ZnO-Si layered structures has been given by Fahmy and Adler [109]. However, a basic assumption in their derivation is to neglect diffusion and thus the results are only valid within a certain range of semiconductor conductivity and frequency. Kino and Reeder [110] have used a normal mode expansion of the Rayleigh wave piezoelectric fields to calculate the amplification in a separated medium amplifier. An alternative approach which uses a perturbational method based on field theory has been developed by Ingebrigtsen [111], [112]. Basic to the analysis is the introduction of an electric surface impedance Z, which relates at the surface the electric potential ϕ (associated with the surface acoustic wave) to the normal component of the electric displacement D_3. The effective dielectric constant or permittivity ϵ_{eff} which is equivalent to the electric surface impedance was later introduced by Greebe et al. [113]. Although other definitions for the effective permittivity are possible [114], [115], the definition given by Greebe et al. suits the problem to calculate the SAW amplification in the ZnO-SiO$_2$-Si layered structure:

$$\epsilon_{eff} = \frac{j}{v_{ph} Z} = \frac{D_3}{k\phi} \tag{3.17}$$

In the equation above, k is the wave number and v_{ph} the phase velocity of the acoustic wave. The use of electric surface impedances or effective permittivities is rather simple and direct in comparison with the normal mode theory. Lakin and Shaw [97] used this perturbational method for analyzing their separated medium amplifier. Their numerical results are in close agreement with the normal mode theory and with experiments.

3.5.2 Perturbation Theory

The perturbational method introduced in this subsection to determine the amplification (or attenuation) and velocity of Rayleigh-wave modes in

ZnO-SiO$_2$-Si layered structures, is based on the application of the effective permittivity in Eq. 3.17. Lossless SAW propagation is considered as the unperturbed situation and is used to start the perturbational method. The numerical programs for lossless SAW propagation and transduction developed by Ghijsen [116] have already been used in Chapter 2 to obtain the velocity and piezoelectric coupling as a function of layer thicknesses, frequency and temperature.

The effective permittivity has the dimension of a dielectric permittivity and is equal to it in the case of an isotropic dielectric half-space. In the effective permittivity of a half-space the surface charge must be included and the x_3-axis points into the interior. A structure divided into two half-spaces, each characterized by an effective permittivity and only electrically coupled, yields the dispersion relation

$$\epsilon_{eff,1}(k, v_{ph}) + \epsilon_{eff,2}(k, v_{ph}) = 0 \tag{3.18}$$

where $\epsilon_{eff,1}$ and $\epsilon_{eff,2}$ are the effective permittivities of both half-spaces. The mechanical and electrical fields are assumed to be plane-wave solutions of the form

$$e^{j(kx_1 - \omega t)} \qquad \omega = k v_{ph} \tag{3.19}$$

In the case of lossless SAW propagation real values for the effective permittivities, k and v_{ph} are obtained. Otherwise these variables become complex (but the radial frequency ω remains real and constant)

$$k' = k + \Delta k_r + j k_i \tag{3.20}$$

$$v'_{ph} = v_{ph} + \Delta v_{ph,r} + j v_{ph,i} \tag{3.21}$$

The perturbation technique discussed in this subsection can be used because

$$|\Delta k_r|, |k_i| \ll k \tag{3.22}$$

$$|\Delta v_{ph,r}|, |v_{ph,i}| \ll v_{ph} \tag{3.23}$$

The dispersion relation in Eq. 3.18 gives an exact solution, but is only of practical interest when expressions for the effective permittivities for both half-spaces can be formulated. As long as dielectric and semiconducting materials are involved, analytic expressions for the effective permittivity of a half-space can be obtained in a straightforward manner (see Section 3.5.3). In the case of Bleustein-Gulyaev waves an analytic expression for the effective permittivity of a piezoelectric half-space can also

be calculated [113]. However, for the more complicated Rayleigh waves it is not possible and here the Ingebrigtsen approximation for the effective permittivity of a piezoelectric half-space can be used [111], [112]

$$\epsilon_{eff} = \epsilon \left(\frac{v_{ph} - v_{open,1}}{v_{ph} - v_m} \right) \tag{3.24}$$

where

ϵ = $\sqrt{\epsilon_{11}\epsilon_{33} - \epsilon_{13}^2}$
v_{ph} = SAW phase velocity
$v_{open,1}$ = SAW phase velocity in the case of an adjoining medium with zero effective permittivity
v_m = SAW phase velocity in the case of a metalized surface

As soon as the half-spaces are not only electrically, but also are mechanically coupled, the mechanical boundary conditions enter the problem. It is no longer possible to divide the structure into two independent half-spaces. Only half-spaces with nonpiezoelectric material keep an effective permittivity independent of the other half-space. Therefore, Ingebrigtsen's approximation no longer holds when a piezoelectric substrate is covered with a semiconducting layer of arbitrary layer thickness. However, by redefining $v_{open,1}$ and v_m as

$v_{open,1}$ = SAW phase velocity in the case of a semiconducting layer with zero permittivity
v_m = SAW phase velocity in the case of a metalized piezoelectric-semiconductor interface

the mechanical and electrical boundary conditions are satisfied for both these velocities. The effective permittivity of the piezoelectric half-space for these velocities can be considered as the unperturbed (exact) value. Perturbations are caused by changes in the electrical parameters in the semiconducting layer. This approach has proven to be successful by Voges [117], who used an approximation to obtain $v_{open,1}$.

To calculate the gain and velocity the ZnO-SiO_2-Si layered structure of Fig. 3.1 must be divided into two half-spaces. The lower, independent one (Section 3.5.3) contains the silicon substrate, epitaxial layer and the silicon dioxide layer. The upper, dependent one (Section 3.5.4) consists

of the ZnO layer and vacuum. Thus by only demanding the continuity of ϵ_{eff} at one interface the amplification can be calculated. The electrical boundary conditions are satisfied not only in the unperturbed, but also in the perturbed situation. The mechanical boundary conditions however, are only satisfied in the unperturbed system. This of course influences the electrical boundary conditions (because of the piezoelectricity), but this effect is neglected (weak coupling approximation from Eqs. 3.20–3.23).

3.5.3 Effective Permittivity of the Lower Half-Space

The effective permittivity ϵ_{eff} of an isotropic nonpiezoelectric semiconducting layer with dielectric permittivity ϵ, electrical conductivity σ and a normalized layer thickness kh on a substrate with an effective permittivity ϵ_{sub} can be derived from the quasi-static approximation for the potential ϕ and the Maxwell equations

$$\underline{E} = -\nabla\phi \tag{3.25}$$

$$\underline{D} = \epsilon\underline{E} \tag{3.26}$$

$$\nabla \cdot \underline{D} = -qn_1 = \rho \tag{3.27}$$

with n_1 the perturbation from the equilibrium electron density, ρ the space charge and $-q$ the charge of an electron. The electric current densities J_1 and J_3 (including diffusion effects and the presence of drifting electrons) are given by

$$J_1 = \sigma E_1 - qn_1 v_d + qD_n \frac{\partial n_1}{\partial x_1} \tag{3.28}$$

$$J_3 = \sigma E_3 + qD_n \frac{\partial n_1}{\partial x_3} \tag{3.29}$$

$$\nabla \cdot J = q\frac{\partial n_1}{\partial t} \tag{3.30}$$

This last equation is the continuity equation. D_n is the electron diffusion constant and v_d is the electron drift velocity. E_1 and E_3 are the electric fields generated by the piezoelectric material. The drift velocity v_d is caused by an externally applied DC electric field. Using plane wave solutions of the form

$$e^{jkbx_3} e^{jk(x_1 - v_{ph}t)} \tag{3.31}$$

the following relation is obtained

$$(1+b^2)\left(j\omega(1-\frac{v_d}{v_{ph}})-\frac{\sigma}{\epsilon}-D_n k^2(1+b^2)\right)=0 \qquad (3.32)$$

Eq. 3.32 has four solutions for b

$$b=\pm j \quad or \quad b=\pm a \qquad (3.33)$$

with

$$a=j\frac{\omega_m}{\omega}\sqrt{-j\frac{\delta\omega}{\omega_c}+\left(\frac{\omega}{\omega_m}\right)^2+1} \qquad (3.34)$$

where

ω_c	=	σ/ϵ	the dielectric relaxation frequency
ω_D	=	v_{ph}^2/D_n	the diffusion frequency
ω_m	=	$\sqrt{\omega_c\omega_D}$	
δ	=	$1-(v_d/v_{ph})$	the normalized electron drift velocity

The solutions $b=\pm j$ correspond to the solution of Laplace's equation and don't carry space charge. Therefore, these solutions for b do not contribute to the amplification. The solutions $b=\pm a$ are associated with space charge. In order to obtain a decay of the mechanical displacements and electric potential for increasing positive x_3 values, only positive values of the imaginary part of b can be accepted. Thus only two solutions for b are left.

The boundary conditions require $J_3=0$ at $x_3=0$ and $x_3=kh$ and $D_3/k\phi=\epsilon_{sub}$ at $x_3=kh$. The problem is thus restricted to structures with insulators adjoining the semiconducting layer. The effective permittivity of a semiconducting layer is then given by [112]

$$\epsilon_{eff}=\frac{D_3}{k\phi}=ja\epsilon\left(1-j\frac{\delta\omega}{\omega_c}\right)\frac{T}{N} \qquad (3.35)$$

where

$$\begin{aligned}T &= ja\left(1-j\frac{\delta\omega}{\omega_c}\right)\tanh(kh)\tanh(jakh)+\\ &+a\frac{\epsilon_{sub}}{\epsilon}\frac{\delta\omega}{\omega_c}\tanh(jakh)+\frac{\epsilon_{sub}}{\epsilon}\tanh(kh)\end{aligned}$$

$$\begin{aligned}N &= ja\left(1-j\frac{\delta\omega}{\omega_c}\right)\left(\tanh(kh)+a\frac{\delta\omega}{\omega_c}\tanh(jakh)\right)+\\ &+\frac{\epsilon_{sub}}{\epsilon}\left(1+a^2\frac{\delta^2\omega^2}{\omega_c^2}\right)\tanh(kh)\tanh(jakh)+\\ &+2a\frac{\epsilon_{sub}}{\epsilon}\frac{\delta\omega}{\omega_c}\left(1-\frac{1}{\cosh(kh)\cosh(jakh)}\right)\end{aligned}$$

For $kh\to\infty$ Eq. 3.35 reduces to

$$\epsilon_{eff}=\epsilon\left(\frac{1+j\omega_c/\delta\omega}{1-\omega_c/a\delta\omega}\right) \qquad (3.36)$$

The diffusion of the charge bunches by the thermal motion of the charge carriers can be neglected when the Debye screening length is much smaller than the surface acoustic wavelength. The Debye screening length λ_D is given by

$$\lambda_D=\sqrt{\frac{D}{\omega_c}} \qquad (3.37)$$

Thus the diffusion free limit ($\omega/\omega_m\to 0$, $k\lambda_D\ll 1$) of Eq. 3.36 is

$$\epsilon_{eff}=\epsilon\left(1+j\frac{\omega_c}{\delta\omega}\right) \qquad (3.38)$$

Eq. 3.36 reduces in the case of $\delta=0$ ($v_d=v_{ph}$) to

$$\epsilon_{eff}=\epsilon\sqrt{1+\frac{\omega_c\omega_D}{\omega^2}} \qquad (3.39)$$

The diffusion effects cause a finite value for the effective permittivity. For $\sigma\to 0$ Eq. 3.34 reduces to $a=j$ and Eq. 3.35 reduces to

$$\epsilon_{eff}=\epsilon\left(\frac{\epsilon\tanh(kh)+\epsilon_{sub}}{\epsilon+\epsilon_{sub}\tanh(kh)}\right) \qquad (3.40)$$

The effective permittivity of the ZnO-SiO$_2$-Si layered structure, as shown in Fig. 3.1 can be calculated by repeatedly using Eq. 3.35 or one of the four Eqs. 3.36, 3.38–3.40. The silicon substrate has an effective permittivity defined by Eq. 3.36. The depletion layer can be taken into account by using Eq. 3.40. For the epitaxial layer the complete Eq. 3.35 must be taken and with Eq. 3.40 the SiO$_2$ layer is brought into the effective permittivity of the lower half-space. In this way the effective permittivity of every nonpiezoelectric half-space can be evaluated. The only, already mentioned, restriction is that two semiconducting layers must be separated by a dielectric one.

3.5.4 Effective permittivity of the Upper Half-Space

In this subsection expressions for the effective permittivity of a half-space containing one piezoelectric layer are derived. A generalization of Ingebrigtsen's approximation for the effective permittivity of a ZnO layer (with a c-axis normal orientation) is in analogy with Eqs. 3.24 and 3.40

$$\epsilon_{eff} = \epsilon \left(\frac{\epsilon \tanh(bkh) + \epsilon_{vac}}{\epsilon + \epsilon_{vac} \tanh(bkh)} \right) \left(\frac{v_{ph} - v_{open,1}}{v_{ph} - v_m} \right) \tag{3.41}$$

where

$$\begin{aligned} \epsilon &= \sqrt{\epsilon_{11}\epsilon_{33}} \\ b &= \sqrt{\epsilon_{11}/\epsilon_{33}} \\ kh &= \text{the normalized piezoelectric layer thickness} \\ \epsilon_{vac} &= \text{the permittivity of vacuum} \end{aligned}$$

When the ZnO layer is not piezoelectric $v_{open,1} = v_m$ and Eq. 3.41 reduces to the effective permittivity of a nonisotropic dielectric layer. The phase velocities $v_{open,1}$ and v_m can exactly be calculated with the numerical programs used in Chapter 2.

To obtain a higher accuracy the effective permittivity of a ZnO layer as a function of the phase velocity is examined by using Fig. 3.2. For simplicity a ZnO-SiO$_2$-Si layered structure with a thick epitaxial layer is assumed. Rayleigh wave propagation is only possible when the real part of the effective permittivity is negative. When a particular Rayleigh-wave mode is considered, variation of the electrical parameters of the adjoining half-spaces result in phase velocities

$$v_m < v_{ph} < v_{open,1} \tag{3.42}$$

All mechanical material constants and layer thicknesses are kept constant. As soon as the dielectric permittivities are chosen the phase velocity can, dependent on the conductivities, vary according to

$$v_m < v_{ph} < v_0 \tag{3.43}$$

When only the silicon conductivity is varied, the possible phase velocities are

$$v_\infty < v_{ph} < v_0 \tag{3.44}$$

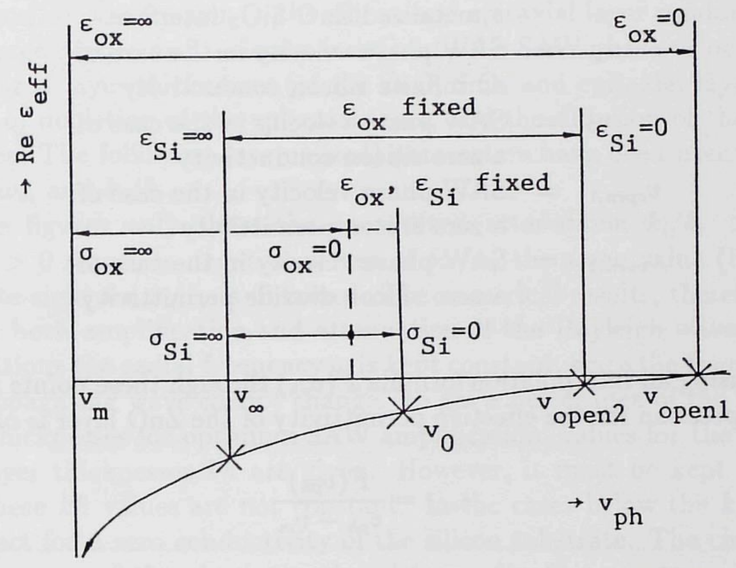

Figure 3.2: *Real part of the effective permittivity of a ZnO layer half-space as a function of the phase velocity. The influence of the electrical parameters of the adjoining half-space is shown. The subscript "ox" is an abbreviation for SiO_2.*

with the corresponding wave numbers

$$k_\infty = \frac{\omega}{v_\infty} \tag{3.45}$$

$$k_0 = \frac{\omega}{v_0} \tag{3.46}$$

The parameter ω can be chosen arbitrarily, but is kept constant during variation of the electrical parameters. In this way the effective permittivity (for lossless SAW propagation) can be calculated for five different phase velocities

v_m = SAW phase velocity in the case of a metalized ZnO-SiO_2 interface

v_∞ = SAW phase velocity in the case of an infinite silicon conductivity

v_0 = SAW phase velocity in the case of a zero silicon conductivity

$v_{open,1}$ = SAW phase velocity in the case of a zero silicon permittivity

$v_{open,2}$ = SAW phase velocity in the case of a zero silicon dioxide permittivity

By using an interpolation formula $F(v_{ph})$ through these points an analytic expression for the effective permittivity of the ZnO layer is obtained

$$\epsilon_{eff} = \frac{F(v_{ph})}{v_{ph} - v_m} \tag{3.47}$$

In the case of a second-order Lagrange interpolation polynomial through v_∞, v_0 and $v_{open,1}$

$$F(v_{ph}) = \frac{(v_m - v_\infty)\epsilon_{SiO_2}}{\tanh(kh_{SiO_2})} \tag{3.48}$$

$$F(v_0) = (v_m - v_0)\epsilon_{SiO_2}\left(\frac{\epsilon_{SiO_2}\tanh(kh_{SiO_2}) + \epsilon_{Si}}{\epsilon_{SiO_2} + \epsilon_{Si}\tanh(kh_{SiO_2})}\right) \tag{3.49}$$

$$F(v_{open,1}) = 0 \tag{3.50}$$

The accuracy of the effective permittivity in Eq. 3.47 can be obtained with a minimum of numerical calculations and is more accurate than Eq. 3.41. Further improvement can be obtained if $v_{open,2}$ is also used in the interpolation formula for $F(v_{ph})$.

3.6 NUMERICAL RESULTS

In the numerical calculations for the ZnO-SiO_2-Si layered structure a monocrystalline approximation for the layers is used. The corresponding material constants are listed in Chapter 2. Calculations have been carried out for Si(100)[001], but the perturbational method is applicable to other silicon crystal cuts and directions of Rayleigh-wave propagation as well. The amplification/attenuation and velocity of the Rayleigh-wave

modes in the ZnO-SiO_2-Si layered structure depend on a number of parameters, i.e. the frequency, the silicon and epitaxial layer conductivities, the charge carrier drift velocity (relative to the SAW phase velocity), the normalized layer thicknesses (of the ZnO, SiO_2 and epitaxial layers), the extent of depletion of the epitaxial layer, and the diffusion of the charge bunches. The following (normalized) parameters have been used: $\delta\omega/\omega_c$, kh, ω/ω_m and k_i/k_r.

The figures only show the normalized attenuation $k_i/k_r > 0$ for $\delta\omega/\omega_c > 0$ since for negative values of $\delta\omega/\omega_c$ the same value (but with opposite sign) for k_i/k_r is obtained. The numerical results, therefore, apply for both amplification and attenuation of the Rayleigh waves. In all calculations the radial frequency ω is kept constant, since the frequency of the propagating wave cannot change. To get a better idea of the required layer thicknesses for optimum SAW amplification, values for the normalized layer thicknesses kh are given. However, it must be kept in mind that these kh values are not constant. In the cases below the kh values are exact for a zero conductivity of the silicon substrate. The changes in kh when one of the above-mentioned (normalized) parameters is varied are small (Eqs. 3.20–3.23).

In Figs. 3.3–3.8 a thick (with respect to the acoustic wavelength) epitaxial layer is assumed, thus $kh_{epi} \to \infty$ and Eq. 3.36 together with Eq. 3.40 are used. The normalized thickness kh_{epi} is defined in Fig. 3.1. Figs. 3.9 and 3.10 show the SAW amplification in the case of a finite epitaxial layer thickness and the influence of its depletion on the amplification.

The influence of the normalized ZnO and SiO_2 layer thicknesses on the amplification/attenuation of the fundamental Rayleigh-wave mode are shown in Figs. 3.3 and 3.4, respectively. The diffusion is neglected ($\omega/\omega_m \to 0$). The amplification is proportional to the piezoelectric coupling coefficient κ^2, as expected (Section 3.3). The maximum amplification is obtained for $\delta\omega/\omega_c \approx 0.6$.

In Figs. 3.5 and 3.7 the phase velocities of the fundamental Rayleigh-wave mode and the second Rayleigh-wave mode are shown as a function of $\delta\omega/\omega_c$ with ω/ω_m as parameter. The phase velocities vary between v_0 and v_∞. To obtain $\delta\omega/\omega_c = 0$ either $\sigma = \infty$ (which results in $\omega/\omega_m = 0$) or $\delta = 0$. In the latter case the effective permittivity does not become infinite as a result of the diffusion and the phase velocity is not equal to v_∞. Figures 3.6 and 3.8 show the corresponding normalized amplification. It is clear that the diffusion effects can only be neglected when $\omega/\omega_m \ll 1$.

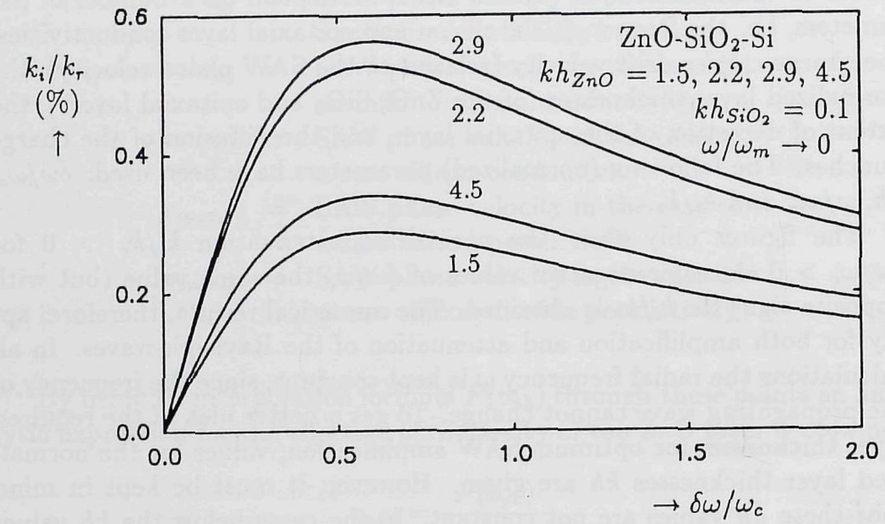

Figure 3.3: *Normalized amplification of the fundamental Rayleigh-wave mode as a function of $\delta\omega/\omega_c$. The values for ωh_{ZnO} are 5012, 6763, 8484, 12510 rad m/s.*

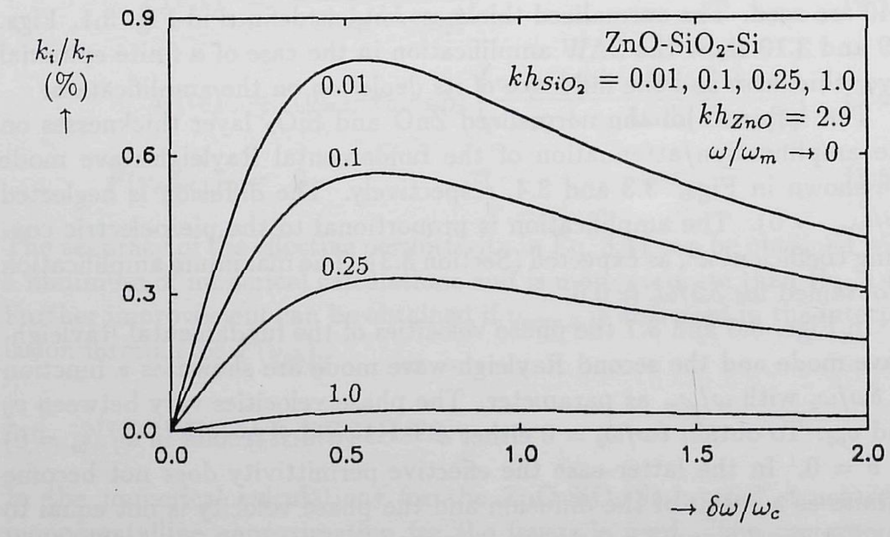

Figure 3.4: *Normalized amplification of the fundamental Rayleigh-wave mode as a function of $\delta\omega/\omega_c$. The values for ωh_{SiO_2} are 29.50, 292.5, 722.3, 2780 rad m/s.*

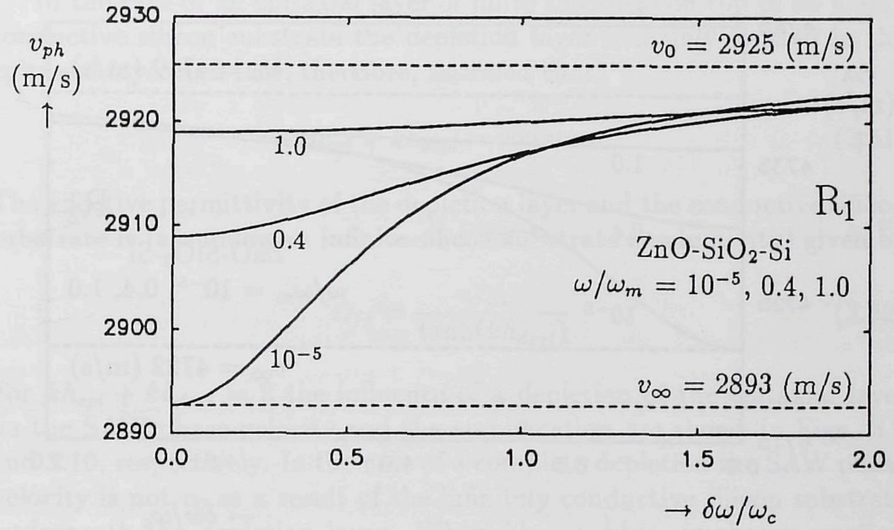

Figure 3.5: *Phase velocity of the fundamental Rayleigh-wave mode for ωh_{ZnO} = 8484 rad m/s as a function of $\delta\omega/\omega_c$. The normalized layer thicknesses for $\sigma_{Si} = 0$ are $kh_{ZnO} = 2.9$ and $kh_{SiO_2} = 0.1$.*

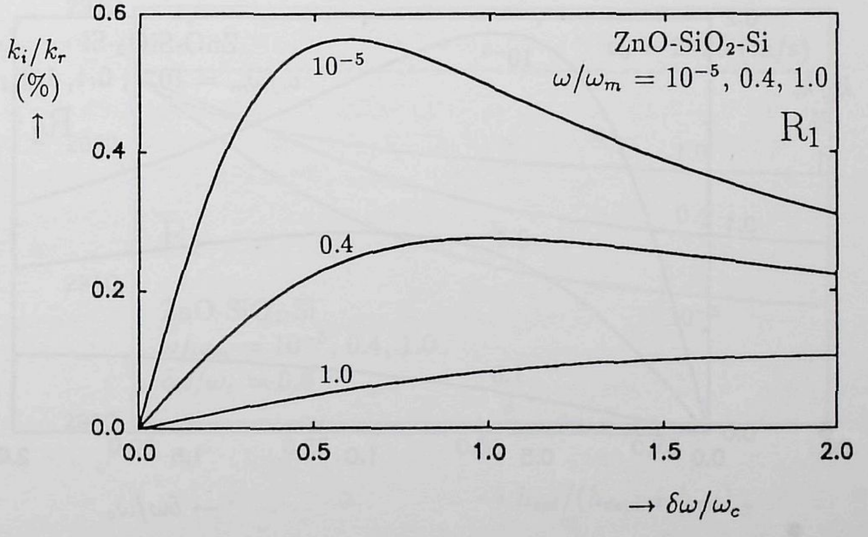

Figure 3.6: *Normalized amplification of the fundamental Rayleigh-wave mode for ωh_{ZnO} = 8484 rad m/s as a function of $\delta\omega/\omega_c$. The normalized layer thicknesses for $\sigma_{Si} = 0$ are $kh_{ZnO} = 2.9$ and $kh_{SiO_2} = 0.1$.*

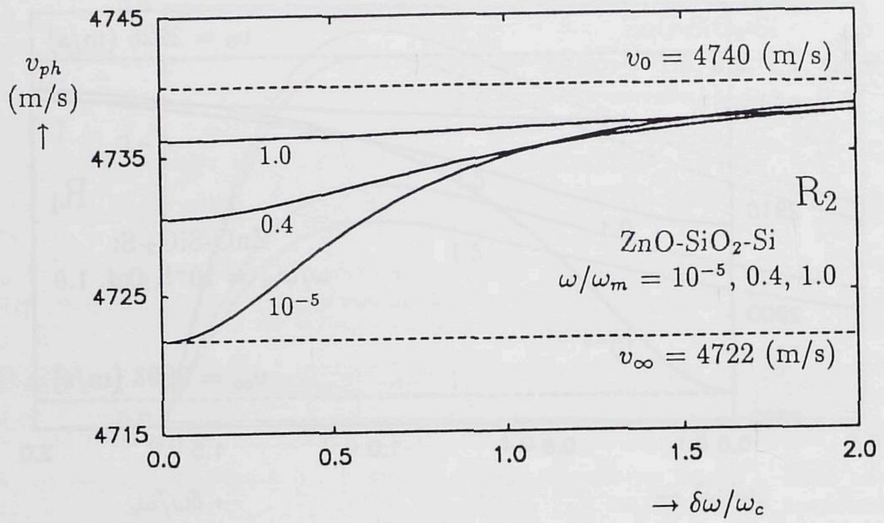

Figure 3.7: *Phase velocity of the second Rayleigh-wave mode for* $\omega h_{ZnO} = 13746$ *rad m/s as a function of* $\delta\omega/\omega_c$. *The normalized layer thicknesses for* $\sigma_{Si} = 0$ *are* $kh_{ZnO} = 2.9$ *and* $kh_{SiO_2} = 0.1$.

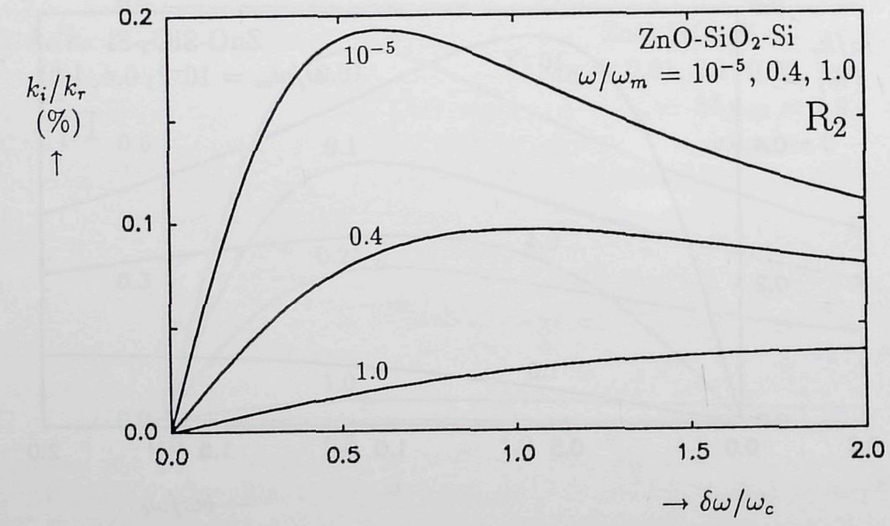

Figure 3.8: *Normalized amplification of the second Rayleigh-wave mode for* $\omega h_{ZnO} = 13746$ *rad m/s as a function of* $\delta\omega/\omega_c$. *The normalized layer thicknesses for* $\sigma_{Si} = 0$ *are* $kh_{ZnO} = 2.9$ *and* $kh_{SiO_2} = 0.1$.

In the case of an epitaxial layer of finite thickness on top of an highly conductive silicon substrate the depletion layer is mainly located in the epitaxial layer and it is, therefore, assumed that

$$kh_{epi} + kh_{depl} = constant \tag{3.51}$$

The effective permittivity of the depletion layer and the conductive silicon substrate is (assuming an infinite silicon substrate conductivity) given by

$$\epsilon_{eff} = \frac{\epsilon_{Si}}{\tanh(kh_{depl})} \tag{3.52}$$

For $kh_{epi} + kh_{depl} = 2$ the influence of a depletion of the epitaxial layer on the SAW phase velocity and the amplification are shown in Figs. 3.9 and 3.10, respectively. In the case of a complete depletion the SAW phase velocity is not v_0 as a result of the infinitely conductive silicon substrate underneath the depletion layer. When $kh_{epi} + kh_{depl}$ is chosen smaller, the influence of the substrate increases. For $kh_{epi}/(kh_{epi} + kh_{depl}) = 1$ the velocity and amplification approach the values given in Figs. 3.5 and 3.6, respectively (for $\delta\omega/\omega_c = 0.6$).

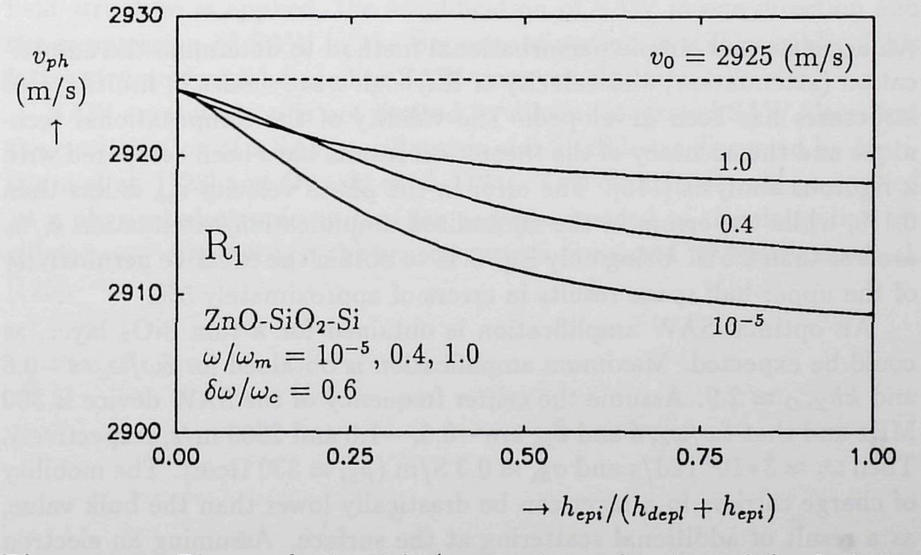

Figure 3.9: *Phase velocity at* $\delta\omega/\omega_c = 0.6$ *as a function of the depletion of the epitaxial layer. Layer thicknesses are* $kh_{epi} + kh_{depl} = 2.0$, $kh_{ZnO} = 2.9$ *and* $kh_{SiO_2} = 0.1$ *(for* $\sigma_{Si} = 0$*).*

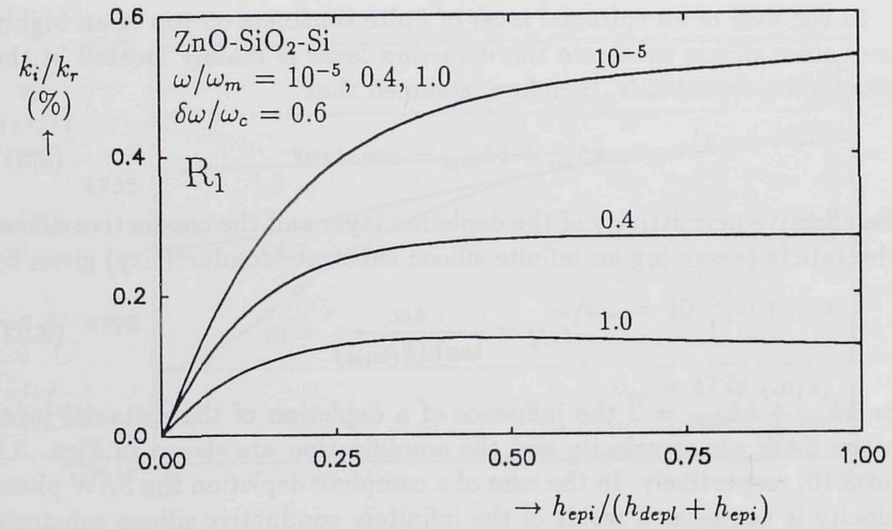

Figure 3.10: *Normalized amplification at $\delta\omega/\omega_c = 0.6$ as a function of the depletion of the epitaxial layer. Layer thicknesses are $kh_{epi} + kh_{depl} = 2.0$, $kh_{ZnO} = 2.9$ and $kh_{SiO_2} = 0.1$ (for $\sigma_{Si} = 0$).*

3.7 DISCUSSION AND CONCLUSIONS

An accurate and simple perturbational method to determine the amplification (attenuation) and velocity of Rayleigh wave modes in multilayered structures has been developed. The validity of the computational technique and the accuracy of the theoretical results have been compared with a rigorous analysis [116]. The error in the phase velocity v_{ph} is less than 0.1%, while the errors in the normalized amplification/attenuation k_i/k_r are less than 0.5%. Using only Eq. 3.41 to obtain the effective permittivity of the upper-half space results in errors of approximately 5%.

An optimal SAW amplification is obtained for a thin SiO_2 layer, as could be expected. Maximum amplification is obtained for $\delta\omega/\omega_c \approx -0.6$ and $kh_{ZnO} \approx 2.9$. Assume the center frequency of the SAW device is 300 MHz and that $\delta\omega/\omega_c$, δ and v_{ph} are -0.6, -1.0 and 2900 m/s, respectively. Then $\omega_c \approx 3{*}10^9$ rad/s and $\sigma_{Si} \approx 0.3$ S/m ($\rho_{Si} \approx 330$ Ωcm). The mobility of charge carriers in a layer can be drastically lower than the bulk value, as a result of additional scattering at the surface. Assuming an electron mobility $\mu_n \approx 750$ cm^2/Vs [118], the diffusion coefficient $D_n \approx 20$ cm^2/s, where

$$D_n = \left(\frac{k_B T}{q}\right)\mu_n = 26 * 10^{-3}\mu_n \qquad (\mathrm{T} = 300\mathrm{K}) \qquad (3.53)$$

with k_B the Boltzmann constant, T the absolute temperature and q the charge of an electron. Hence $\omega_m = 3.6{*}10^9$ rad/s and $\omega/\omega_m \approx 0.5$. In that case a normalized amplification of 0.002 is feasible as shown in Fig. 3.6. This results in an amplification of about 10 dB/mm. With smaller SiO_2 layer thicknesses an even higher amplification is possible. The required DC electric field E_{DC} can be calculated from

$$v_d = \mu_n E_{DC} \qquad (3.54)$$

and is in the case of $\delta = -1.0$ approximately 75 V/mm. The dissipation is approximately 3 mW/mm in the case of an acoustic beamwidth of 1 mm and a normalized epitaxial layer thickness $kh_{epi} = 1$. This layer thickness does not reduce the amplification as shown in Fig. 3.8.

Using the segmented-drift-field structure as introduced by Turner et al. [119], the applied voltages can be reduced. The applied DC electric field produced by the surface drift electrodes can no longer be considered uniform. As a result the amplification is reduced as calculated and experimentally verified by Hsu and White [120]. A symmetric segmented-drift-field structure can be used to obtain a bidirectional amplification, as shown by Solie [121], [122]. This can be used to amplify the surface acoustic waves in SAW resonator filters. When an asymmetric segmented-drift-field structure is applied, the amplification of SAW in one direction and the suppression of SAW in the opposite direction is still possible. This latter structure can be used in SAW transversal filters.

SAW amplification is not limited to silicon-integrated SAW filters but the construction of a SAW oscillator is also feasible, as discussed by Morizumi et al. [123] and Owashi et al. [124]. This oscillator could be applied as a physical-electronic system for sensors, instead of the delay-line oscillator now employed in the sensor system presented by Vellekoop et al. [125].

Chapter 4

TECHNOLOGY

4.1 INTRODUCTION

In this chapter the fabrication technology for SAW filters in ZnO-SiO_2-Si (and other, related) layered structures is discussed. Since SAW filters on silicon substrates are of particular interest in the case of a monolithic integration with electronic circuitry, the fabrication process to obtain SAW filters must be compatible with IC processing. Such an integration of SAW filters with electronic circuitry in one silicon substrate has been realized.

In Section 4.2 the high-resolution etch technology required to obtain an accurate and reproducible aluminum electrode width and shape, is the subject of investigation. This high-resolution technology is necessary, because of the relatively low phase velocity of Rayleigh waves in the ZnO-SiO_2-Si layered structure and because of the strong tendency to use SAW filters with higher center frequencies (up to 1 GHz) in electronic systems. The high-resolution technology is based on electron-beam (e-beam) lithog-

raphy, dry etching of the bilayer mask system in a low pressure O_2-plasma and patterning of the aluminum layer in a $SiCl_4$-plasma.

The monolithic integration of SAW devices with electronic circuitry in the modified Delft BIFET process is discussed in Section 4.3. The on-chip aluminum interconnect between SAW device and electronic circuitry has been realized. In these monolithic devices, both wet etching and the (above-introduced) high-resolution etch technology have been used to obtain the aluminum interdigital pattern.

Section 4.4 deals with the technology to fabricate piezoelectric ZnO layers by DC magnetron sputtering. The problem of packaging and bonding of the SAW devices is discussed in Section 4.5. This chapter on fabrication ends with a discussion and conclusions in Section 4.6. Most photographs in this chapter are Scanning Electron Micrographs (SEM), obtained with a Jeol JSM-840. To improve the quality of the photos the devices have been coated with a 2–3 nm (sputtered) Au layer.

4.2 INTERDIGITAL PATTERN FABRICATION

In this section the interdigital pattern fabrication in different layered structures is discussed. An extensive review on SAW device fabrication on monocrystalline substrates has been given by Smith [126]. The ohmic losses in the interdigital pattern must be small enough to prevent a deterioration of the SAW filter performance as has been shown by Männer et al. [127]. The influence of electrode width and shape on SAW filter performance has been investigated by Asakawa et al. [128], Engan [129], and Veith [130], however, further research especially for high-frequency and silicon-integrated SAW filters is necessary and can be carried out with the technology described in this section.

Especially the transfer function of SAW resonator filters depends strongly on the width and shape of the electrodes, as found by Takahashi et al. [131] and Veith. The width and shape of the electrodes in the reflector arrays of SAW resonator filters influence the center frequency of the transfer function. This is caused by mass loading, short circuiting of the piezoelectric fields and by the energy storage in the electrode walls. To give an example, Veith reports on a ± 15 ppm shift in the 461 MHz center frequency of quartz resonators when the electrode width varies with a standard deviation of ± 30 nm (and an aluminum layer thickness variation of ± 0.4 nm).

The use of submicron technology can be circumvented when the SAW device is operated at a higher-harmonic frequency. Campbell [132] has reported on the efficient operation up to at least the eleventh harmonic (on monocrystalline substrates). Especially the use of the stepped-finger interdigital transducer enables the suppression of all but the desired harmonic. Up to now, only GHz harmonic SAW delay lines have been realized.

4.2.1 Inventory of Fabrication Techniques

Six different structures to obtain an interdigital pattern are discussed. Experimental results are given when these structures have been experimentally realized. The six structures are shown in Fig. 4.1 and are fabricated by implantation, anodic oxidation, wet (chemical) etching, lift-off technology or dry etching. The IDTs consist of a metal interdigital pattern, except for the junction IDT. Aluminum is the favored metal, because of its good conductivity, good acoustic impedance matching with the substrate and its compatibility with IC processing. Gold is incompatible with a monolithic integration of the SAW device with electronic circuitry. Not shown in Fig. 4.1 are the possible deposition of a metal layer on top of the ZnO layer (as discussed in Chapter 2) and the possible deposition of a thin silicon nitride layer (as discussed in Section 4.4).

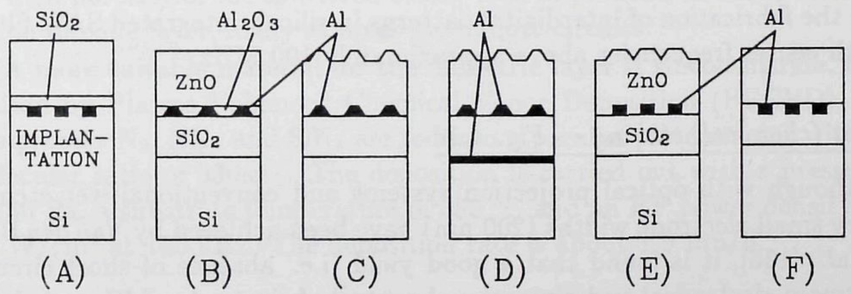

Figure 4.1: *Six different interdigital patterns: a) implantation (junction IDT); b) anodic oxidation; c) wet etching or lift-off; d) structure with an additional metal layer on the silicon substrate; e) dry etching and f) dry etching with the IDT incorporated in the SiO_2 layer (buried IDT).*

Implantation (junction IDT) — Fig. 4.1a

An interdigital pattern for surface acoustic wave generation and detection can be obtained with the junction interdigital transducer. In a junction IDT a highly doped inlay in the silicon substrate (or epitaxial layer) form

the electrodes as realized by Borden et al. [133] and Venema et al. [134]. A flat surface is thus obtained which results in a minimum of mechanical reflections of the acoustic waves. This flat substrate surface forms a good starting point for the piezoelectric film deposition. Passivation of the silicon surface by thermal oxidation is crucial to prevent short circuits by surface states. Successful operation of SAW junction interdigital transducers has been reported by Borden et al. [133], but the (present) losses in these devices are too high for practical application in SAW filters at this moment.

Anodic oxidation — Fig. 4.1b

By using anodic oxidation, as described by Schwartz et al. [135], the aluminum is converted to an insulating film of aluminum oxide. The process is carried out in a oxalic acid solution and the required voltages are compatible for semiconductor device fabrication. An additional metal layer is required at the SiO_2-Al interface to enable the anodic oxidation. The most suitable underlay is found to be a thin layer of hafnium which is thermally oxidized after completion of the anodic oxidation. Anodic oxidation is attractive for its inherent planarization. Electrode widths down to 2–3 μm can be obtained. This technology is, therefore, not suited for the fabrication of interdigital patterns in silicon-integrated SAW filters with center frequencies above approximately 100 MHz.

Wet (chemical) etching — Fig. 4.1c

Although with optical projection systems and conventional wet etching very small electrode widths (200 nm) have been achieved by Van den Berg et al. [136], it is found that a good yield (i.e. absence of short circuits between electrodes) and dimensional control of electrode width and shape are only guaranteed in the case of electrodes wider than several micrometer (which result in an operating frequency of the SAW device below 100 MHz).

Lift-off technology — Fig. 4.1c

To fabricate high-frequency SAW devices, e-beam lithography and lift-off techniques are commonly used and described in detail by Pendergrass and Studebaker [137], and by Yamanouchi et al. [138]. However, lift-off technology depends critically on the resist development, it cannot produce electrodes with high aspect ratios and the requirement of normal incidence

deposition limits the accuracy in the case of full wafer deposition or of fabrication of long SAW devices. The main advantage (compared with dry etching) is that the substrate surface is not damaged during processing.

Additional metal layer on the silicon substrate — Fig. 4.1d

To increase the suppression of the electromagnetic feedthrough an additional metal layer on top of the silicon substrate is required. Experimental results of this structure are discussed in more detail in Chapter 5, here only the technological aspects are discussed. After the metal layer is deposited (by evaporation) on the silicon substrate, it is not possible to grow a SiO_2 layer thermally. A low temperature IC compatible deposition of a dielectric layer is required. Devices with a sputter deposited SiO_2 layer and with a plasma deposited silicon nitride layer have been realized.

The sputtered SiO_2 layers are fabricated with a magnetron sputter unit (Alcatel SCM600), with a SiO_2 target using Ar and 10% O_2. The substrate holder is water-cooled. The sputter rate is about 2.5 μm/h. To prevent the oxidation or melting of the aluminum layer annealing of the sputtered SiO_2 layer is not possible. The etch rate of the sputtered oxide is much larger than that of the thermally grown oxide, probably due to the high porosity of the sputtered oxide. Due to pinholes in the sputtered silicon dioxide layer, many samples have short-circuits.

A more suitable material for the dielectric layer is silicon nitride, deposited by Plasma-Enhanced Chemical Vapor Deposition (PECVD). In this process N_2, NH_3 and SiH_4 are fed into a parallel plate reactor with a molecular ratio of 330:3:1. The deposition is carried out with a pressure of 130 Pa, a substrate temperature of 350 °C and an RF power density of 0.1 W/cm^2 at 100 kHz. The deposition rate is about 1.5 μm/h.

Dry (plasma) etching — Fig. 4.1e

To fabricate silicon-integrated SAW filters at frequencies from 100 MHz to above 1 GHz and to do research on the influence of electrode width and shape on SAW filter performance, a high-resolution technology to etch aluminum electrode patterns (down to a 200 nm electrode width) has been developed. To obtain the desired dimensional control, e-beam lithography and the highly anisotropic reactive ion etching are used. This plasma etching requires a bilayer mask system to compensate for the low selectivity. In the next subsection the fabrication process is discussed in full detail.

Dry etching with buried IDT — Fig. 4.1f

A planarization can be obtained when the interdigital pattern is incorporated in the SiO_2 layer. The structure is especially attractive for thick (relative to the ZnO layer thickness) and narrow electrodes. The realization of this layered structure is the subject of current research.

4.2.2 High-Resolution Aluminum Etch Technology

All devices are fabricated on standard 2 inch p-type (100) silicon wafers (2–5 Ωcm), as used in the Delft high-frequency BIFET process. The SiO_2 layer is obtained by thermal oxidation. In order to obtain a high resolution in the fabrication of the electrode structures, a bilayer resist system is used, as depicted in Fig. 4.2. For electrode widths down to 0.5 μm, it consists

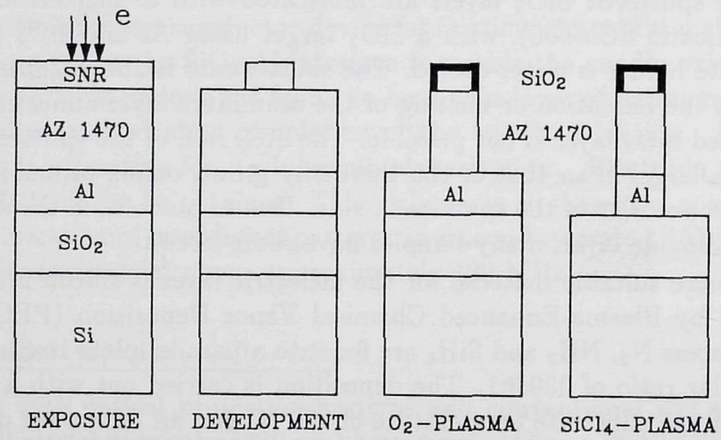

Figure 4.2: *Processing scheme of the high-resolution technology, using e-beam lithography, bilayer masking and plasma etching.*

of a 1 μm thick bottom layer of hard-baked (200 °C, 1 h) photoresist AZ 1470 (Shipley) and a 50 nm thick Silicon-based Negative e-beam Resist – SNR – (Toyo Soda) on top. For an electrode width below 0.5 μm a thinner AZ layer is to be preferred for reasons of mechanical stability. SNR as an e-beam resist has been introduced by Kakuchi et al. [139].

Direct-write electron beam exposure is carried out with a Philips EBPG/03 operating at 50 kV. The nominal electron beam diameter is chosen to be 50 nm and 200 nm for electrode widths of 0.2 μm and 1.0 μm, respectively. The SAW device covers several scan fields of the EBPG. The stitching error between adjacent scan fields is about 30 nm. The

required dose depends somewhat on the periodicity in the electrode structure and is about 60 $\mu C/cm^2$. After development in xylene (10 s) and a rinse in isopropyl alcohol (30 s) the sample is dried.

The subsequent etching step of the bilayer mask in a low pressure (0.5 Pa) O_2-plasma is described in detail by Van der Drift et al. [140]. A parallel-plate plasma reactor (Leybold-Heraeus Z401) is used which operates at 13.56 MHz in the Reactive Ion Etch (RIE) mode, i.e. with the sample on the driven quartz electrode. A surface layer (a few tens of nm) of the SNR is converted into SiO_2 which is an excellent mask for the AZ resist layer (etched in this same process step). The aspect ratio obtained in this mask process is in the order of 50 to 100, yielding a lateral resolution of about 10 nm. A 0.3 μm width electrode pattern in resist is shown in Fig. 4.3.

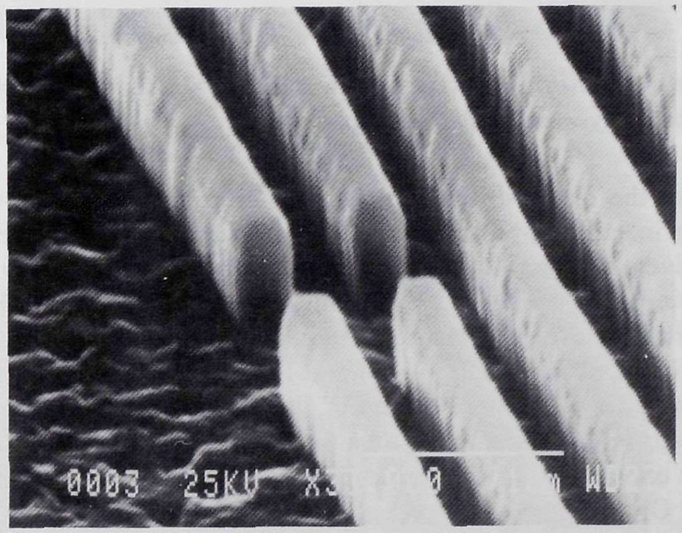

Figure 4.3: *Electrode (width 0.3 μm) pattern in the bilayer mask.*

An earlier approach had a multilayer masking which consisted of a 1 μm layer of AZ resist, a 15 nm Ge layer and a 200 nm PMMA layer. This is a more complicated masking system and requires a longer e-beam writing since PMMA is not a negative e-beam resist. The PMMA and AZ resist layers are etched in a O_2 plasma, while Ge is etched in a SF_6 plasma. This fabrication technology has been used by Van der Drift et al. [140]. Because of the above-mentioned reasons this multilayer system has been used only at the start of this project.

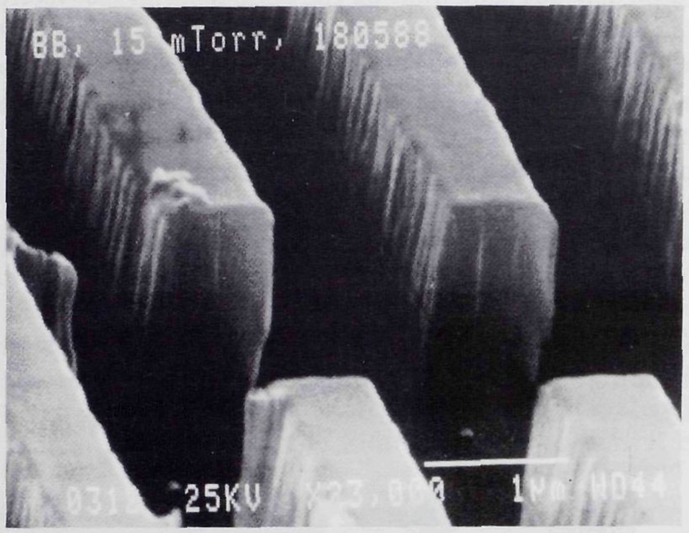

Figure 4.4: *Electrode structure (width 1 μm) after the $SiCl_4$ plasma etch with the bilayer resist still on top.*

Next the electrode pattern is transferred to the aluminum layer by etching in a $SiCl_4$-plasma. Details on aluminum plasma etching have been given by Hess [141] and Purdes [142]. The anisotropy is not only determined by the gas pressure, but also depends on the passivation of the vertical surfaces of the etched structure, as has been examined by Allred et al. [143]. Figure 4.4 shows the result for an electrode width of 1 μm with the resist still on top of the aluminum. The Cl-based plasma processing was carried out in a Leybold-Heraeus Z401 S reactor (load lock version of the Z401), with the substrate on an electrode of either SiO_2 of Al_2O_3. Optimum anisotropy and an acceptable selectivity with respect to the mask (3.6) and to the SiO_2 underlayer (7.2) are obtained at a power density of 0.25 W/cm^2, a gas pressure of 1.3 Pa and a gas flow of 28 sccm. The aluminum etch rate is 42 $\pm$1 nm/min. Below a power level of about 0.2 W/cm^2 the etch rate is negligible due to the etch resistance of the native aluminum oxide layer. Throughout, the electrode temperature is kept at 64 °C. After the plasma etch residual chlorine is removed in a rinse of H_2O and the mask is removed in 100% HNO_3. The results for 1 μm electrodes are shown in Figs. 4.5 and 4.6. Figure 4.7 shows the obtained result for 0.2 μm electrode widths.

Figure 4.5: *Aluminum electrode structure (1 μm electrode width).*

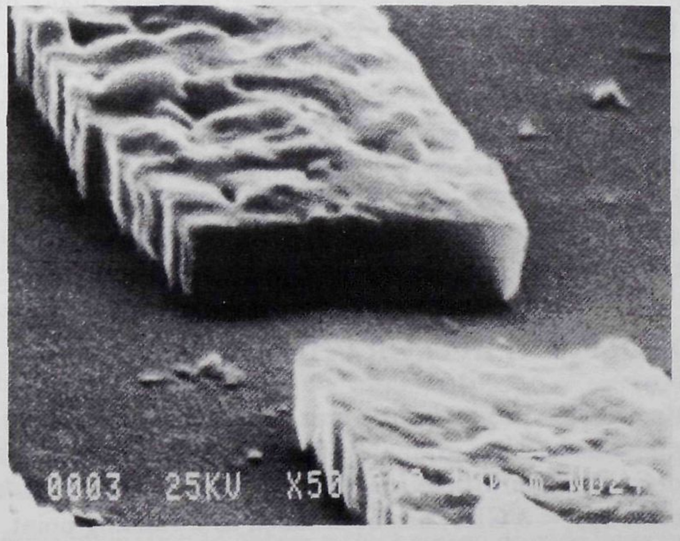

Figure 4.6: *Detail of Fig. 4.5, electrode width 1 μm.*

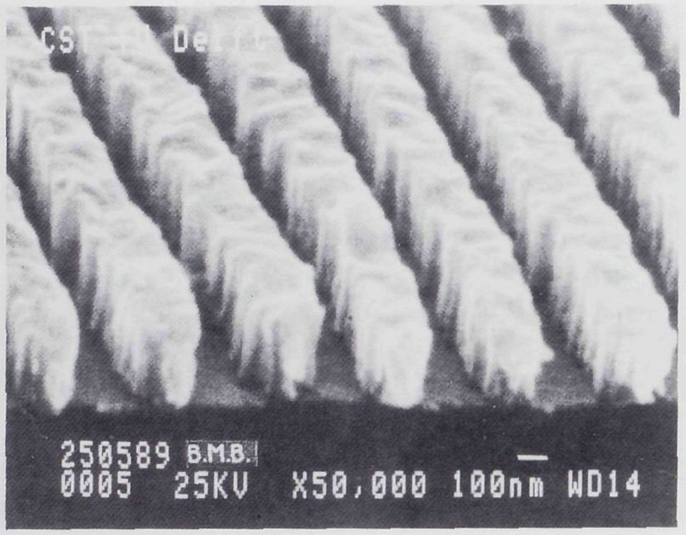

Figure 4.7: *Aluminum electrode structure (0.2 μm electrode width).*

The aluminum electrode structures have been searched for chlorine because it is known that aluminum patterns obtained in a chlorine containing plasma can easily and very fast corrode. However, no chlorine has been detected by Auger electron spectroscopy and after many months no corrosion of the aluminum pattern could be detected.

Instead of a single layer metalization, an aluminum layer on top of a thin underlay of chromium (used for better adhesion to the substrate) can be used. Chromium is etched in a plasma of Cl_2/O_2 (1:1). In future research the aluminum etching can be further optimized (with respect to selectivity and etch rate) by using mixtures of $SiCl_4$ and Cl_2. In particular, the improved selectivity will further reduce the plasma induced damage to the substrate.

4.3 MONOLITHIC INTEGRATION

To integrate SAW devices with electronic circuitry, the IC processing must be slightly modified. As an example of the feasibility of the monolithic integration of SAW filters with electronic circuitry, the Delft high-frequency BIFET process (f_T = 3 GHz) has been taken as a starting point. This IC process has been developed by Nanver [144]. However, other comparable processes are also suitable. The process flowchart in Fig. 4.8 shows the standard Delft BIFET process with the addition of the following steps

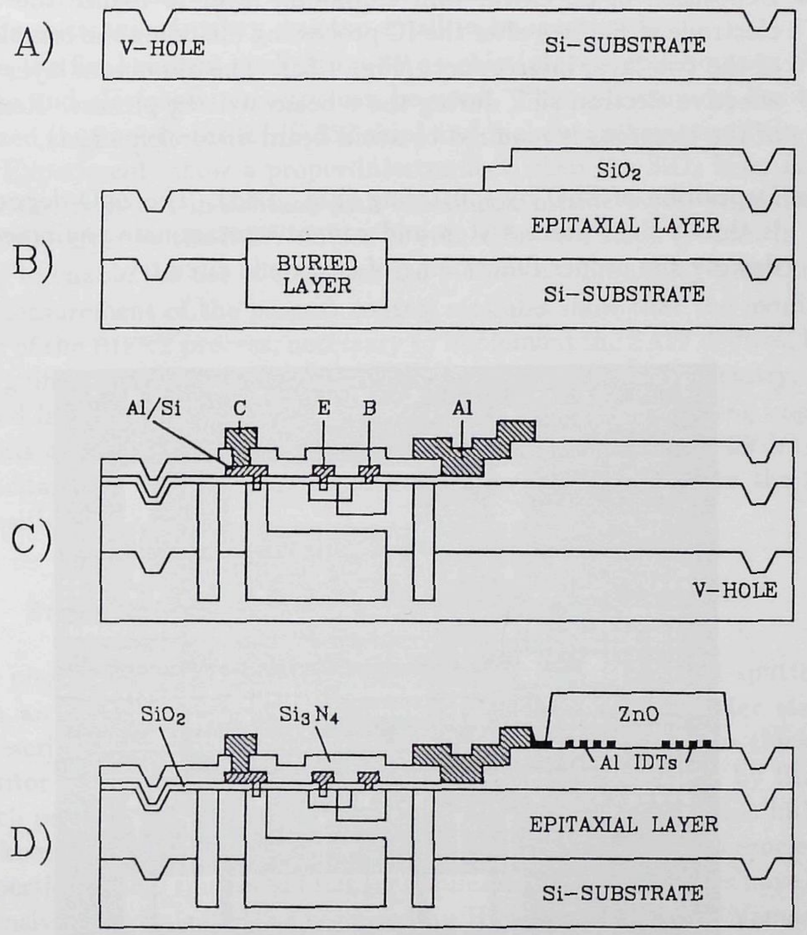

Figure 4.8: *Process flowchart for a SAW device integrated with electronic circuitry: a) V-hole markers; b) Thermal silicon dioxide in SAW area; c) NPN transistor; d) ZnO-SiO_2-Si layered SAW structure.*

- Fabrication of V-hole makers to align the SAW electrode pattern to the electronic circuitry and to the silicon crystal axes via Mix and Match lithography (Fig. 4.8a). Mix and Match lithography has been described in detail by Verhaar et al. [145].
- Thermal oxidation to obtain a thick silicon dioxide layer in the SAW device area. This process step is performed directly after the buried layer and the epitaxial layer are fabricated, but before any critical diffusion or implantation steps (Fig. 4.8b).

- Deposition of an extra, thin aluminum layer to realize the SAW electrode structures after the IC processing including the completion of the two-layer interconnect (Fig. 4.8c). The aluminum layer is an effective electron sink during the e-beam writing process. Removal of the electrons is required to avoid beam distortion effects.

- Deposition of ZnO by sputtering (Fig. 4.8d). The ZnO deposition is thus a final process step and cannot contaminate equipment or destroy the proper functioning of electronic circuitry.

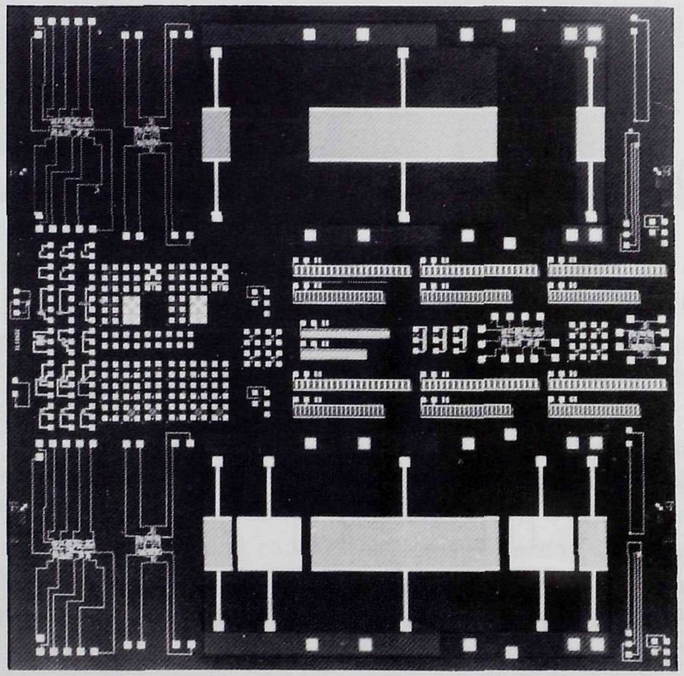

Figure 4.9: *ELIS-552 chip: SAW devices integrated with electronic circuitry on one single chip. The ZnO layer is not yet deposited, see Fig. 4.13.*

Figure 4.9 shows the *ELIS-552* chip, as a result of an integration of SAW devices with BIFET electronic circuitry. Besides SAW delay lines (center frequency 100 MHz), the chip contains bipolar switching mixers, balanced transimpedance amplifiers and process control modules. The total chip measures 10x10 mm. The electronic circuitry is located either under the ZnO layer in the propagation path of the acoustic wave (see

Fig. 4.13) or outside this region. The influence of surface acoustic waves on the electronic circuitry was too small to be measured.

In the final system-application an on-chip interconnect between SAW device and electronic circuitry can be used. This interconnect has been realized (but not in the *ELIS-552* chip) and is shown schematically in Fig. 4.8. Experiments show a proper interconnect when the SiO_2 layer in the SAW device is not in contact with the silicon nitride layer. In addition, the SiO_2 layer in the SAW device is etched in two steps (shown in Fig. 4.8b) to enable the use of the standard 1.4 μm aluminum layer thickness.

Measurement of the process control modules show that the modifications of the BIFET process, necessary to implement the SAW devices, have no significant influence on the performance of the electronic circuitry. The buried layer which could have been diffused into the neighboring implantations or diffusions shows normal breakdown voltages (< -60 V) and capacitances. The measurements have been carried out after the ZnO deposition.

4.4 ZnO DEPOSITION

The piezoelectric ZnO layers are deposited by DC magnetron sputtering with an S-gun sputter unit (Varian, 3119 R&D). This sputter station is described in more detail by Defranould [146]. Because no thickness monitor was installed, the desired layer thickness is obtained by timing, which proved to be not a very accurate method. The variations in layer thickness in different runs were $\pm 10\%$. The structural and piezoelectric properties of ZnO sputtered films for application in SAW devices have been extensively investigated, as reviewed by Hickernell [147] and Yamamoto et al. [148].

The ZnO layer consists of hexagonal crystallites, oriented perpendicular to the plane of the substrate. This is the "c-axis normal orientation." For application of ZnO in SAW devices the following parameters must be considered: the c-axis orientation, the grain size, the electrical conductivity of the thin film, the presence of voids, the difference in growth on metalized and non-metalized regions of the substrate, and the surface roughness. These parameters are interrelated and cannot, in general, all be optimized. Furthermore, for different substrate materials the optimum choice of the sputter parameters will be different. In this work a fixed recipe has been used for ZnO sputtering on SiO_2-Si substrates which proved to give high-quality piezoelectric layers on relatively thick SiO_2 layers ($h_{SiO_2} > 0.5\mu m$). The sputter parameters are listed in Table 4.1.

On other substrates like sputtered SiO_2 layers on silicon substrates or silicon nitride layers on silicon substrates the quality of the piezoelectric ZnO layers is less.

Table 4.1: *ZnO DC magnetron sputter conditions.*

Target composition	Zn
Sputtering gas	100 % O_2
Sputtering gas pressure	1 Pa
Substrate heater temperature	400 °C
Target-to-substrate distance	9 cm
RF power	1.5 kW
Deposition rate	6 μm/h

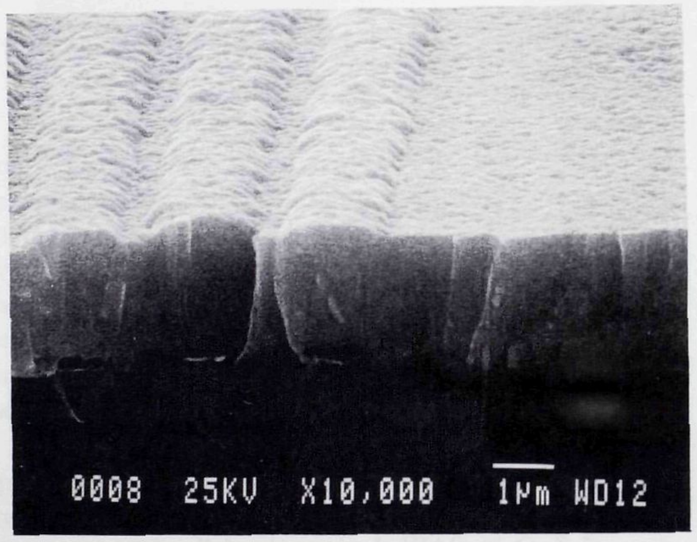

Figure 4.10: *ZnO layer (6 μm) on top of an interdigital transducer with an electrode width of 1 μm.*

In this work the sputtered ZnO films are characterized SEM photographs, X-ray diffraction, Auger electron spectroscopy, and by their piezoelectric and acoustic properties. The latter properties have already been discussed in Chapter 2. The other measuring methods and obtained experimental results will be discussed below. The electrical conductivity of the (semiconducting) ZnO layer in SAW devices can be neglected. A

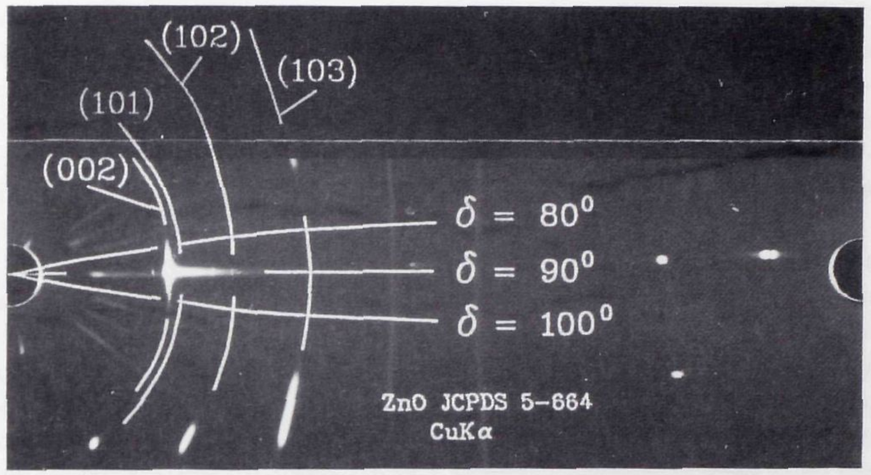

Figure 4.11: *X-ray diffraction pattern of a ZnO layer of thickness 11 μm on a SiO_2-Si substrate, showing a standard deviation angle in the c-axis normal orientation of approximately 5°.*

qualitative measurement of the presence of voids between the crystallites can be obtained by a pole figure which gives a rotation distribution of the crystallite axes parallel to the plane of the substrate, as shown by Venema [149] for a vapor deposited CdS layer on glass.

Figure 4.10 shows an approximately 6 μm thick ZnO layer on top of an interdigital pattern with electrode widths of 1 μm. The aluminum interdigital pattern ($h_{Al} = 0.3$ μm) is placed on a thermally grown SiO_2 layer ($h_{SiO_2} \approx 1.6$ μm) on a p-type silicon wafer.

The crystallographic texture is measured by X-ray diffraction using a Debye-Scherrer apparatus and a CuKα source. The c-axis has to be normal to the plane of the substrate. When the c-axis is randomly oriented on the substrate, circles long the (002) and other orientations would be observed. Figure 4.11 shows a typical X-ray diffraction pattern of a ZnO layer. In this case for a 11 μm ZnO layer thickness (on a 2 μm SiO_2 layer on a silicon substrate) a standard deviation angle of the c-axis normal orientation of approximately 5° has been found. The measured dots in the right-hand side of Fig. 4.11 are caused by the X-ray diffraction at the monocrystalline silicon substrate. The horizontal distribution in the pattern is caused by impurity of the X-ray source. The ZnO layer of approximately 6 μm thickness (as shown in Fig. 4.10) shows a standard deviation angle of the c-axis normal orientation of about 2.5°. In both

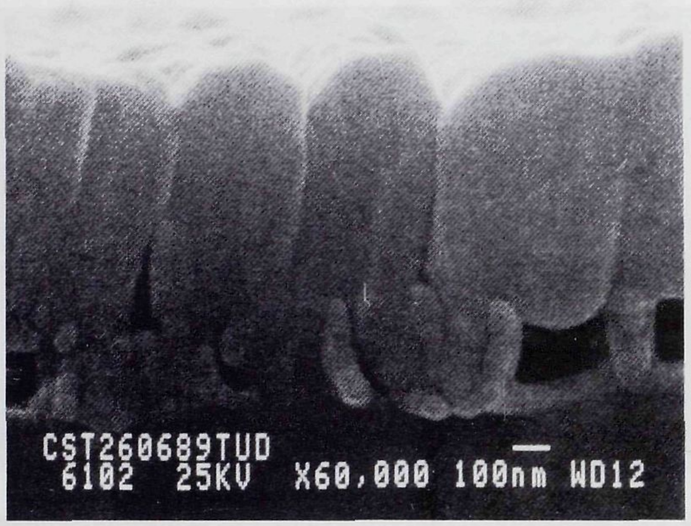

Figure 4.12: *ZnO layer (0.8 μm) on top of an interdigital transducer with an electrode width of 0.2 μm.*

cases no significant differences in c-axis orientation have been observed when an aluminum interdigital pattern under the ZnO layer is present or not. Better results in c-axis orientation have been obtained, but the results listed above correspond to the SAW delay line, SAW transversal filter, and SAW resonator filter presented in Chapter 5.

ZnO is a very reactive material, a property that can cause stability problems in device operation, when it is in contact with its environment. By covering the ZnO layer with another material it can be passivated. A simple technology for the passivation of ZnO with silicon nitride has been reported by Vellekoop et al. [150]. The thin film of silicon nitride is deposited by (low temperature) Plasma-Enhanced Chemical Vapor Deposition (PECVD). This silicon nitride layer proved to be without pinholes and internal stress. In addition, a conformal step coverage at the edge of the zinc oxide layer can be realized with nitride thicknesses of at least 30% of the step-height. The additional silicon nitride layer does not significantly influence the propagation and transduction properties of the layered structure. The center frequency drift and instability caused by the presence of gases decreased by at least one order of magnitude, as shown by Visser, Vellekoop, et al. [151]. An advantage of this passivation method is its compatibility with the standard IC processing, where silicon nitride is often used as a scratch protection layer for integrated circuits.

The packaging of silicon-integrated microacoustic devices in air instead of in an inert gas is one of the important potential applications.

Figure 4.12 shows the insufficient ZnO coverage in the case of 0.2 μm electrode widths (0.3 μm thick). This might be the reason why the fabricated GHz devices did not show any response. By reducing the aluminum electrode thickness, by adapting the ZnO sputter conditions or by applying the buried interdigital transducer (as introduced in Section 4.2) a conformal step coverage of the aluminum electrodes will be realizable.

The ZnO layers have been obtained by using a stainless steel sputter mask because the device must not be completely covered with ZnO to be able to contact the interdigital transducer under the ZnO layer. As a result the uniformity of the layer thickness was not optimal, as already described in Chapter 2. At the edges of this sputter mask the aluminum leads were frequently destroyed, probably by discharge (despite proper grounding of the sputter mask). Auger electron spectroscopy revealed the presence of typical stainless steel elements like Fe, Cr, Ni and Mo at (only) the regions of destruction. This problem is best solved by deposition of ZnO over the entire wafer and a subsequent etch step, as described by Vellekoop et al. [150]. In this way a better layer thickness uniformity can be obtained. This method is also better suited to mass production.

4.5 PACKAGING

The aging mechanisms and the related (long-term) performance of a SAW filter are not only determined by the fabrication process and the way it is used (temperature, driving power etc.), but also by the SAW filter packaging. Packaging and reliability of SAW filters have been studied by Meeker and Grise [152]. The frequency response, in particular the center frequency, of microacoustic devices is sensitive to substrate strain. The effects of strain on the propagation of surface acoustic waves in ZnO thin films on fused quartz substrates have been investigated by Nalamwar et al. [153]. Packaging is critical due to differences in thermal expansion of the SAW device and package. The SAW device must, therefore, be mounted with a rubber adhesive. This adhesive should preferably be electrically conductive to effectively ground the silicon substrate which is necessary for an adequate electromagnetic feedthrough suppression. This rubber adhesive also reduces the reflections of bulk waves at the bottom of the substrate. Other methods to prevent spurious bulk waves from reaching the output transducer are the roughening or canting of the bottom surface and the fabrication of a notch in the bottom of the substrate [130]. The

devices presented here have been mounted with a conductive silver in methyl-isobutyl-ketane glue (Electrodag 1415 from Acheson), 1–1.5 hours at 100 °C.

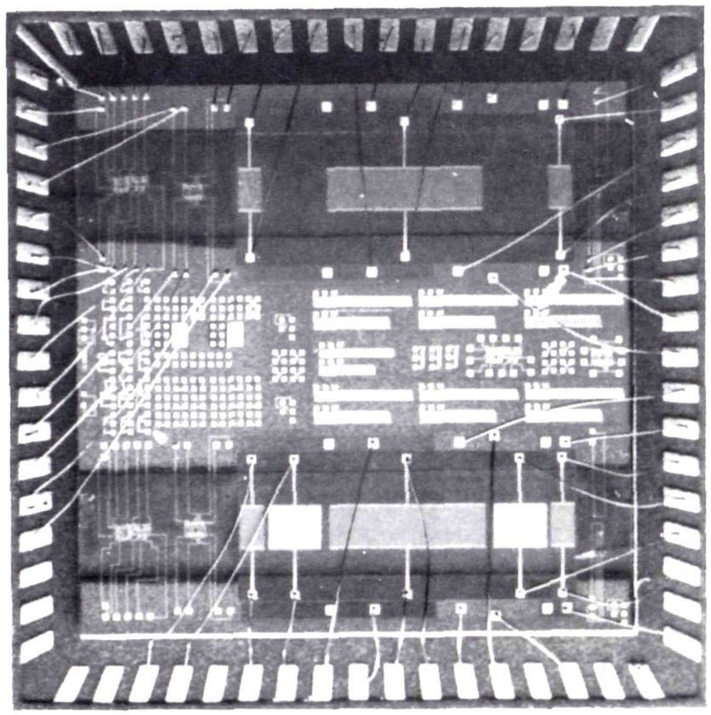

Figure 4.13: *ELIS-552 chip mounted on a 68 pins SLAM package. Two ZnO layers are visible and no acoustic absorber has been applied at the substrate edges. For protection, the chip can be sealed with a metal cover.*

An acoustic absorber is necessary in order to reduce reflections of the surface waves at the edges of the substrate. These reflections cause spurious time responses which results in a degradation of the frequency response. In the devices described in this thesis, Rhodorsil Silicones CAF4 (from Rhône-Poulenc) has been used, but a better absorber (especially for high frequencies) is required. Furthermore, for mass production these (often manually applied) silicones are not suited. Polyimide seems to be a good acoustic absorber in high-frequency SAW devices with the advantages of being fabrication compatible with the silicon planar technology and of displaying good high-temperature behavior, as demonstrated by Johnson et al. [154].

Two types of packages have been used: a 28 pins dual-in-line IC package (suited for maximal chip size of 15x13 mm) and a 68 pins SLAM package (maximal chip size 10x10 mm). The 28 pins DIL package in combination with the inevitable long bonding wires caused a considerable electromagnetic feedthrough between the input and output interdigital transducers of the SAW device. This feedthrough has been reduced by using the 68 pins SLAM package. The 68 pins package was also required for the bonding and subsequent testing of the ELIS-552 chip, as shown in Fig. 4.13. In a final realization of an electronic system with on-chip SAW filters, the on-chip interconnect will be used and will thus reduce the length and the number of bonding wires drastically.

4.6 DISCUSSION AND CONCLUSIONS

An IC compatible high-resolution technology has been obtained for patterning aluminum electrodes in silicon-integrated SAW devices with yields approaching 100%. Reproducible electrode widths down to 200 nm have been fabricated successfully. No rests of chlorine or corrosion could be detected. On ST-X quartz this would result in center frequencies up to 4 GHz (single-electrode interdigital transducers). In the ZnO-SiO_2-Si layered structures the maximal obtainable center frequencies depend on the choice of layer thicknesses. Taking the configuration with the interdigital transducers at the ZnO-SiO_2 interface, center frequencies up to at least 3 GHz are feasible. For these small electrode widths the thickness of the aluminum should be reduced to enable proper ZnO deposition or the ZnO sputter conditions should be modified. A more attractive solution is the embedding of the aluminum pattern in the silicon dioxide layer. Where a larger group delay variation in the passband of the filter and a larger spread in center frequencies of fabricated devices is acceptable, the interdigital transducer can be placed on top of the ZnO layer as well. In this latter case the ZnO layer thickness for optimum coupling at an acoustic wavelength of 800 nm will be approximately 150 nm. The quality of such films with respect to its piezoelectric properties should be investigated. The e-beam lithography is a drawback in mass production but can be replaced by UV or X-ray lithography.

Concerning the technology aspects described in this thesis, at the start of this work only the fabrication of piezoelectric, sputtered ZnO layers and a monolithic physical-electronic system for sensors (in an $f_T = 500$ MHz bipolar process) had been realized. Now, an IC compatible high-resolution technology for patterning aluminum electrodes, and an integration of SAW

devices and electronic circuitry in an $f_T = 3$ GHz BIFET process have been realized. In addition an on-chip interconnect between the SAW device and the electronic circuitry has been tested. Such an integration can be accomplished in comparable IC processes as well. In even higher-frequency processes the fabrication of the SiO_2 layer in the SAW device by thermal oxidation could become a problem. If, however, the center frequency of the SAW device also increases, the silicon dioxide layer thickness can be reduced in proportion. This in turn reduces the expansion of the buried layer by diffusion processes and no malfunction of transistors is expected. The thermal oxidized silicon dioxide layer could be replaced by a (low temperature) sputtered one, but experiments show a very low yield due to short circuits in the interdigital patterns which is caused by pinholes. Other methods of SiO_2 deposition (for example Chemical Vapor Deposition – CVD) can be considered. When the thermally grown silicon dioxide layer is replaced by a silicon nitride layer, this critical and time-consuming process step can be omitted. The silicon nitride layer is now only used in the double-layer metalization. The effect on the propagation and transduction properties must be considered. Initial experimental results show an increase in phase velocity. Furthermore, the sputter conditions for growing high-quality piezoelectric layers on silicon nitride must be sorted out.

In order to obtain a better reproducibility in the frequency characteristic of the SAW devices, the reproducibility in quality and thicknesses of the ZnO layers requires further attention, but its achievement is certainly possible. The encountered problems of the destruction of aluminum patterns by sputter masks is circumvented by ZnO deposition over the entire wafer and subsequent etching of the ZnO. This method will also result in a better uniformity of the film thickness and is suited to mass production. To ensure the (long-term) stability and functioning of the device, the ZnO layers must be passivated against gases by the deposition of a thin silicon nitride layer. This passivation layer can at the same time serve as a scratch protection for the electronic circuitry which is integrated in the same chip with the SAW filters.

Chapter 5

SAW FILTERS IN SILICON

5.1 INTRODUCTION

This chapter discusses the experimental results obtained with SAW filters in ZnO-SiO_2-Si layered structures. SAW filter design has been split up into two parts. The first part consists of the determination of the optimum layer thicknesses and the determination of the transducer configuration, as discussed in Chapter 2. The design of the metal interdigital pattern is the other part. This is an extensively studied problem and because the here realized silicon-integrated SAW filters have been designed by using first-order models only, the problem of the interdigital pattern layout is only briefly discussed in Section 5.2. Treated in more detail are the electromagnetic feedthrough suppression and the problem how to drive and load silicon-integrated SAW filters. The experimental results obtained from SAW delay lines, SAW transversal filters and (two-port) SAW resonator filters in ZnO-SiO_2-Si layered structures are presented in Section 5.3. Discussion and conclusions can be found in Section 5.4.

5.2 SAW FILTER THEORY

The two basic SAW filter structures are briefly discussed, i.e. the SAW transversal filter and the SAW resonator filter. The SAW delay line is a SAW transversal filter with uniform interdigital transducers, as explained in Chapter 1.

SAW transversal filter

The geometry of uniform and apodized interdigital transducers corresponds in first order to a spatially sampled version of the impulse response of the SAW transversal filter. In the delta-function model each pair of electrodes is considered as an independent source of acoustic wave generation with an amplitude proportional to the overlap of the electrodes. By applying this delta-function model SAW transversal filters can be designed, as discussed in more detail by Tancrell [155] and Morgan [156].

In this work only linear-phase SAW transversal filters with symmetric passbands have been designed. The design of these FIR filters is extensively treated by Rabiner and Gold [157]. To obtain a rectangular-shaped frequency response on a substrate of finite length, the corresponding $\sin x/x$ impulse response must be truncated. A deterioration of both amplitude and phase response is the result. The optimum transducer layout can be obtained by windowing, as reviewed by Harris [158], by applying the Remez Exchange Algorithm, as discussed by McClellan et al. [159] or by using linear programming techniques as developed by Ruppel et al. [160].

The SAW transversal filters presented in this thesis have been designed by using the Remez Exchange Algorithm. Only beam-centered apodized transducers, i.e. the overlap regions of the electrodes are symmetrical about the center of the acoustic beam, have been fabricated (see Fig. 1.3). A study on the effects of apodized transducer geometries on the filter performance has been presented by Vigil et al. [161].

The equivalent first-order circuit model, as introduced by Smith et al. [162] can be applied to calculate the transducer admittance in piezoelectric substrates. A more accurate numerical determination of the IDT admittance in a layered, anisotropic, semiconducting structure, assuming weak coupling has been carried out by Quak and Den Boon [163]. Also assuming weak coupling, Venema [164] has presented a flexible lumped network approximation for the IDT admittance in a SiO_2-Si structure covered with a (6mm) piezoelectric layer. In this network approximation the effect of depletion and the presence of surface states have been included. In a rigorous acoustoelectric field analysis of multilayered SAW devices, Ghijsen [165] has calculated the IDT admittance including piezoelectric coupling.

SAW resonator filter

In SAW resonator filter design there are two approaches: the coupled-mode formalism or the transmission matrix formalism. The SAW resonators described in this thesis have been designed by using the latter approach. This transmission matrix formalism is described in more detail by Datta [166] and Eikenbroek [167].

In a practical realization of a SAW resonator different types of reflector arrays (metal or dielectric electrodes, grooves, diffused or implanted electrodes) and interdigital patterns (single or double electrodes, unidirectional IDTs, buried electrodes) can be applied. The different types have been reviewed by Coldren and Rosenberg [168]. Here double electrodes have been used in the interdigital pattern to minimize the distortion in the SAW resonator transfer function as a result of reflections at the edges of the electrodes. The reflector array consists of metal electrodes spaced by half the wavelength of the center frequency. These metal reflector arrays are made in the same fabrication step as the interdigital patterns.

ZnO film on glass substrate SAW resonators have been presented by Ono et al. [169]. SAW resonator filters have been realized in ZnO-SiO_2-Si layered structures by Martin et al. [170]–[172]. However, in their two-port resonators the interdigital pattern is placed on top of the ZnO layer to obtain a low propagation loss and a high Q. This low propagation loss can be obtained since the maximum piezoelectric coupling in this configuration is obtained at smaller ZnO layer thicknesses. However, the variations in phase velocity due to fabrication tolerances in the ZnO layer deposition and thus in center frequency are much higher. This is a serious problem, in particular for high-Q devices. Therefore, in this work the interdigital pattern is located at the ZnO-SiO_2 interface. To compensate for the propagation losses in order to obtain high-Q resonators the SAW amplification mechanism, as described in Chapter 3, could be used. The metal reflector arrays are made in the same fabrication step as the interdigital patterns.

The equivalent electrical circuit of the two-port SAW resonator filter can be modeled by a series *RLC* resonant circuit with a parallel capacitor. This latter capacitor is the interdigital transducer static capacitance. This two-port SAW resonator equivalent circuit was first described by Shreve [173]. The stopband rejection can be improved by the application of coupled SAW resonators, as discussed by Cross and Schmidt [174].

5.3 EXPERIMENTAL RESULTS

Electromagnetic feedthrough

Electromagnetic feedthrough occurs as a consequence of the direct capacitive and inductive coupling between input and output interdigital and interconnecting patterns (on the substrate), bonding wires and connector pins. The direct feedthrough signal interferes with the delayed acoustic signal, deteriorating the overall transfer function. SAW devices in ZnO-SiO_2-Si layered structures exhibit a higher electromagnetic feedthrough than SAW devices on (non-conductive) piezoelectric substrates, as shown by Visser and Venema [175]. Since the difference in dielectric constants cannot account for this difference, it is concluded that the feedthrough between the input and output interdigital transducers mainly takes place through the conductive silicon substrate and can, therefore, not be adequately eliminated with a good packaging technique.

A metal plane, placed perpendicularly between the input and output transducers to suppress the electromagnetic feedthrough more than 100 dB has been applied by Oates [176]. He used an edge-bonded transducer. An IC-compatible analogon could be a grounded p^+ diffusion between both interdigital transducers. However, in practice this diffusion does not reach deep enough. Increasing the distance between the transducers reduces the feedthrough, but is not a very attractive solution in the case of a monolithic integration. In SAW two-port resonator filters it is not even possible. Symmetrically driving the transducers has proven to be successful, as shown by Venema et al. [177] and can easily be implemented when amplifiers that drive the SAW filter are monolithically integrated. Grounding the epitaxial layer and substrate decreases the electromagnetic feedthrough, but not sufficiently [177]. Implantation or diffusion of a highly doped layer on top of the epitaxial layer or on the substrate (buried layer) to improve the conductivity and subsequently grounding of these layers does not noticeably improve the feedthrough suppression. This is also found in the case of a grounded metal plane between the metal interdigital patterns.

Therefore, the use of a grounded, metal layer between the silicon substrate and the interdigital pattern should reduce the feedthrough more effectively. For this purpose the IDT configuration D (in Fig. 2.1) could be used. However, optimum piezoelectric coupling in this configuration is obtained for ZnO layer thicknesses approximately one order of magnitude smaller. This results in a higher phase and group velocity and in an increased dispersion, when compared with the configuration with the

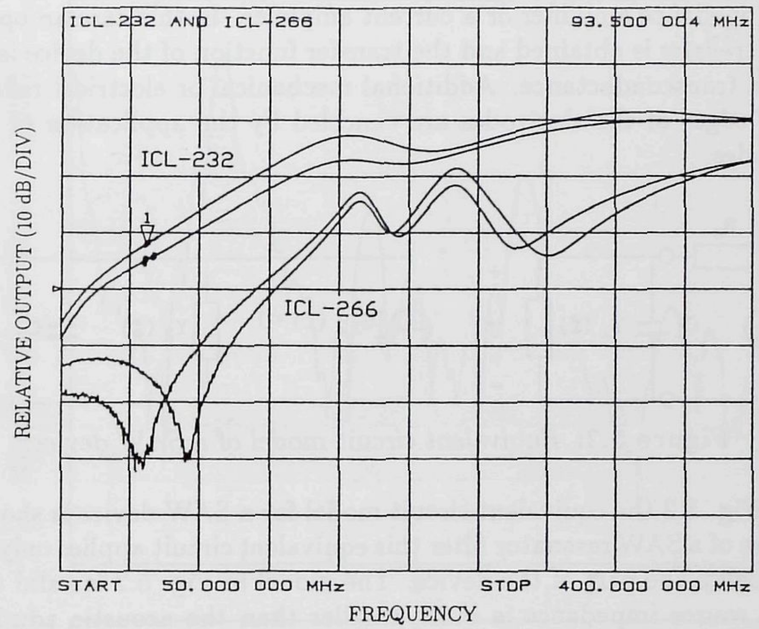

Figure 5.1: *Electromagnetic feedthrough in SAW filters in a ZnO-SiO_2-Si layered structure with (ICL-266) and without (ICL-232) a metal layer on top of the silicon substrate. The SAW filters ICL-266 have a 2 μm thick dielectric layer of silicon nitride (see also Chapter 4).*

interdigital transducer at the ZnO-SiO_2 interface. By inserting a metal layer on top of the silicon substrate, as shown in Fig. 4.1d, the electromagnetic feedthrough can be suppressed by 10–15 dB as shown in Fig. 5.1. The technology for this configuration has already been described in Chapter 4.

Driving and loading

To determine the optimum source and load of the SAW filter the application must be known. However, SAW filters are mainly used in signal processing applications, where signal transfer instead of power transfer is desired. To avoid a regeneration of the surface acoustic wave at the interdigital transducers, both IDTs should form a short-circuit for a bypassing acoustic wave. For the input transducer this means that a voltage source must drive the SAW filter. The output transducer should be loaded with a short-circuit. The current is then the output signal. In practice this can be realized by using an amplifier with a low input impedance, such as a

transimpedance amplifier or a current amplifier. In this case an optimum signal transfer is obtained and the transfer function of the device is essentially a transconductance. Additional mechanical or electrical reflections at the edges of the electrodes are canceled by the application of double electrodes.

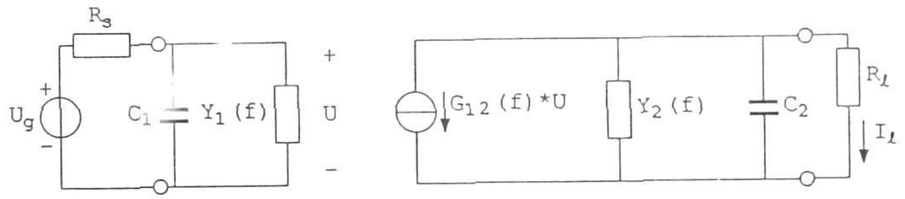

Figure 5.2: *Equivalent circuit model of a SAW device.*

In Fig. 5.2 the equivalent circuit model for a SAW device is shown. In the case of a SAW resonator filter this equivalent circuit applies only to the SAW delay line part of the device. The model in Fig. 5.2 is valid as long as the source impedance is much smaller than the acoustic admittance $Y_1(f)$. The capacitances C_1 and C_2 are the static IDT capacitances. The real parts of the frequency dependent admittances $Y_1(f)$ and $Y_2(f)$ can be interpreted as radiation conductances and represent the conversion of electrical power to acoustic power, as described by Smith [162]. The optimum aperture of the SAW device with respect to the noise attribution to the complete system is treated by Van Zeijl [178].

Figure 5.3 shows the effect of driving and loading circuitry on the impulse response of a SAW transversal filter on a $LiNbO_3$ substrate. Figure 5.3a shows the impulse response when power matching of the SAW filter (and an inductor tuning of the IDT capacitance) is used. In the case of a short circuiting of both transducers (in this case with 10 Ω) an improved triple transit echo and bulk wave suppression is obtained. In addition, the SAW filter bandwidth is no longer disturbed by the circuit effect [156].

SAW delay line

The experimental results of the SAW delay lines integrated on chip *ELIS*–552, as shown in Figs. 4.9 and 4.13 are now presented. The ZnO and SiO_2 layer thicknesses are 11.8 and 2.0 μm, respectively. With external transformers, the device is driven by a balanced voltage and loaded with a differential short circuit. The transconductance in the 100 MHz passband is about 1 mA/V, as shown in Fig. 5.4. The $\sin x/x$ delay line responses of the first- and second-order Rayleigh-wave modes are severely disturbed

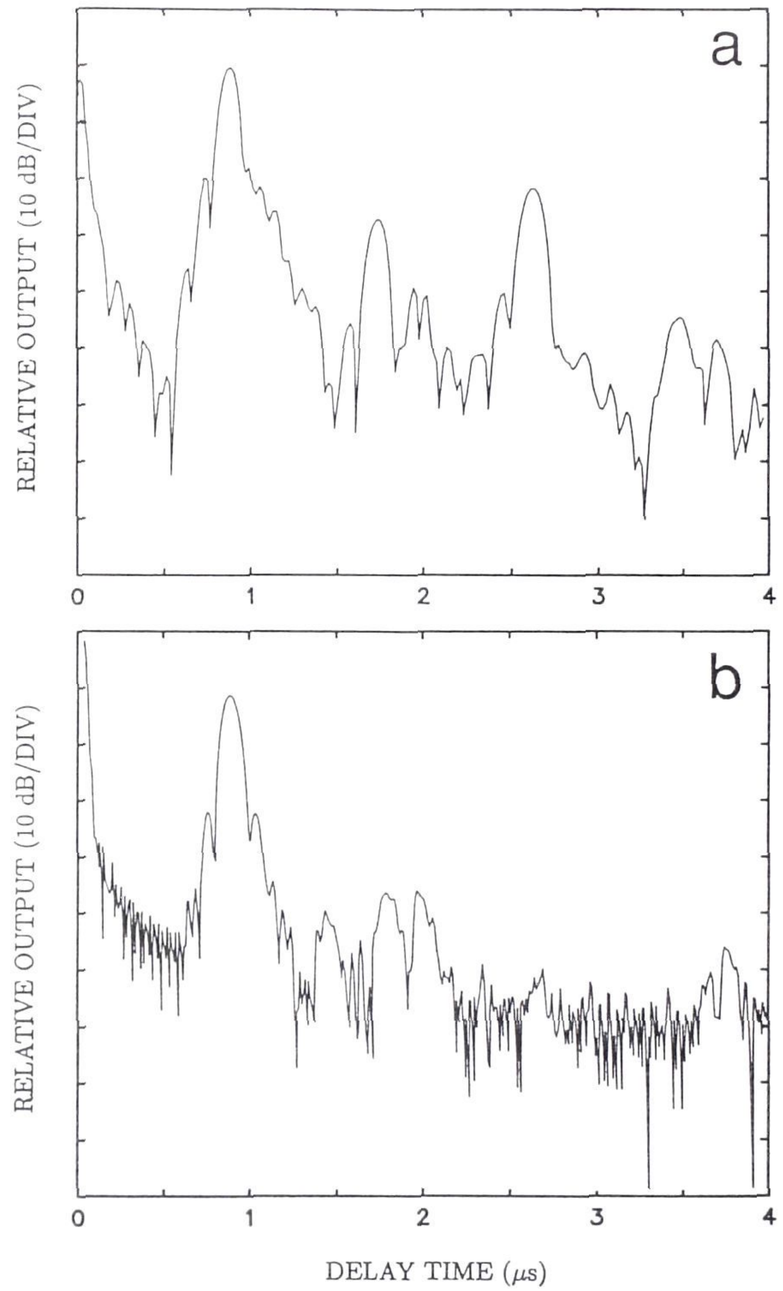

Figure 5.3: *Impulse response of a SAW filter on $LiNbO_3$ in the case of optimum power transfer (A) and in the case of optimum signal transfer (B).*

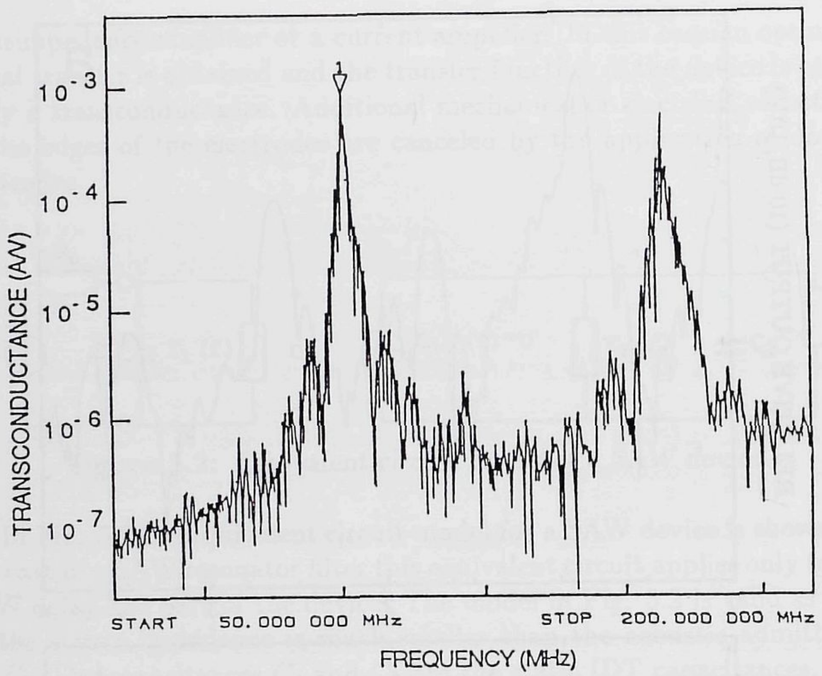

Figure 5.4: *Amplitude response of the SAW delay line in a ZnO-SiO$_2$-Si layered structure. The marker indicates the center frequency of 100.4 MHz.*

by electrode reflections since only single electrodes have been used in this device. The aperture is about 0.7 mm. The electromagnetic feedthrough between input and output transducer increases with frequency, but is adequately suppressed. In Fig. 5.5 the third-order intermodulation distortion of the SAW delay line is shown. Two signals with equal amplitude (1.2 V_{eff}) have been applied to the large IDT (100 pairs of electrodes). The intermodulation components at 100.7 and 101.3 MHz are about 70 dB lower. When the small IDT (15 pairs of electrodes) is chosen, the intermodulation is less (as shown by the lower curve in Fig. 5.5). Noise measurements performed on this delay-line show that the noise (referred to the input) generated by the SAW device is less than 10 nV/$\sqrt{\text{Hz}}$ at 100 MHz. From these measurements it is concluded that for a 180 kHz bandwidth (as used in the FM upconversion receiver discussed in the next chapter) the dynamic range is at least 130 dB, while the third-order intermodulation-free dynamic range amounts to at least 105 dB. The SAW delay line and the SAW transversal filter have a noise behavior which is less than their equivalent transimpedance.

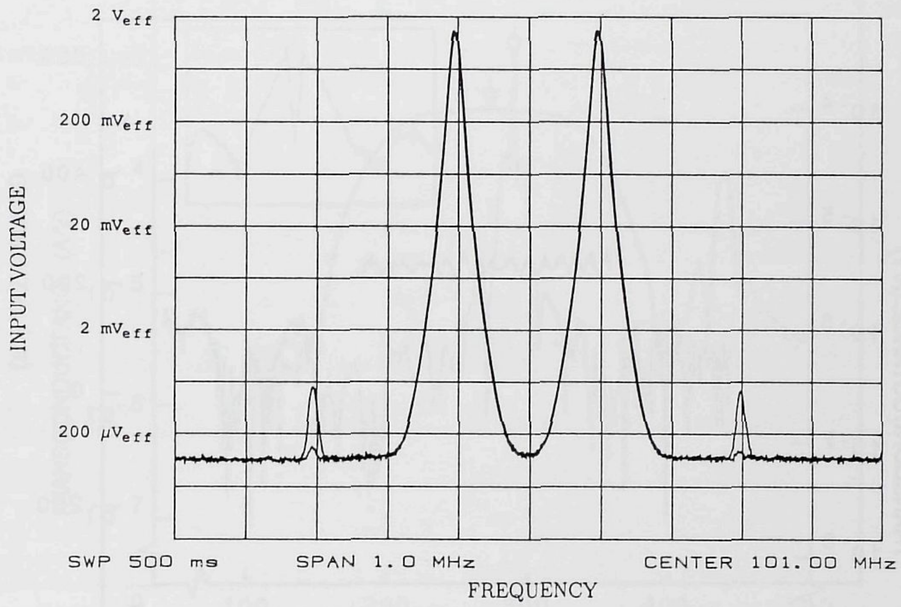

Figure 5.5: *The SAW delay line (in a ZnO-SiO$_2$-Si layered structure) third-order intermodulation.*

SAW transversal filter

Figure 5.6 shows the frequency characteristic of a SAW transversal filter with a 18.7 MHz bandwidth at a center frequency of 283 MHz. The aluminum layer thickness of the electrodes is 0.3 μm. The ZnO and SiO$_2$ layer thicknesses are approximately 5.8 μm and 1.6 μm, respectively. For optimum performance the ZnO layer thickness should have been approximately 4.5 μm. The 5.8 μm ZnO layer thickness results not only in a second Rayleigh-wave mode, but also in a third. This SAW filter has double and dummy electrodes. The aperture is $35\lambda_0$ ($\lambda_0 = 9.33$ μm). The uniform IDT consists of 10 pairs of electrodes and the apodized IDT has 64 pairs. The designed bandwidth is in good agreement with the measured bandwidth. A constant group delay in the passband has been realized, despite the large bandwidth and the layered structure. The peak-to-peak ripple in group delay is about 25 ns. No special measures have been taken to suppress the electromagnetic feedthrough in this device. Instead, the direct feedthrough has been removed by gating (−10 ns – 30 ns) in the time domain with the network analyzer.

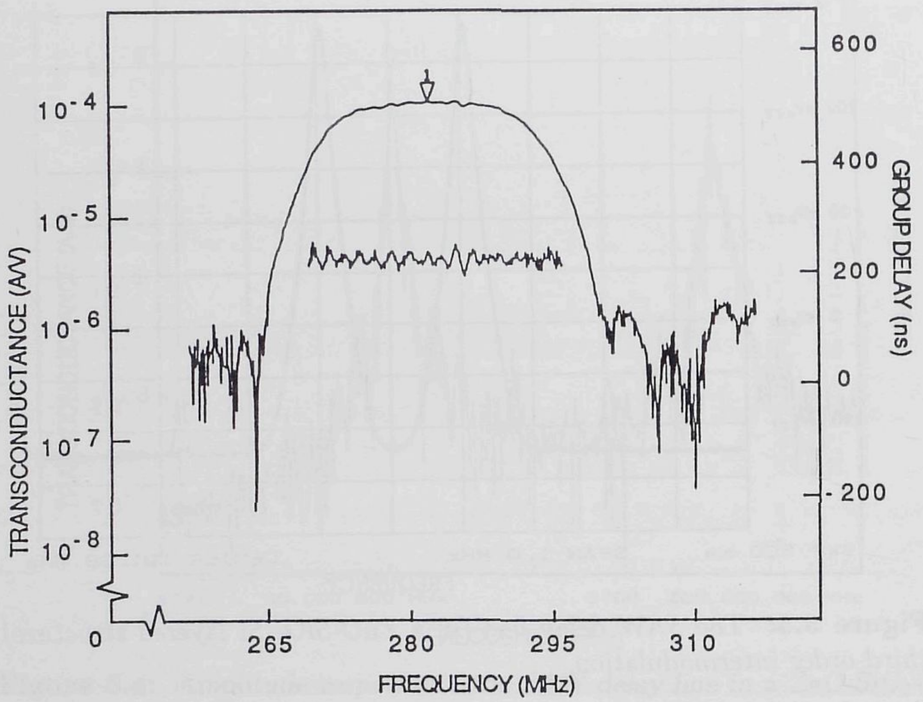

Figure 5.6: *Amplitude response (upper curve) and group delay (in the passband) of a SAW transversal filter in a ZnO-SiO_2-Si layered structure. The marker indicates the center frequency of 283 MHz.*

SAW resonator filter

The frequency characteristic of a SAW resonator filter (500 kHz bandwidth) is shown in Fig. 5.7. It consists of a resonance peak superposed on the ordinary SAW delay line response. The presence of a second delay line passband is caused by the second Rayleigh-wave mode. However, on this passband no resonance peak is present. The interdigital transducers consist of 20 pairs of (double) electrodes. The antinodal reflection of the surface acoustic wave at the reflector array results in a distance between the edge of the reflector and the center of the electrodes in the interdigital transducer of $\frac{1}{2}n\lambda_0$ (n integer). This result has also been obtained by Martin et al. [170], however for a different configuration. The layer thicknesses are the same as for the SAW transversal filter. In this case the electromagnetic feedthrough has also been gated by the network analyzer. The distance between the reflector arrays is $50.5\lambda_0$ ($\lambda_0 = 9\ \mu m$). The reflector arrays consist of 250 electrodes. No difference between shorted

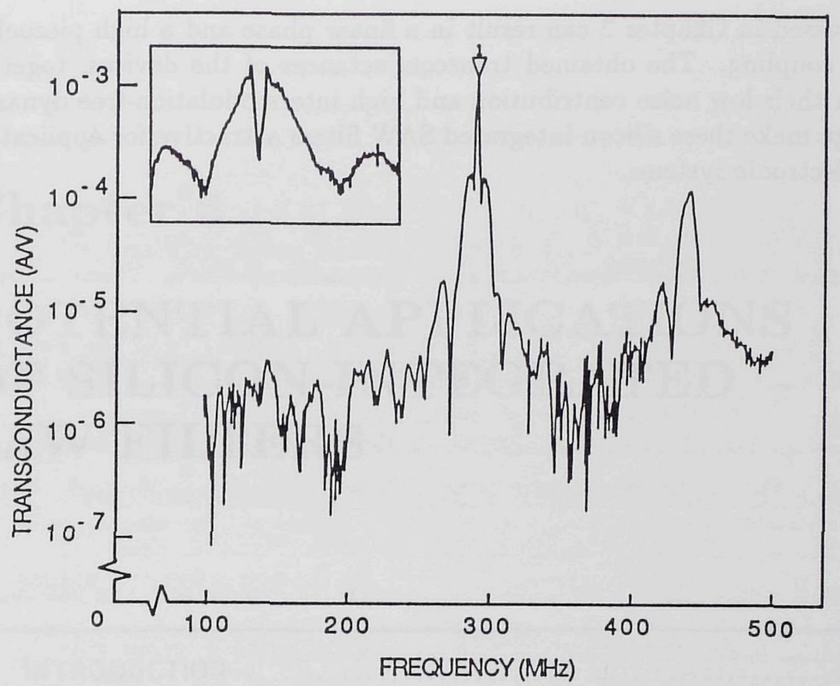

Figure 5.7: *Amplitude response of a SAW resonator filter in a ZnO-SiO_2-Si layered structure with a distance of $1/2\lambda_0$ between reflector and transducer. The marker indicates the center frequency of 292.25 MHz. The inset shows the frequency characteristic for a $3/4\lambda_0$ distance.*

and open reflector arrays is found. No transverse modes are detected, which is expected since the aperture is $40\lambda_0$. Preliminary noise measurements of the SAW resonator filter show a noise behavior equivalent to the impedance R in the series RLC equivalent circuit of the resonator filter.

5.4 DISCUSSION AND CONCLUSIONS

SAW delay lines, SAW transversal filters and SAW resonator filters have been realized in a ZnO-SiO_2-Si layered structure. An optimal signal transfer is obtained when the device is driven with a balanced voltage source and loaded with a differential short-circuit. Under these conditions no regeneration of acoustic waves at the IDTs is possible. Balanced driving and loading of the device suppresses the electromagnetic feedthrough, which can be further reduced by the insertion of a thin metal layer on top of the silicon substrate. Double electrodes are necessary to prevent a severe distortion in the passband. A proper choice of the layer thicknesses, as

discussed in Chapter 2 can result in a linear phase and a high piezoelectric coupling. The obtained transconductances of the devices, together with their low noise contribution and high intermodulation-free dynamic range make these silicon-integrated SAW filters attractive for application in electronic systems.

Chapter 6

POTENTIAL APPLICATIONS OF SILICON-INTEGRATED SAW FILTERS

6.1 INTRODUCTION

Surface Acoustic Wave (SAW) filters realized in a ZnO-SiO_2-Si layered structure offer the opportunity for monolithic integration with electronic circuitry, as demonstrated in Chapters 4 and 5 of this thesis. Since the fabrication of these filters is compatible with the silicon planar IC technology and no adjustment of the fabricated devices is required, a high-volume production of compact electronic systems with high-performance on-chip selectivity becomes feasible. The reduced size and weight of the complete system will be an advantage in cordless telephone, car radio, all kinds of portable consumer electronics products, and military applications. Taking the general trend in IC technology into account (as described in Chapter 1), the price/performance ratio of these fully integrated electronic systems with on-chip SAW filters might very well be superior to that of systems

built up of a number of discrete components.

Moreover, receiver architectures, such as in radio [179], television [180], [181] and other telecommunication systems, are making increasing use of higher Intermediate Frequencies (IF) to improve the interfering signal rejection and to allow for the use of wider bandwidths. These wider bandwidths are in demand for new systems, such as High-Definition TeleVision (HDTV) and Direct Broadcast Satellite (DBS) television. The IF selectivity is obtained by using SAW (transversal) filters. These high-IF systems give a better performance, even when the tuned front-end filters are replaced by fixed-frequency filters. At these high frequencies, the use of discrete SAW components is not very attractive because of the increased pin-to-pin feedthrough between the different components. The cost of packaging is an overriding cost. Therefore, reducing the number of packages in the total system can substantially reduce its cost. It can be concluded that silicon-integrated SAW filters will be attractive in the above-mentioned applications.

In Section 6.2 the performance, crucial to the future application of SAW filters in ZnO-SiO$_2$-Si layered structures is reviewed and compared with implementations on conventional monocrystalline substrates. As an example of the use of silicon-integrated SAW filters, Section 6.3 deals with the overall system design of an FM upconversion radio receiver with on-chip SAW filters, while taking the discussed performance into account. This chapter ends with a discussion and conclusions in Section 6.4.

6.2 PERFORMANCE OF Si-INTEGRATED SAW FILTERS

Considering the SAW filter as an isolated component, the performance of such a filter realized in the ZnO-SiO$_2$-Si layered structure can be compared with a realization on conventional (monocrystalline) substrates. The main differences have already been discussed in various sections of this thesis. For reasons of clarity the differences are reviewed below and the theoretical and (present) experimental results of SAW filters in a ZnO-SiO$_2$-Si layered structure are summarized.

Phase velocity and piezoelectric coupling

For monolithic integration of SAW filters and electronic circuitry to be attractive, the device length of the SAW filters should be minimal. The length of a SAW transversal filter is in first order determined by the group velocity, while the length of a SAW resonator filter is (in first order) determined by the phase velocity. The phase or group velocity of the fundamental Rayleigh-wave mode in the ZnO-SiO$_2$-Si layered structure can be 10–30% lower than on substrates like quartz and lithium niobate, thus reducing the length of the device by 10–30% (for a given bandwidth). In addition, the piezoelectric coupling in the ZnO-SiO$_2$-Si layered structure is better than on quartz, but lower than on lithiumniobate. These low velocities and high piezoelectric couplings are obtained when the interdigital transducer is located at the ZnO-SiO$_2$ interface and

$$f_0 h_{SiO_2} \geq 400 \tag{6.1}$$

$$f_0 h_{ZnO} \approx 1200 \tag{6.2}$$

All experimental results show high-quality ZnO sputtered layers when

$$1\mu m < h_{ZnO} < 10\mu m \tag{6.3}$$

For ZnO layer thicknesses of

$$10\mu m < h_{ZnO} < 20\mu m \tag{6.4}$$

the quality is less, but still acceptable, as shown in Chapter 4. In the case of thick ZnO layers, it is advisable to choose a layer thickness smaller than Eqs. 6.1 and 6.2 require. This reduces the theoretical piezoelectric coupling but increases the actual, realized piezoelectric coupling. Another possibility, especially for low frequency applications, is the fabrication of the interdigital transducer on top of the ZnO layer. The theoretical piezoelectric coupling is lower, but since it can be obtained at

$$f_0 h_{ZnO} \approx 120 \tag{6.5}$$

the actually obtained piezoelectric coupling (as a result of the smaller ZnO layer thickness) can be as good as in the case described above. However, in this configuration the reproducibility of the center frequency is more difficult to control and the phase velocity and dispersion are higher, as discussed in Chapter 2. In the research described in this thesis, the silicon dioxide layer thickness was limited to 2 μm (corresponding to 8 hours of thermal oxidation at 1200 °C).

Higher-order Rayleigh-wave modes

In the ZnO-SiO$_2$-Si layered structures, higher-order Rayleigh-wave modes can be generated. The degree of generation of these surface acoustic wave

modes depends on the normalized layer thicknesses. Especially the generation of the second-order mode is difficult to circumvent, as shown in Chapter 2. In SAW filters, these higher-order modes result in multiple passbands, thus deteriorating the stopband rejection. This deterioration is most critical in SAW transversal filters (and SAW delay lines), while in SAW two-port resonator filters the higher-order modes are not effectively reflected by the reflector arrays, as shown in Chapter 5. The application of SAW amplification (Chapter 3) by the interaction of the propagating acoustic wave with the drifting charge carriers in the silicon substrate will be an attractive and adequate solution to reduce these spurious passbands.

Using the higher-order modes can double the surface wave phase velocity, which results in a doubling of the maximal obtainable center frequency for a given minimal realizable interdigital electrode width. However, doubling of the phase velocity (and larger group velocity) also increases the device length for a given frequency response.

Dispersion

In contrast to the homogeneous substrates, the layered structure is a dispersive medium for surface acoustic wave propagation, with a dispersion determined by the layer thicknesses of the ZnO and SiO_2 layers. As shown in Chapters 2 and 5, a constant group delay can be obtained in these layered structures by the proper choice of the layer thicknesses, even for wide band SAW transversal filters. Not only the phase and group velocities depend on the layer thicknesses, but the piezoelectric coupling as well. This is an advantage when the frequencies in the passband of the SAW filter have a higher piezoelectric coupling than frequencies in the stopband.

Reproducibility and (long-term) stability

The center frequency of the SAW filter is proportional to the phase velocity of the surface acoustic wave. Variations in material properties and layer thicknesses limit the reproducibility and (long-term) stability of the center frequency of the SAW filter. These variations are critical in narrow band filters. Improvement of the stability of the ZnO layer is enabled by the deposition of a silicon nitride layer on top of it. A reproducibility and stability as obtained on polished, homogeneous crystals will be more difficult to obtain, and thus limit the applicability of narrow band silicon-integrated SAW filters. However, with the constantly improving fabrication techniques and the possible use of compensation as is discussed in

the following item, these limitations will not hamper a widespread use of narrow band SAW filters in ZnO-SiO_2-Si layered structures.

Temperature coefficient of frequency (TCF)

The temperature stability of a SAW device in a ZnO-SiO_2-Si layered structure depends on layer thicknesses and material constants. A temperature coefficient of frequency better than on lithium niobate is easily obtained, a temperature stability comparable to that of ST-X quartz can be obtained. Theoretical and experimental data show a zero temperature coefficient of frequency in the case

$$f_0 h_{SiO_2} \approx 250 \tag{6.6}$$

In practice, problems of reproducibility and stability in device characteristics reduce the temperature stability. Compensation methods, involving a second SAW device as a reference, are another solution to the improvement of the temperature behavior of these silicon-integrated SAW filters.

Propagation losses

As a result of the presence of polycrystalline layers, the propagation losses of acoustic waves in SAW filters in ZnO-SiO_2-Si layered structures are somewhat higher than in conventional substrates. These propagation losses depend on the layer thicknesses and the surface roughness, and are proportional to the square of the center frequency and can be compensated for in the filter design. At high frequencies the propagation losses can become too high. In this case the insertion of SAW amplification in the filter (as discussed in Chapter 3) can be used to improve the performance.

Electromagnetic feedthrough

As shown in Chapter 5, the electromagnetic feedthrough of SAW filters on conductive silicon substrates is worse than on the conventional (nonconductive) substrates, but can be suppressed to a great extent. In (silicon-integrated) SAW devices the stopband rejection is usually limited by the electromagnetic feedthrough. A choice for a configuration with a high piezoelectric coupling is, therefore, required to obtain a sufficient stopband rejection.

Matching networks

Basically, a SAW filter can be (optimally) matched to the other parts of the electronic system by either optimal power transfer or by optimal signal

transfer. In low power systems, where additional amplification is undesired, an optimal power transfer is preferred. Power matching is difficult to obtain on-chip since it requires tuning by inductors. For most communication and signal processing applications an optimal signal transfer is the best choice. This is obtained by driving the interdigital transducer with a voltage source and loading the transducer with a short-circuit by using an amplifier with a low input impedance (such as current or transimpedance amplifiers).

It is concluded that SAW filters in ZnO-SiO$_2$-Si layered structures have a piezoelectric coupling better than that of quartz substrates and a temperature stability superior to lithium niobate substrates. These silicon-integrated SAW filters can be fabricated with center frequencies from approximately 10 MHz to above 1 GHz. However, with the present technology and the need of a high piezoelectric coupling and a low dispersion, the minimum center frequency is about 100 MHz. Accepting a suboptimal performance can lead to a possible minimum center frequency down to about 10 MHz. The upper limit is determined by the lithography and etch technology used for the interdigital transducer fabrication. The minimum bandwidth of these SAW filters is limited by problems with the (long-term) stability, temperature stability and reproducibility of the center frequencies of the transfer function. Since these problems have a technological origin, great improvement is expected in the near future, not only in the ZnO deposition and in the fabrication of the aluminum interdigital transducers, but also in the availability of new piezoelectric materials. Moreover, compensation methods can be used.

Taking this performance evaluation into account, it is clear that silicon-integrated SAW filters cannot simply replace the conventional (SAW) filters in a system. The complete system should be considered and revised in order to find out whether these on-chip SAW filters can be used and how an optimal (overall) system performance can be obtained. In Section 6.3 such an approach, as a case study to demonstrate the feasibility of on-chip SAW filters, has been carried out for a new, one-chip FM upconversion radio receiver.

6.3 FM RADIO RECEIVER WITH ON-CHIP SAW FILTER

6.3.1 Radio Receiver Architectures

The task of a radio receiver is to reproduce the information originally modulated on a carrier broadcast from a transmitter. This recovery of information is hindered by noise, distortion and by interference from other channels. In the received Radio Frequent (RF) signal at the antenna, noise is already present (galactic, atmospheric or man-made) and noise is generated in the radio receiver. Interference is created in the receiver and limits its performance, especially in the case of a (weak) desired signal in the presence of (strong) undesired signals in adjacent and image channels. This situation increasingly occurs due to the growing density of transmitted electromagnetic signals in the entire RF spectrum.

The tendency today in radio receiver design is towards a fully integrated receiver with a minimal number of adjustments and external components. These types of receivers are feasible because of the recent development of high-frequency IC processes and insight gained into the design of electronic circuitry, and are increasingly popular because of their favorable price/performance ratio and their small size. An introduction to analog communication, including Amplitude Modulation (AM) and Frequency Modulation (FM) is given by Carlson [182].

Nauta [179] has made an extensive inventory and performance comparison of various types of AM radio receiver architectures, taking the possibility of a monolithic integration into account. As has already been mentioned, noise, distortion and the level of interference in the reproduced signal are the parameters which are important in determining the performance. A classification of AM and FM receiver architectures can be made, which is based on the type of detection and on whether or not a frequency conversion in front of this detector is used. Tuned Radio Frequency (TRF) receivers (with a non-selective detector, such as an envelope detector) or direct-detection (homodyne) receivers (with a selective detector), as depicted in Fig. 6.1, constitute the most basic receiver architecture. These

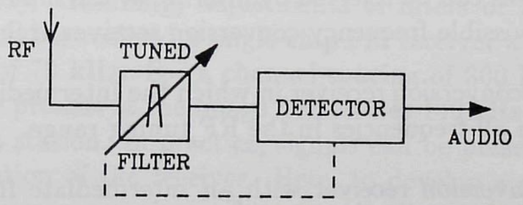

Figure 6.1: *General block diagram of tuned radio frequency or direct-detection receiver architecture.*

receivers use no frequency conversion and different signals can be selected by tuning the filter to the proper channel frequency. In practice tuned

bandpass filters are not easily implemented and a sufficient overall dynamic range of the receiver in the order of 100 dB is not feasible without the use of very complicated electronic circuitry, which makes these receiver architectures of theoretical interest only.

Using a frequency conversion before detection offers the advantage of applying fixed-frequency filters for channel selectivity, which results in "heterodyne" radio receivers. The general block diagram of a single-conversion receiver architecture is shown in Fig. 6.2. The frequency con-

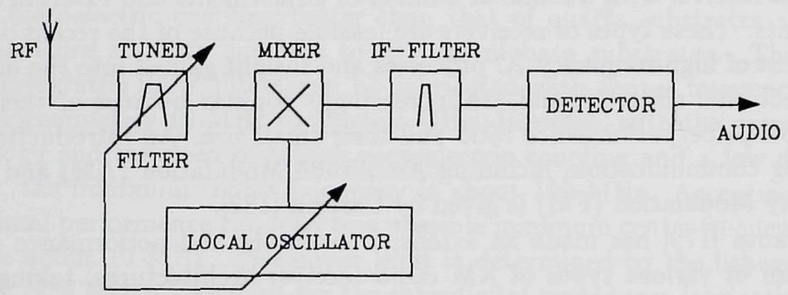

Figure 6.2: *General block diagram of a heterodyne (single-conversion) receiver architecture.*

version is obtained by a multiplication of the input signal with a local-oscillator signal. In practice this multiplication is realized by using a mixer. Apart from the desired frequencies, this type of receiver also exhibits an increased sensitivity to other input frequencies: image frequencies (inherent to the frequency conversion) and frequencies related to the harmonics of the local-oscillator signal and the switching action of the mixer (and their associated image frequencies). The resulting image and spurious responses can be rejected by filtering at the input of the receiver. There are two possible frequency conversion receiver architectures:

- The *downconversion* receiver in which the intermediate frequency is lower than all frequencies in the RF tuning range.
- The *upconversion* receiver with an intermediate frequency higher than all frequencies in the RF tuning range.

The conventional (consumer) FM radio receiver with an IF frequency of 10.7 MHz and an RF frequency broadcast range of 87.5–108 MHz is thus a downconversion receiver. The image frequencies are at a distance of only 21.4 MHz from the broadcast channels and located in the 66.1–86.6

MHz or 108.9–129.4 MHz bands for local-oscillator frequencies below and above the broadcast channels, respectively. These frequency bands are extensively used for air traffic control and other purposes. Therefore, the input filter must be a bandpass filter tuned to the receiving frequency in order to adequately suppress image and spurious responses. Due to the tunable bandpass filter at the input and its required coupling to the local oscillator, the architecture of a downconversion receiver is not very attractive for monolithic integration. In the case of an upconversion receiver with the signals at the intermediate frequency and local-oscillator frequencies higher than all RF input signals, a better reduction of image and spurious sensitivities can be obtained, even in the case of a non-tuned low-pass input filter. With the high-frequency IC processes now available, Nauta [179] concluded that the upconversion receiver in a monolithic implementation is on a price/performance basis more attractive than the classical downconversion receivers. Nordholt et al. [183] and Nauta et al. [184] realized an AM upconversion car radio receiver for the long-wave (150–365 kHz) and medium-wave (512–1625 kHz) bands. Eikenbroek [185] investigated the AM upconversion receiver front-end, including the short-wave (1.8–30 MHz) band.

Here, the analysis, design and partial realization of an FM upconversion radio receiver with on-chip SAW filters is discussed. This research has been carried out in cooperation with Van Zeijl, his Ph.D. Thesis [186] contains detailed information on system and electronic circuitry design. Results have been published by Visser et al. [187] and Van Zeijl et al. [188].

6.3.2 FM Upconversion Receiver with On-Chip IF Selectivity

The aim is to develop a fully monolithic integration of an FM radio receiver without any (trimming) adjustments of filters or offset voltages. Kasperkovitz [189] has realized a single-chip FM receiver with an intermediate frequency of 70 kHz. For a channel spacing of 300 kHz, in theory, no signals will be present at the image frequencies 140 kHz away from the chosen broadcast station. In practice, signals can be present and disturb the proper operation of the receiver. Here, to develop a single-chip FM radio receiver, the upconversion architecture has been chosen.

The IF frequency selectivity (for the FM signals with a bandwidth of approximately 180 kHz [182]) must be realized on-chip to prevent pin-to-pin feedthrough (between ICs or other components) and to reduce the overall size and cost of the receiver. At low frequencies switched-capacitor filters or continuous-time active filters can be made on-chip, but these

filters have a limited dynamic range. High-performance on-chip filters, i.e. with a low noise contribution and a high intermodulation-free dynamic range in the frequency band of 50 MHz – 1 GHz, are available in the form of acoustic wave filters. The two basic types are:

- The thin-film (or composite) bulk wave resonator.
- The SAW transversal filter or the SAW (coupled) resonator filter.

Both acoustic wave filters can be realized on a silicon substrate and have a piezoelectric ZnO thin film for generation and detection of the waves. The thin-film or composite resonator [190], [191] is a bulk acoustic wave resonator consisting of a piezoelectric membrane on a silicon diaphragm. Typical membrane dimensions are 200–500 μm (square) with a thickness of 5–30 μm. To construct resonators with a low temperature coefficient of frequency (TCF) double or triple layer thin-film composite membranes can be used [192], as shown in Fig. 6.3. Recently, the need for etching the back of the silicon substrate has been eliminated with the introduction of air-gap type thin film resonators [193], [194]. The advantage of the composite resonator is its small size. The center frequency is, however, directly related to the ZnO layer thickness. In SAW filters, the variations in layer

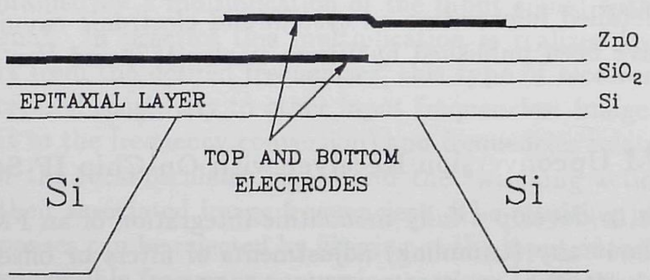

Figure 6.3: *Schematic cross-section of a (temperature compensated) ZnO-SiO$_2$-Si thin film bulk wave resonator.*

thicknesses are a second-order effect, while the lithography determines the center frequency in first order, resulting in a better reproducibility. Moreover, the SAW transversal filters have the advantage of an independent design of amplitude and phase characteristic.

Now a summary of the FM upconversion receiver system design and some of the experimentally obtained performance results will be discussed [188]. The block diagram of the FM upconversion receiver is shown in

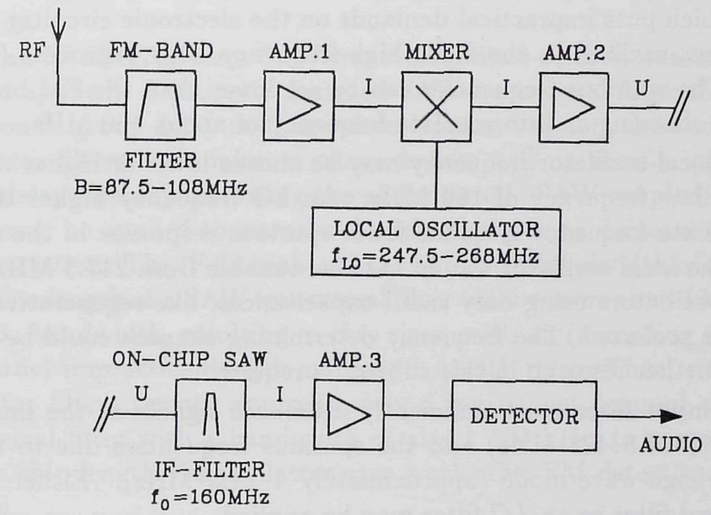

Figure 6.4: *Block diagram of the FM upconversion radio receiver.*

Fig. 6.4. The voltage from the whip antenna passes through a bandpass filter (with a bandwidth covering the entire FM band from 87.5–108 MHz) to the input amplifier (amp.1). By using the local-oscillator (LO) signal and the mixer, the RF signal is converted to a signal at the intermediate frequency. The second amplifier is used to drive the IF filter with the mixer output signal. The IF filter is loaded with an amplifier (amp.3), which drives succeeding stages for the detection of the FM signal.

The demands placed on each block specified in the diagram of Fig. 6.4 will now be discussed beginning with the choice of the intermediate frequency. The IF filter is an on-chip SAW filter, either a transversal filter or a resonator filter. The most dominant (spurious) passband in the filter is caused by the second Rayleigh-wave mode at approximately 1.7 times the fundamental passband frequency. The signals passing through this spurious passband may disturb the detection of the desired signal. For instance, FM detectors using phase-lock loops may be pulled out of lock. A low-pass filter between the IF SAW filter and the FM detector will attenuate these undesired signals. However, such a filter cannot be made in a form compatible with the intention to fully integrate the receiver. The signal frequencies arriving at the antenna, from which the disturbing signals may originate, can be placed far away from the FM broadcast range by choosing the proper intermediate frequency. Thus maximum attenuation by the input filter is achieved. Choosing these spurious frequencies higher

than the FM broadcast band leads to intermediate frequencies above 500 MHz, which puts impractical demands on the electronic circuitry that is, at present, realized in the Delft high-frequency BIFET process (f_T = 3 GHz). The spurious frequencies can be set lower than the FM broadcast band by choosing an intermediate frequency of about 160 MHz.

The local-oscillator frequency may be chosen lower or higher than the intermediate frequency of 160 MHz. An LO frequency higher than the intermediate frequency gives far fewer spurious responses in the receiver [179]. The local oscillator should then be tunable from 247.5 MHz to 268 MHz. Oscillators using only small capacitances, like regenerative types, are to be preferred. The frequency determining element could be a SAW device, further research in this subject is required.

The input filter must sufficiently attenuate signals at the image frequencies (407.5–428 MHz) and the spurious frequencies due to the second Rayleigh-wave mode (approximately 4–24.5 MHz). Either a SAW transversal filter or an *LC* filter may be applied.

A mixer is used to perform the frequency conversion of signals from the FM broadcast band to signals on the intermediate frequency. The mixer has to handle the total FM broadcast range of signals and must, therefore, be extremely linear to maintain a sufficient selectivity. The linearity can be described by the intermodulation-free dynamic range (IMFDR), the dynamic range in which the intermodulation components cannot be distinguished from the noise. A bipolar current switching mixer is the best circuit with respect to noise and distortion performance [179]. A balanced version is preferable to compensate for local-oscillator feedthrough. Both input and output signals of the mixer are balanced currents.

The input amplifier (amp.1) also has to be extremely linear. A noise floor of 1 μV (B=180 kHz) and a maximum input level of 100 mV for linear operation of the input amplifier are desirable. Furthermore, this amplifier has to terminate the *LC* filter at the input to obtain a signal transfer which is sufficiently independent of the impedance of the whip antenna, which can vary, depending on the position of the antenna relative to the ground plane of the receiver. The output signal of the amplifier must be a current for driving the bipolar switching mixer. Amplifiers employing two feedback loops are to be preferred for a low-noise, linear input impedance for the termination of the filter and for driving the bipolar mixer with a current [195]. Such an amplifier has been realized by Van Zeijl [196].

Amplifier 2 in Fig. 6.4 has a balanced current as input signal and must deliver a balanced voltage for the SAW filter. As this amplifier has to handle the total upconverted FM broadcast range this amplifier must also

be extremely linear. A balanced transimpedance amplifier can fulfill these demands.

As an IF filter, either a SAW transversal filter or SAW resonator filter may be applied. A properly designed SAW transversal filter shows little variation in group delay and, therefore, does not distort the audio signal. Resonator filters are minimum phase devices and do show a variation in group delay, thereby distorting the audio signal. SAW coupled resonator filters may be applied to increase the selectivity or to decrease the group delay variation. The IF filter should have a −3 dB bandwidth of about 180 kHz. The length of a SAW transversal filter will be more than 10 mm for a 180 kHz bandwidth, resulting in chip sizes, with an (according to current standards) impractical length and length/width ratio. Thus, either SAW resonator filters (length approximately 6 mm) must be used or a SAW transversal filter with a bandwidth of about 400 kHz, to comply with a 10 mm chip length. In the latter case a selective FM detector should be applied.

A further important aspect is the fabrication reproducibility and temperature stability of these SAW filters. For a maximum deviation from the center frequency of 50 kHz, the filter must be reproducibly made with a tolerance of maximally 300 ppm, while the center frequency drift must be smaller than 3 ppm/K over a 100 K temperature range. As these demands are quite stringent, techniques such as compensation will have to be applied to circumvent these problems. The extra circuitry and SAW device required for this compensation must be the subject of further investigation.

6.3.3 Conclusions

An FM upconversion radio receiver with (on-chip) SAW filters for IF selectivity can be realized. The chip will have an acceptable length of about 6 mm (SAW resonator filter) or 10 mm (SAW transversal filter). The following front-end specifications can be obtained:

Input frequency range	87.5–108 MHz
Input noise floor (B=180 kHz)	1 μV
Maximum linear input level	100 mV
$IMFDR_3$	> 70 dB
Intermediate frequency	160 MHz
IF filter	SAW (coupled) resonator or SAW transversal filter
LO frequency range	247.5–268 MHz
Suppression of spurious responses	> 50 dB

It is found that the amplifier at the input (ampl.1 in Fig. 6.4) limits the overall performance with respect to noise and dynamic range. Therefore, no signal loss can be accepted in the input filter, because it would lead to deterioration in the overall system performance. A fourth- or higher-order *LC* filter can be used as an input filter. Experiments show a suppression of image and spurious responses of at least 50 dB. A low loss SAW filter with a 20% fractional bandwidth can only be realized with a SAW transversal filter using unidirectional interdigital transducers, matched with inductors, and the use of a substrate with a high piezoelectric coupling, such as lithium niobate. The relatively high propagation losses of surface acoustic waves in silicon-integrated SAW devices, the lower piezoelectric coupling (compared with lithium niobate) and the difficulty of matching the output transducer on-chip with an inductor, make the application of a silicon-integrated SAW filter not very attractive as input filter unless SAW amplification is used.

The main problem in the application of the IF SAW filter lies with the temperature stability of the center frequency (3 ppm/K) and with the reproducibility and (long-term) stability of the center frequency (300 ppm) of the filter. In theory this can be accomplished and the preliminary experimental results point in that direction, but an increased effort in technology will be required.

6.4 DISCUSSION AND CONCLUSIONS

Silicon-integrated filters seem promising at high center frequencies in particular, where pin-to-pin feedthrough and related, expensive packaging problems require the development of (high-performance) on-chip selectivity. At these frequencies only relatively thin, inherently high-quality (with the present technology) layers are required for optimal performance. However, the SAW filter should no longer be considered as a single component,

but a complete system design must be undertaken. The experimentally obtained piezoelectric coupling is high enough to implement these filters in IF stages, without deterioration of the overall system performance.

Integration of SAW filters is especially attractive for wide bandwidth applications (HDTV and DBS receivers), since these bandwidths require only a small-length device and make only moderate demands on reproducibility, (long-term) stability and temperature behavior. With further improvement in technology and design, silicon-integrated filters can be applied as narrow band filters and also as filters in systems that transmit analog signals in digital form, using for example Quadrature Amplitude Modulation (QAM).

For low-loss (front-end) applications the passive silicon-integrated filters are not very suited, because of the propagation losses and the (on-chip) matching problems. The addition of SAW amplification in the filter structure will theoretically improve the filter performance for this application.

In this thesis the feasibility of on-chip selectivity by means of transversal filters and resonator filters in ZnO-SiO_2-Si layered structures has been demonstrated. In addition a monolithic integration of these filters with electronic circuitry in one single chip has been realized. A high resolution IC compatible aluminum etch technology has been developed to fabricate electrodes with 200 nm widths. An incorporation of the aluminum electrode pattern into the silicon dioxide and the realization of reflector arrays in SAW resonator filters, consisting of grooves instead of electrodes, are relevant subjects to be further investigated. In future research, more complicated devices, such as chirp filters, Reflective Array Compressors (RAC) etc. can be realized, while in addition the modeling and technology for realizing accurate SAW transversal and resonator filters can be improved. A practical realization of SAW amplification in a SAW filter, as theoretically investigated in this thesis, is another interesting subject for further research.

REFERENCES

CHAPTER 1 — INTRODUCTION

[1] K. F. Graff, "A history of ultrasonics" in *Physical Acoustics: Principles and Methods*, vol. 15, W. P. Mason and R. N. Thurston, Eds. New York: Academic Press, 1981, ch. 1, pp. 1–97.

[2] J. Curie and P. Curie, "Développement, par pression, de l'électricité polaire dans les cristaux hémièdres à faces inclinées," *Comptes Rendus de l'Académie des Sciences*, August 2, 1880, and *Bull. Soc. Min. de France*, vol. 3, pp. 90–93, 1880.

[3] Lord Rayleigh, "On waves propagated along the plane surface of an elastic solid," *Proc. London Math. Soc.*, vol. 17, pp. 4–11, 1885.

[4] M. F. Lewis, "On Rayleigh waves and related propagating acoustic waves," in *Rayleigh-Wave Theory and Application*, E. A. Ash and E. G. S. Paige, Eds. Berlin: Springer Verlag, 1985, pp. 37–58. See also: W. S. Mortley, *Marconi Review*, pp. 273–290, 1965.

[5] J. H. Rowen, "Tapped ultrasonic delay line and uses therefore," U.S. Patent 3 289 144, November 29, 1966; filed December 24, 1963.

[6] G. S. Kino and H. Matthews, "Signal processing in acoustic surface-wave devices," *IEEE Spectrum*, pp. 22–35, 1971.

[7] R. M. White and F. W. Voltmer, "Direct piezoelectric coupling to surface elastic waves," *Appl. Phys. Lett.*, vol. 7, pp. 314–316, 1965.

[8] J. D. Maines and E. G. S. Paige, "Surface-acoustic-wave components, devices and applications," *Proc. IEE (IEE Reviews)*, vol. 120, pp. 1078–1110, 1973.

[9] M. G. Holland and L.,T. Claiborne, "Practical surface acoustic wave devices," *Proc. IEEE*, vol. 62, pp. 582–611, 1974.

[10] M. F. Lewis, C. L. West, J. M. Deacon, and R. F. Humphryes, "Recent developments in SAW devices," *IEE Proceedings*, vol. 131, Pt. A, pp. 186–215, 1984.

[11] G. Tobolka, W. Faber, G. Albrecht, and D. Pilz, "High volume TV-IF filter design, fabrication, and, applications," *Proc. IEEE 1984 Ultrasonics Symp.*, pp. 1–12.

[12] C. S. Hartmann, "System impact of modern Rayleigh wave technology," in *Rayleigh-Wave Theory and Application*, E. A. Ash and E. G. S. Paige, Eds. Berlin: Springer Verlag, 1985, pp. 238–253.

[13] T. W. Bristol, W. R. Jones, P. B. Snow, and W. R. Smith, "Applications of double electrodes in acoustic surface wave device design," *Proc. IEEE 1972 Ultrasonics Symp.*, pp. 343–345.

[14] G. A. Coquin and H. F. Tiersten, "Analysis of the excitation and detection of piezoelectric surface waves in quartz by means of surface electrodes," *Journal of the Acoustical Soc. of America*, vol. 41, pp. 921–939, 1966.

[15] R. M. White, "Surface elastic waves," *Proc. IEEE*, vol. 58, pp. 1238–1276, 1970.

[16] F. W. Voltmer, R. M. White, and C. W. Turner, "Magnetostrictive generation of surface elastic waves," *Appl. Phys. Lett.*, vol. 15, pp. 153–154, 1969.

[17] V. M. Ristic, *Principles of Acoustic Devices*. New York: John Wiley & Sons, 1983.

[18] S. E. Deggendorf and R. M. White, "Generation and detection of ultrasonic waves arising from resistive heating in functioning integrated circuits," *Proc. IEEE 1983 Ultrasonics Symp.*, pp. 655–658.

[19] D. C. Webb, "AO, SAW, BAW, and MSW technology for frequency sorting," *Proc. IEEE 1986 Ultrasonics Symp.*, pp. 109–118.

[20] S. M. Hanna, "Microwave filters based on coupled MSW resonators and their applications," *Proc. IEEE 1988 Ultrasonics Symp.*, pp. 241–244.

[21] G. W. Farnell, "Elastic surface waves" in *Surface Wave Filters*, H. Matthews, Ed. New York: John Wiley & Sons, 1977, ch. 1, pp. 1–53.

[22] J. J. Campbell and W. R. Jones, "A method for estimating optimal crystal cuts and propagation directions for excitation of piezoelectric surface waves," *IEEE Trans. on Sonics and Ultrasonics*, vol. SU-15, pp. 209–217, 1968.

[23] W. R. Smith, H. M. Gerard, J. H. Collins, T. M. Reeder, and H. J. Shaw, "Analysis of interdigital surface wave transducers by use of an equivalent circuit model," *IEEE Trans. on Microwave Theory and Techniques*, vol. MTT-17, pp. 856–864, 1969.

[24] A. J. Slobodnik, Jr., "Materials and their influence on performance." Chapter 6 in *Acoustic Surface Waves. Topics in Applied Physics*, vol. 24. Berlin: Springer Verlag, 1978, ch. 6, pp. 226–303.

[25] A.J. Slobodnik, Jr., *The Temperature Coefficients of Acoustic Surface Wave Velocity and Delay on Lithium Niobate, Lithium Tantalate, Quartz, and Tellurium Dioxide*, USAF Cambridge Research Laboratories, Report AFCRL–72–0082, December 1972.

[26] K. Iamsakun, W. Elder, C. D. W. Wilkinson and R. M. De La Rue, "Surface acoustic wave devices using electrostrictive transduction," *J. Phys. D: Appl. Phys.*, vol. 8, pp. 266–282, 1975.

[27] B. A. Auld, P. Delval, G. Laguna, D. F. Thompson and W. J. Wang, "SAW devices on electrostrictive substrates," *Proc. IEEE 1986 Ultrasonics Symp.*, pp. 217–223.

[28] H. E. Kallmann, "Transversal filters," *Proc. Institute of Radio Engineers*, vol. 28, pp. 302–310, 1940.

[29] R. H. Tancrell and R. C. Williamson, "Wavefront distortion of acoustic surface waves from apodized interdigital transducers," *Appl. Phys. Lett.*, vol. 19, pp. 456–459, 1971.

[30] E. A. Ash, "Surface wave grating reflectors and resonators," *Proc. IEEE 1970 G-MTT International Microwave Symp.*, pp. 385–386.

[31] S. Butterworth, "On electrically-maintained vibrations," *Proc. Physical Society of London*, vol. 27, pp. 410–424, 1915.

[32] W. G. Cady, *Piezoelectricity*. New York: McGraw-Hill, 1946. Printed in revised form, New York: Dover, 1964.

[33] R. E. Collin, *Foundations of Microwave Engineering*. New York: McGraw-Hill, 1966.

[34] B. G. Malcolm, "The current state of the art of miniature L/C filters," *Proc. IEEE 1985 Ultrasonics Symp.*, pp. 38–42.

[35] F. S. Hickernell, "High-reliability SAW bandpass filters for space applications," *IEEE Trans. on Ultrasonics, Ferroelectrics and Frequency Control*, vol. UFFC-35, pp. 652–656, 1988.

[36] R. T. Webster and P. H. Carr, "Rayleigh waves on gallium arsenide," in *Rayleigh-Wave Theory and Application*, E. A. Ash and E. G. S. Paige, Eds. Berlin: Springer Verlag, 1985, pp. 122–130.

[37] T. W. Grudkowski, G. K. Montress, M. Gilden, and J. F. Black, "GaAs monolithic SAW devices for signal processing and frequency control," *Proc. IEEE 1980 Ultrasonics Symp.*, pp. 88–97.

[38] B. Santo, "BiCMOS circuitry: the best of both worlds," *IEEE Spectrum*, vol. 26, pp. 50–53, 1989.

[39] J. Shibata and T. Kajiwara, "Optics and electronics are living together," *IEEE Spectrum*, vol. 26, pp. 34–38, 1989.

[40] S. Middelhoek and S. A. Audet, *Silicon Sensors*. London: Academic Press, 1989.

[41] M. J. Vellekoop, E. Nieuwkoop, J. C. Haartsen and A. Venema, "A monolithic SAW physical-electronic system for sensors," *Proc. IEEE 1987 Ultrasonics Symp.*, pp. 641–644.

[42] A. Venema, "Transduction and propagation of surface acoustic waves in three-layered media with an electrically conductive substrate," Ph.D. Thesis, Delft University of Technology, Delft, The Netherlands, 1980.

[43] S. J. Martin, R. L. Gunshor and R. F. Pierret, "High Q, temperature stable ZnO-on-silicon SAW resonators," *Proc. IEEE 1980 Ultrasonics Symp.*, pp. 113–117.

[44] B. T. Khuri-Yakub and G. S. Kino, "A monolithic zinc-oxide on silicon convolver," *Appl. Phys. Lett.*, vol. 25, pp. 188–190, 1974.

[45] M. E. Motamedi, M. K. Kilcoyne, and R. K. Asatourian, "Large-scale monolithic SAW convolver/correlator on silicon," *IEEE Trans. on Sonics and Ultrasonics*, vol. SU-32, pp. 663–669, 1985.

[46] F. L. Augustine, R. J. Schwartz, and R. L. Gunshor, "Modeling of charge transfer by surface acoustic waves in a monolithic metal/ZnO/SiO_2/Si system," *IEEE Trans. on Electron Devices*, vol. ED-29, pp. 1876–1883, 1982.

[47] F. S. Hickernell, D. E. Olsen, M. D. Adamo and H. J. Bush, "Monolithic surface wave transversal filter," *Proc. IEEE 1977 Ultrasonics Symp.*, pp. 615–618.

[48] J. B. Green, G. S. Kino, J. T. Walker and J. D. Shott, "The SAW/FET: a new programmable SAW transversal filter," *Proc. IEEE 1982 Ultrasonics Symp.*, pp. 436–441.

[49] J. C. Haartsen and A. Venema, "The barrier-modulated tap: a new SAW detection method in silicon," *Proc. IEEE 1988 Ultrasonics Symp.*, pp. 159–163.

[50] T. Shiosaki and A. Kawabata, "Piezoelectric thin films for SAW applications," in *Piezoelectricity*, G. W. Taylor, Ed. New York: Gordon and Breach Science Publishers, 1985, pp. 327–340.

[51] A. Fiorillo, P. Dario, J. van der Spiegel, C. Domenici and J. Foo, "Spinned P(VDF-TrFE) copolymer layer for a silicon-piezoelectric integrated US transducer," *Proc. IEEE 1987 Ultrasonics Symp.*, pp. 667–670.

[52] O. Yamazaki, T. Mitsuyu, and K. Wasa, "ZnO thin-film SAW devices," *IEEE Trans. on Sonics and Ultrasonics*, vol. SU-27, pp. 369–379, 1980.

[53] T. Shiosaki, "High-speed fabrication of high-quality sputtered ZnO thin-films for bulk and surface wave applications," *Proc. IEEE 1978 Ultrasonics Symp.*, pp. 100–110.

[54] R. H. Tancrell and M. G. Holland, "Acoustic surface wave filters," *Proc. IEEE*, vol. 59, pp. 393–409, 1971.

[55] C. S. Hartmann, D. T. Bell and R. C. Rosenfeld, "Impulse model design of acoustic surface wave filters," *IEEE Trans. on Microwave Theory and Techniques*, vol. MTT-21, pp. 162–175, 1973.

[56] S. Datta, *Surface Acoustic Wave Devices*. Englewood Cliffs (NJ): Prentice-Hall, 1986.

CHAPTER 2 — PROPAGATION AND TRANSDUCTION

[57] G. S. Kino and R. S. Wagers, "Theory of interdigital couplers on nonpiezoelectric substrates," *J. Appl. Phys.*, vol. 44, pp. 1480–1488, 1973.

[58] A. Venema, "Transduction and propagation of surface acoustic waves in three-layered media with an electrically conductive substrate," Ph.D. Thesis, Delft University of Technology, Delft, The Netherlands, 1980.

[59] A. Venema and J. J. M. Dekkers, "Enhancement of surface-acoustic-wave piezoelectric coupling in three-layer substrates," *IEEE Trans. on Microwave Theory and Techniques*, vol. MTT-23, pp. 765–767, 1975.

[60] W. J. Ghijsen, "The acousto-electric field analysis of multilayered surface acoustic wave devices," Ph.D. Thesis, Delft University of Technology, Delft, The Netherlands, 1987.

[61] W. J. Ghijsen and P. M. van den Berg, "A rigorous computational technique for the acousto-electric field problem in SAW devices," *IEEE Trans. on Ultrasonics, Ferroelectrics, and Frequency Control*, vol. UFFC-33, pp. 375–384, 1986.

[62] S. Ono, K. Wasa and S. Hayakawa, "Surface-acoustic-wave properties in ZnO-SiO_2-Si layered structure," *Wave Electronics*, vol. 3, pp. 35–49, 1977.

[63] A. K. Sinha, H. J. Levinstein, and T. E. Smith, "Thermal stresses and cracking resistance of dielectric films (SiN, Si_3N_4, and SiO_2) on Si substrates," *J. Appl. Phys.*, vol. 49, pp. 2423–2426, 1978.

[64] T. F. Retajczyk, Jr., and A. K. Sinha, "Elastic stiffness and thermal expansion coefficients of various refractory silicides and silicon nitride films," *Thin Solid Films*, vol. 70, pp. 241–247, 1980.

[65] M. J. Vellekoop, C. C. G. Visser. P. M. Sarro, and A. Venema, "Compatibility of zinc oxide with silicon IC processing." Presented at *Transducers '89*. Accepted for publication in *Sensors & Actuators*, 1989.

[66] M. Lewis, "Temperature compensation techniques for SAW devices," *Proc. IEEE 1979 Ultrasonics Symp.*, pp. 612–622.

[67] Y. Nakagawa, "Elastic-surface-wave temperature coefficients of delay line with ZnO thin film," *Appl. Phys. Lett.*, vol. 31, pp. 56–57, 1977.

[68] Ph. Defranould, "Surface acoustic waves bandpass filters on ZnO/pyrex substrate with zero temperature coefficient," *Proc. IEEE 1983 Ultrasonics Symp.*, pp. 341–344.

[69] S. J. Martin, R. L. Gunshor and R. F. Pierret "High Q, temperature stable ZnO-on-silicon SAW resonators," *Proc. IEEE 1980 Ultrasonics Symp.*, pp. 113–117.

[70] K. Dransfeld and E. Salzmann, "Excitation, detection, and attenuation of high-frequency elastic surface waves," in *Physical Acoustics: Principles and Methods*, vol. 7, W. P. Mason and R. N. Thurston, Eds. New York: Academis Press, 1970, ch. 4, pp. 219–272.

[71] F. S. Hickernell, "Surface acoustic wave propagation loss in zinc oxide films," *Proc. IEEE 1982 Ultrasonics Symp.*, pp. 325–328.

[72] V. M. Ristic, *Principles of Acoustic Devices.* New York: John Wiley & Sons, 1983.

[73] G. S. Kino, *Acoustic Waves: Devices, Imaging, and Analog Signal Processing.* Englewood Cliffs (NJ): Prentice-Hall, 1987.

[74] O. L. Anderson, "Determination and some uses of isotropic constants of polycrystalline aggregates using single-crystal data" in *Physical Acoustics: Principles and Methods*, vol. 3B, W. P. Mason, Ed. New York: Academic Press, 1965, ch. 2, pp.43–95.

[75] Z. X. Qian, X. Z. Zhang, M. Z. Zhao, X. Z. Wu, and Y. J. Wu, "A modified ZnO film model for calculating elastic and piezoelectric properties," *IEEE Trans. on Sonics and Ultrasonics*, vol. SU-32, 1985, pp. 630–633.

[76] G. Carlotti, G. Socino, A. Petri, and E. Verona, "Elastic constants of sputtered ZnO films," *Proc. IEEE 1987 Ultrasonics Symp.*, pp. 295–299.

[77] K. Tsubouchi, K. Sugai, and N. Mikoshiba, "Zero temperature coefficient surface-acoustic-wave devices using epitaxial AlN films," *Proc. IEEE 1982 Ultrasonics Symp.*, pp. 340–345.

[78] K. Tsubouchi and N. Mikoshiba, "Zero temperature coefficient SAW delay line on AlN epitaxial films," *Proc. IEEE 1983 Ultrasonics Symp.*, pp. 299–310

[79] K. Tsubouchi, K. Sugai, and N. Mikoshiba, "AlN material constants evaluation and SAW properties on AlN/Al_2O_3 and AlN/Si," *Proc. IEEE 1981 Ultrasonics Symp.*, pp. 375–380.

[80] A.J. Slobodnik, Jr. and E. D. Conway, *Microwave Acoustics Handbook – Volume 1. Surface Acoustic Wave Velocities*, USAF Cambridge Research Laboratories, Report AFCRL–70–0164, March 1970.

[81] K. L. Davis, "Surface acoustic waves with nearly dispersion-free propagation in a layered silicon configuration," *J. Appl. Phys.*, vol. 45, pp. 3255–3257, 1974.

CHAPTER 3 — SAW AMPLIFICATION

[82] G. Chao, "Parametric amplification of surface acoustic waves," *Appl. Phys. Lett.*, vol. 16, pp. 399–401, 1970.

[83] S. Minagawa, T. Kugaya, K. Tsubouchi, and N. Mikoshiba, "Parametric amplification of surface acoustic waves on monolithic MIS structure," *Proc. IEEE 1977 Ultrasonics Symp.*, pp. 629–632.

[84] S. Minagawa, T. Kugaya, K. Tsubouchi, and N. Mikoshiba, "Parametric amplification and generation of surface acoustic waves on a monolithic MIS structure," *Appl. Phys. Lett.*, vol. 33, pp. 687–689, 1978.

[85] B. T. Khuri-Yakub and G. S. Kino, "A detailed theory of the monolithic zinc oxide on silicon convolver," *IEEE Trans. on Sonics and Ultrasonics*, vol. SU-24, pp. 34–43, 1977.

[86] J. R. Pierce, *Traveling-Wave Tubes.* Princeton: Van Nostrand, 1950.

[87] G. S. Kino and L. A. Coldren, "Noise figure calculation for the Rayleigh wave amplifier," *Appl. Phys. Lett.*, vol. 22, pp. 50–52, 1973.

[88] R. Adler, "A simple theory of acoustic amplification," *IEEE Trans. on Sonics and Ultrasonics*, vol. SU-18, pp. 115–118, 1971.

[89] J. H. McFee, "Transmission and amplification of acoustic waves in piezoelectric semiconductors," in *Physical Acoustics: Principles and Methods*, vol. 4A, W. P. Mason Ed. New York: Academic Press, 1966, ch. 1, pp. 1–45.

[90] A. R. Hutson, J. H. McFee, and D. L. White, "Ultrasonic amplification in CdS," *Physical Review Lett.*, vol. 7, pp. 237–239, 1961.

[91] A. R. Hutson and D. L. White, "Elastic wave propagation in piezoelectric semiconductors," *J. Appl. Phys.*, vol. 33, pp. 40–47, 1962.

[92] D. L. White, "Amplification of ultrasonic waves in piezoelectric semiconductors," *J. Appl. Phys.*, vol. 33, pp. 2547–2554, 1962.

[93] J. E. May, Jr., "Electronic signal amplification in the UHF range with the ultrasonic traveling wave amplifier," *Proc. IEEE*, vol. 53, pp. 1465–1485, 1965.

[94] R. M. White and F. W. Voltmer, "Ultrasonic surface-wave amplification in cadmium sulfide," *Appl. Phys. Lett.*, vol. 8, pp. 40–42, 1966.

[95] P. K. Tien, U.S. Patent 3 158 819, November 24, 1964.

[96] Yu. V. Gulyaev and V. I. Pustovoit, "Amplification of surface waves in semiconductors," *Zh. Eksp. Theor. Fiz.*, vol. 47, pp. 2251–2253, 1964. See also *Sov. Phys. JETP*, vol. 20, 1965.

[97] K. M. Lakin and H. J. Shaw, "Surface wave delay line amplifiers," *IEEE Trans. on Microwave Theory and Techniques*, vol. MTT-17, pp. 912–920, 1969.

[98] L. A. Coldren and G. S. Kino, "Monolithic acoustic surface-wave amplifier," *Appl. Phys. Lett.*, vol. 18, pp. 317–319, 1971. See also: L. A. Coldren, "Monolithic acoustic surface-wave amplifiers," Ph.D. Thesis, Stanford University, Palo Alto (CA), U.S.A., 1972.

[99] R. Hannebrekke and K. A. Ingebrigtsen, "Acoustoelectric amplification of surface waves in structure of cadmium-selenide film on lithium niobate," *Electronic Letters*, vol. 6, pp. 520–521, 1970.

[100] U. Tarakci and R. M. White, "Layered media active microwave acoustic delay lines," *Proc. IEEE 1972 Ultrasonics Symp.*, pp. 440–445.

[101] A. Venema, "Influence of SiO_2-Si interface states on SAW transduction in SiO_2-Si layered medium covered with a piezoelectric overlay," *Proc. IEEE 1981 Ultrasonics Symp.*, pp. 474–478.

[102] S. Zemon and E. M. Conwell, "Effects of surface states on surface wave amplification," *Appl. Phys. Lett.*, vol. 17, pp. 218–220, 1970.

[103] A. R. Moore and R. W. Smith, "Effect of traps on acoustoelectric current saturation in CdS," *Physical Review*, vol. 138, pp. A1250–A1258, 1965.

[104] I. Uchida, T. Ishiguro, Y. Sasaki, T. Suzuki, "Effects of trapping of free carriers in CdS ultrasonic amplifier," *Journal of the Physical Society of Japan*, vol. 19, pp. 674–680, 1964.

[105] J. H. McFee, "Ultrasonic amplification and non-ohmic behavior in CdS and ZnO," *J. Appl. Phys.*, vol. 34, pp. 1548–1553, 1963.

[106] A. R. Moore, "Acoustoelectric current saturation in CdS as a fluctuation process," *J. Appl. Phys.*, vol. 38, pp. 2327–2339, 1967.

[107] H. Skeie, "Current saturation and oscillations in piezoelectric semiconductors due to the acoustoelectric effect," *IEEE Trans. on Sonics and Ultrasonics*, vol. SU-16, pp. 136–144, 1969.

[108] J. T. Hanlon, "Noise induced gain saturation in the ultrasonic traveling wave amplifier," *Proc. IEEE*, vol. 55, pp. 1128–1135, 1967.

[109] A. H. Fahmy and E. L. Adler, "Perturbation theory for multilayered surface-wave amplifiers," *Proc. IEEE 1973 Ultrasonics Symp.*, pp. 275–277.

[110] G. S. Kino and T. M. Reeder, "A normal mode theory for the Rayleigh wave amplifier," *IEEE Trans. on Electron Devices*, vol. ED-18, pp. 909–920, 1971.

[111] K. A. Ingebrigtsen, "Surface waves in piezoelectrics," *J. Appl. Phys.*, vol. 40, pp. 2681–2686, 1969.

[112] K. A. Ingebrigtsen, "Linear and nonlinear attenuation of acoustic surface waves in a piezoelectric coated with a semiconducting film," *J. Appl. Phys.*, vol. 41, pp. 454–459, 1970.

[113] C. A. A. J. Greebe, P. A. van Dalen, T. J. B. Swanenburg and J. Wolter, "Electrical coupling properties of acoustic and electric surface waves," *Physics Reports (Section C of Physics Lett.) 1*, pp. 235–268, 1971.

[114] A. H. Fahmy and E. L. Adler, "On the effective permittivity charaterizing electrical coupling in surface-wave devices," *J. Appl. Phys.*, vol. 44, pp. 3949–3952, 1973.

[115] R. F. Milsom, N. H. C. Reilly and M. Redwood, "Analysis of generation and detection of surface and bulk acoustic waves by interdigital transducers," *IEEE Trans. on Sonics and Ultrasonics*, vol. SU-24, pp. 147–166, 1977.

[116] W. J. Ghijsen, "The acousto-electric field analysis of multilayered surface acoustic wave devices," Ph.D. Thesis, Delft University of Technology, Delft, The Netherlands, 1987.

[117] E. Voges, "Dispersion and acoustoelectric amplification of elastic surface waves in a layered medium," *Archiv für Elektrotechnik und Übertragungstechnik (AEÜ)*, vol. 26, pp. 513–519, 1972. See also: E. Voges, "Ausbreitung elastischer Oberflachenwellen, piezoelektrische Kopplung und akustoelektrische Wechselwirkung in Schichtstrukturen," Ph.D. Thesis, TU-Braunschweig, Braunschweig, Germany (BRD), 1973.

[118] S. M. Sze, *Physics of Semiconductor Devices*, 2nd Edition. New York: John Wiley & Sons, 1981.

[119] C. W. Turner, A. Shomon, and R. M. White, "Reduced-voltage operation of a surface-elastic-wave amplifier," *Electronics Letters*, vol. 5, pp. 244–246, 1969.

[120] T. H. Hsu and R. M. White, "Two-dimensional layered analysis of a surface elastic wave amplifier having a segmented drift structure," *IEEE Trans. on Sonics and Ultrasonics*, vol. SU-20, pp. 2–6, 1973.

[121] L. P. Solie, "An integrated surface wave convolver/amplifier," *Proc. IEEE 1973 Ultrasonics Symp.*, pp. 175–177.

[122] L. P. Solie, "A new mode of operation for the surface-wave convolver," *Proc. IEEE*, vol. 64, pp. 760–763, 1976.

[123] T. Moriizumi, K. Kyuma, J. Hyakutake, and T. Yasuda, "A monolithic surface-wave oscillator using a SAW amplifier and periodic gratings," *Proc. IEEE 1977 Ultrasonics Symp.*, pp. 932–935.

[124] H. Owashi, K. Matsumoto, S. Shiokawa, T. Moriizumi, and T. Yasuda, "Experimental realization of SAW amplifier oscillation," *Proc. IEEE 1979 Ultrasonics Symp.*, pp.891–895.

[125] M. J. Vellekoop, E. Nieuwkoop, J. C. Haartsen and A. Venema, "A monolithic SAW physical-electronic system for sensors," *Proc IEEE 1987 Ultrasonics Symp.*, pp. 641–644.

CHAPTER 4 — TECHNOLOGY

[126] H. I. Smith, "Surface wave device fabrication," in *Surface Wave Filters*, H. Matthews, Ed. New York: John Wiley & Sons, 1977, ch. 4, pp. 165–217.

[127] O. Männer, E. Ehrmann-Falkenau, H. Stocker, "Analysis of electrode resistance effects in SAW filters on strongly coupling substrates," *Proc. IEEE 1984 Ultrasonics Symp.*, pp. 77–81.

[128] K. Asakawa, M. Itoh, H. Gokan, S. Esho and K. Nishikawa, "Low loss 1–2 GHz SAW filters with submicron finger period electrodes," *Proc. of 1st Symp. on Ultrasonic Electronics, Tokyo, 1980, Japanese Journal of Applied Physics*, vol. 20, suppl. 20–3, pp. 93–97, 1981.

[129] H. Engan, "Excitation of elastic surface waves by spatial harmonics of interdigital transducers," *IEEE Trans. on Electron Devices*, vol. ED-16, pp. 1014–1017, 1969.

[130] R. Veith, "The fabrication technology of Rayleigh wave devices", in *Rayleigh-Wave Theory and Application*, E. A. Ash and E. G. S. Paige, Eds.Berlin: Springer Verlag, 1985, pp. 254–272.

[131] S. Takahashi, Y. Ebata and T. Kodama, "Surface acoustic wave device applications to consumer electronics," *Proc. of 3rd Symp. on Ultrasonic Electronics, Tokyo, 1982, Japanese Journal of Applied Physics*, vol. 22, suppl. 22-3, pp. 7–11, 1983.

[132] C. K. Campbell, *Surface Acoustic Wave Devices and Their Signal Processing Applications.* Boston: Academic Press, 1989.

[133] P. Borden, B. T. Khuri-Yakub, H. C. Tuan, and G. S. Kino, "ZnO convolver development," *Proc. IEEE 1976 Ultrasonics Symp.*, pp. 171–173.

[134] A. Venema and E. A. Wolsheimer, "A SAW junction interdigital transducer in silicon," *Proc. IEEE 1982 Ultrasonics Symp.*, pp. 461–465.

[135] G. C. Schwartz and V. Platter, "Anodic processing for multilevel LSI," *J. Electrochem. Soc.: Solid-State Science and Technology*, vol. 123, pp. 34–37, 1976.

[136] H. A. M. van den Berg, R. F. Humphryes, J. J. M. Ruigrok and A. Venema, "Sub-micron IDT fabrication," *Proc. IEEE 1977 Ultrasonics Symp.*, pp. 767–769.

[137] L. L. Pendergrass and L. G. Studebaker, "SAW resonator design and fabrication for 2.0, 2.6 and 3.3 GHz," *IEEE Trans. on Ultrasonics, Ferroelectrics and Frequency Control*, vol. UFFC-35, pp. 372–379, 1988.

[138] K. Yamanouchi, Y. Cho and T. Meguro, "SHF-range surface acoustic wave interdigital transducers using electron beam exposure," *IEEE 1988 Ultrasonics Symp.*, pp. 115–118.

[139] M. Kakuchi, M. Hikita and T. Tamamura, "Amorphous carbon films as resist masks with high reactive ion etching resistance for nanometer lithography," *Appl. Phys. Lett.*, vol. 48, pp. 835–837, 1986.

[140] E. van der Drift, K. Kerkhof, J. Romijn and T. M. Klapwijk, "Nanometer-scale lithography for Aharonov-Bohm magnetoconductance oscillation studies," *Microcircuit Engineering 86: Proc. International Conference on Microlithography*, pp. 257–263.

[141] D. W. Hess, "Plasma etching of aluminum," *Solid State Technology*, pp. 189–194, 1981.

[142] A. J. Purdes, "Aluminum plasma etch rate limitations," *J. Vac. Sci. and Technol. A.*, pp. 712–715, 1983.

[143] D. Allred, S. Jäckel, C. Mazuré, H. J. Barth, H. Cerva, and W. Hösler, "Film redeposition on vertical surfaces during reactive ion etching," *J. Vac. Sci. and Technol. B.*, pp. 505–511, 1989.

[144] L. K. Nanver, "High-performance BIFET process for analog integrated circuits," Ph.D. Thesis, Delft University of Technology, Delft, The Netherlands, 1987.

[145] R. D. J. Verhaar, J. W. Barben, J. G. Dil, C. A. H. Juffermans, J. J. M. J. de Klerk, H. Lifka, "E-beam lithography for sub-micron MOS-devices," *Microcircuit Engineering 85: Proc. International Conference on Microlithography*, pp. 511–518.

[146] Ph. Defranould, "High deposition rate sputtered ZnO thin films for BAW and SAW applications," *Proc. IEEE 1981 Ultrasonics Symp.*, pp. 483–488.

[147] F. S. Hickernell, "Zinc oxide films for acoustoelectric device applications," *IEEE Trans. on Sonics and Ultrasonics*, vol. SU-32, pp. 621–629, 1985.

[148] T. Yamamoto, T. Shiosaki, and A. Kawabata, "Characterization of ZnO piezoelectric films prepared by rf planar-magnetron sputtering," *J. Appl. Phys.*, vol. 51, pp. 3113–3120, 1980.

[149] A. Venema, "Transduction and propagation of surface acoustic waves in three-layered media with an electrically conductive substrate," Ph.D. Thesis, Delft University of Technology, Delft, The Netherlands, 1980.

[150] M. J. Vellekoop, C. C. G. Visser. P. M. Sarro, and A. Venema, "Compatibility of zinc oxide with silicon IC processing." Presented at *Transducers '89.* Accepted for publication in *Sensors & Actuators*, 1989.

[151] J. H. Visser, M. J. Vellekoop, A. Venema, E. van der Drift, P. J. M. Rek, A. J. Nederlof, and M. S. Nieuwenhuizen, "Surface acoustic wave filters in ZnO-SiO$_2$-Si layered structures." Accepted for publication in *Proc. IEEE 1989 Ultrasonics Symp.*

[152] T. R. Meeker and W. R. Grise, "Packaging and reliability of SAW filters," *Proc. IEEE 1983 Ultrasonics Symp.*, pp.117–124.

[153] A. L. Nalamwar and M. Epstein, "Effects of applied strain in ZnO thin-film SAW devices," *IEEE Trans. on Sonics and Ultrasonics*, vol. SU-23, pp. 144–147, 1976.

[154] C. A. Johnson, T. L. Bagwell, J. L. Henderson, R. C. Bray, "Polyimide as an acoustic absorber for high frequency SAW applications," *Proc. IEEE 1988 Ultrasonics Symp.*, pp. 279–284.

CHAPTER 5 — SAW FILTERS IN SILICON

[155] R. H. Tancrell, "Principles of surface wave filter design," in *Surface Wave Filters*, H. Matthews, Ed. New York: John Wiley & Sons, 1977, ch. 3, pp. 109–164.

[156] D. P. Morgan, *Surface-Wave Devices for Signal Processing.* Amsterdam: Elsevier, 1985.

[157] L. R. Rabiner and B. Gold, *Theory and Application of Digital Signal Processing.* Englewood Cliffs (NJ): Prentice-Hall, 1975.

[158] F. J. Harris, "On the use of windows for harmonic analysis with the discrete fourier transform," *Proc. IEEE*, vol. 66, pp. 51–83, 1978.

[159] J. H. McClellan, T. W. Parks and L. R. Rabiner, "A computer program for designing optimum FIR linear phase digital filters," *IEEE Trans. Audio and Electroacoustics*, vol. AU-21, pp. 506–526, 1973.

[160] C. Ruppel, E. Ehrmann-Falkenau, H. R. Stocker, R. Veith, "Optimum design of SAW-filters by linear programming," *Proc. IEEE 1983 Ultrasonics Symp.*, pp. 23–26. See also: C. Ruppel, "Entwurf von Oberflächenwellenfiltern," Ph.D. Thesis, Technische Universität Wien, Wien, Austria, 1986.

[161] A. J. Vigil, B. P. Abbott and D. C. Malocha, "A study of the effects of apodized structure geometries on SAW filter parameters," *Proc. IEEE 1987 Ultrasonics Symp.*, pp. 139–144.

[162] W. R. Smith, H. M. Gerard, J. H. Collins, T. M. Reeder, and H. J. Shaw, "Analysis of interdigital surface wave transducers by use of an equivalent circuit model," *IEEE Trans. on Microwave Theory and Techniques*, vol. MTT-17, pp. 856–864, 1969.

[163] D. Quak and G. den Boon, "Electric input admittance of an interdigital transducer in a layered, anisotropic, semiconducting structure," *IEEE Trans. on Sonics and Ultrasonics*, vol. SU-25, pp. 44–50, 1978.

[164] A. Venema, "Transduction and propagation of surface acoustic waves in three-layered media with an electrically conductive substrate," Ph.D. Thesis, Delft University of Technology, Delft, The Netherlands, 1980.

[165] W. J. Ghijsen, "The acousto-electric field analysis of multilayered surface acoustic wave devices," Ph.D. Thesis, Delft University of Technology, Delft, The Netherlands, 1987.

[166] S. Datta, *Surface Acoustic Wave Devices.* Englewood Cliffs (NJ): Prentice-Hall, 1986.

[167] J. W. Th. Eikenbroek, "Development of an integrated AM shortwave upconversion receiver front-end," Ph.D. Thesis, Delft University of Technology, Delft, The Netherlands, 1989.

[168] L. A. Coldren and R. L. Rosenberg, "SAW resonator filter overview: design and performance tradeoffs," *Proc. IEEE 1978 Ultrasonics Symp.*, pp. 422–432.

[169] S. Ono, O. Yamazaki, K. Ohji, K. Wasa, and S. Hayakawa, "SAW resonators using rf-sputtered ZnO films on glass substrates," *Appl. Phys. Lett.*, vol. 33, pp. 217–218, 1978.

[170] S. J. Martin, R. L. Gunshor, and R. F. Pierret, "Zinc-oxide-on-silicon surface acoustic wave resonators," *Appl. Phys. Lett.*, vol. 37, pp. 700–701, 1980.

[171] S. J. Martin, R. L. Gunshor, and R. F. Pierret, "High Q, temperature stable ZnO-on-silicon SAW resonators," *Proc. IEEE 1980 Ultrasonics Symp.*, pp. 113–117.

[172] S. J. Martin, R. L. Gunshor, R. F. Pierret, S. Datta and S. S. Schwartz, "Zinc oxide-on- silicon surface acoustic wave resonators," School of Electrical Engineering, Purdue University, West Lafayette (IN), USA, Report TR–EE 83–31, September 1983.

[173] W. R. Shreve, "Surface-wave two-port resonator equivalent circuit," *Proc. IEEE 1975 Ultrasonics Symp.*, pp. 295–298.

[174] P. S. Cross and R. V. Schmidt, "Coupled surface-acoustic-wave resonators," *The Bell System Technical Journal*, vol. 56, pp. 1447–1482, 1977.

[175] J. H. Visser and A. Venema, "Silicon SAW devices and electromagnetic feedthrough," *Proc. IEEE 1988 Ultrasonics Symp.*, pp. 299–301.

[176] D. E. Oates and R. W. Ralston, "A SAW tapped delay line with short (15-ns) pedestal of delay and high (>110 dB) feedthrough isolation," *Proc. IEEE 1981 Ultrasonics Symp.*, pp. 44–47.

[177] A. Venema, M. J. Vellekoop, E. Nieuwkoop and J. C. Haartsen, "A silicon SAW physical-electronic system for sensors," *Proc. of the 4th International Conference on Solid-State Sensors and Actuators*, pp. 482–486, 1987.

[178] P. T. M. van Zeijl, "Fundamental aspects and design of an integrated FM upconversion receiver front-end with on-chip SAW filters," Ph.D. Thesis, Delft University of Technology, Delft, The Netherlands, 1990.

CHAPTER 6 — POTENTIAL APPLICATIONS

[179] H. C. Nauta, "Fundamental aspects and design of monolithically integrated AM radio receivers," Ph.D. Thesis, Delft University of Technology, Delft, The Netherlands, 1986.

[180] D. Ash, "An improved high-performance tv receiver," *Proc. IEEE*, vol. 70, pp. 1345–1357, 1982.

[181] J. Yamada, A. Yuhara, T. Shiba, and T. Toyama, "High frequency SAW filters stretched over non-overlapped electrodes for satellite broadcast receivers," *IEEE Trans. on Consumer Electronics*, vol. CE-31, pp. 673–679, 1985.

[182] A. B. Carlson, *Communication Systems.* New York: McGraw-Hill Book Company, 1986, part 2 ("Analog Communication"), pp. 193–377.

[183] E. H. Nordholt, H. C. Nauta and C. A. M. Boon, "A high-dynamic-range front end for an upconversion car-radio receiver," *IEEE Journal of Solid-State Circuits*, vol. SC-20, pp. 688–696, 1985.

[184] H. C. Nauta and E. H. Nordholt, "An integrated IF amplifier and detector for an AM upconversion radio," *IEEE Journal of Solid-State Circuits*, vol. SC-20, pp. 697–702, 1985.

[185] J. W. Th. Eikenbroek, "Development of an integrated AM shortwave upconversion receiver front-end," Ph.D. Thesis, Delft University of Technology, Delft, The Netherlands, 1989.

[186] P. T. M. van Zeijl, "Fundamental aspects and design of an integrated FM upconversion receiver front-end with on-chip SAW filters," Ph.D. Thesis, Delft University of Technology, Delft, The Netherlands, 1990.

[187] J. H. Visser, P. T. M. van Zeijl, L. K. Nanver, "On-chip SAW filters in integrated radio systems," *Digest of Technical Papers IEEE 1989 International Conference on Consumer Electronics*, pp. 90–91.

[188] P. T. M. van Zeijl, J. H. Visser and L. K. Nanver, "FM radio receiver front-end circuitry with on-chip SAW filters," *IEEE Trans. on Consumer Electronics*, vol. CE-35, pp. 512–519, 1989.

[189] W. G. Kasperkovitz, "FM-ontvangers voor mono en stereo op één 'chip'," *Philips Technisch Tijdschrift*, vol. 41, pp. 177–191, 1983. See also *Philips Technical Review.*

[190] K. Nakamura, H. Sasaki and H. Shimizu, "A piezoelectric composite resonator consisting of a ZnO film on an anisotropically etched silicon substrate," *Proc. 1st Symp. on Ultrasonic Electronics, Tokyo, 1980, Japanese Journal of Applied Physics*, vol. 20, pp. 111–114, 1981.

[191] K. M. Lakin, J. S. Wang, G. R. Kline, A. R. Landin, Y. Y. Chen, and J. D. Hunt, "Thin film resonators and filters," *Proc. IEEE 1982 Ultrasonics Symp.*, pp. 466–475.

[192] Y. Miyasaka, S. Hoshino and S. Takahashi, "Temperature compensated ZnO-SiO_2-Si thin film resonator for VHF voltage controlled oscillator," *Proc. IEEE 1985 Ultrasonics Symp.*, pp. 346–351.

[193] K. Yamanouchi and M. Oba, "New air gap type piezoelectric composite thin film resonators," *Proc. IEEE 1987 Ultrasonics Symp.*, pp. 415–418.

[194] H. Satoh, H. Suzuki, C. Takahashi, C. Narahara and Y. Ebata, "A 400 MHz one-chip oscillator using an air-gap type thin film resonator," *Proc. IEEE 1987 Ultrasonics Symp.*, pp. 363–368.

[195] E. H. Nordholt, *Design of High-Performance Negative-Feedback Amplifiers.* Amsterdam: Elsevier, 1983.

[196] P. T. M. van Zeijl, "A new high-dynamic range dual-loop power-to-current amplifier," *IEEE Journal of Solid-State Circuits*, vol. SC-24, pp. 646–650, 1989.

SUMMARY

The research work presented in this thesis deals with the design and technology of Surface Acoustic Wave (SAW) filters in ZnO-SiO_2-Si layered structures. SAW propagation and transduction properties with respect to dispersion, higher-order Rayleigh-wave modes and fabrication tolerances in the piezoelectric layer thickness have been studied. In addition, the conditions for SAW amplification by the interaction of the acoustic wave with the drifting charge carriers in the silicon substrate are examined. The monolithic integration of these SAW filters with electronic circuitry in one single chip and the fabrication of interdigital patterns with electrode widths down to 200 nm have successfully been realized. Experimental results of SAW delay lines, SAW transversal filters and SAW resonator filters are given. Application of silicon-integrated SAW filters in an FM upconversion radio receiver (on one single chip) is discussed.

Chapter 1. The propagation and transduction properties of surface acoustic waves on homogeneous piezoelectric substrates are shortly reviewed and the two basic SAW filter types, i.e. the SAW transversal filter and the SAW resonator filter are introduced. Silicon-integrated SAW filters are low-noise devices with an high intermodulation-free dynamic range and are, therefore, excellently suited to obtain high-performance on-chip frequency selectivity in electronic systems. The design of SAW filters in ZnO-SiO_2-Si layered structures is split into two parts. The first part consists of the determination of the layer thicknesses and the location of the interdigital transducer. The second part deals with the design of the metal interdigital pattern. This latter part is not discussed in detail in this thesis since only first-order models for SAW filter design have been used, which are well known and identical to the models used for SAW filter design on monocrystalline piezoelectric substrates.

Chapter 2. The layered structure for silicon-integrated SAW filters is investigated with respect to acoustic wave propagation and transduc-

tion properties. It is shown that a monocrystalline approximation of the sputtered ZnO layer results in values of the phase velocity up to 10% too high and values for the piezoelectric coupling up to 20% too high. For ZnO and AlN the phase and group velocity, and the piezoelectric coupling are given as a function of ωh, with ω the radial frequency and h the layer thickness. The numerical results are obtained for a constant ratio of the piezoelectric and dielectric layer thicknesses. The figures, therefore, can be used to estimate the dispersion in acoustic wave propagation in the layered structures. Further, the influence of the piezoelectric layer thickness variations (due to the fabrication tolerances) on the center frequency is given. With respect to the ZnO-SiO_2-Si layered structure, it is shown that the AlN-SiO_2-Si layered structure has more dispersion, a lower piezoelectric coupling, a higher phase and group velocity and the device center frequency is more vulnerable for piezoelectric layer thickness variations. The only advantage of AlN is the possible absence of higher-order Rayleigh-wave modes.

Chapter 3. The SAW amplification mechanism, to be applied in SAW filters or oscillators, is studied. Amplification is possible by the interaction between the surface acoustic wave and the drifting charge carriers in the silicon substrate. In this way not only amplification can be obtained, but a suppression of triple transit echoes, higher-order Rayleigh-wave modes and bulk waves as well. First, a one-dimensional model to understand the SAW amplification mechanism is given, then a perturbational method, based on the continuity of the effective permittivity at the ZnO-SiO_2 interface is discussed. A new approximation for the effective permittivity of a piezoelectric layer is given and the phase velocities and amplification/attenuation of the Rayleigh waves are calculated with errors smaller than 0.1% and 0.5%, respectively. The numerical results show the influence of the frequency, the silicon and epitaxial layer conductivities, the charge carrier drift velocity (relative to the SAW phase velocity), the normalized layer thicknesses (of the ZnO, SiO_2 and epitaxial layers), the extent of depletion of the epitaxial layer, and the diffusion of the charge bunches.

Chapter 4. The technology to fabricate silicon-integrated SAW devices is discussed. An inventory of interdigital pattern fabrication is given. A high-resolution aluminum etch technology based on electron beam lithography, dry etching of the bilayer mask system in a low pressure O_2-plasma and patterning of the aluminum layer in a $SiCl_4$-plasma has

been developed for accurate dimensional control of the electrode width and shape. Electrode widths down to 200 nm have been fabricated. Further, a monolithic integration of electronic circuitry and SAW devices on one chip has been realized in a modified version of the Delft high-frequency BIFET process. Attention is paid to ZnO deposition (by DC magnetron sputtering) and its passivation.

Chapter 5. Experimental results of SAW delay lines, SAW transversal filters and SAW resonator filters are presented in this chapter. A new configuration to suppress the electromagnetic feedthrough in silicon-integrated SAW devices is presented and a 10–15 dB additional suppression is experimentally obtained. For an optimal signal transfer the input and output transducers must be short-circuited for the signal. Therefore, the device is driven by a voltage source and loaded with a short-circuit. The short-circuit current is the output signal and the transfer function is essentially a transconductance. Noise and intermodulation measurements show an excellent performance when compared with the electronic circuitry.

Chapter 6. The performance of silicon-integrated SAW filters is reviewed and possible applications of these filters are discussed. As an example of the use of silicon-integrated SAW filters, the (single chip) FM upconversion radio receiver with on-chip SAW filters is discussed in more detail. The SAW device determines to a large extent the total chip area of this receiver. The performance is mainly limited by the input amplifier.

SAMENVATTING

Het onderzoek dat in dit proefschrift wordt gepresenteerd gaat over het ontwerp en de technologie van akoestische oppervlaktegolf (SAW) filters in ZnO-SiO_2-Si gelaagde structuren. De eigenschappen van akoestische oppervlaktegolfpropagatie en -transductie met betrekking tot dispersie, hogere-orde Rayleigh-golf modi en fabricagetoleranties in de dikte van de piezoelektrische laag zijn bestudeerd. Bovendien zijn de voorwaarden voor akoestische oppervlaktegolfversterking door de interactie van de akoestische golf met driftende ladingsdragers in het silicium substraat onderzocht. De monolithische integratie van deze SAW filters met elektronische schakelingen op één enkele 'chip' en de fabricage van interdigitale patronen met elektrodebreedtes tot 200 nm zijn succesvol gerealiseerd. Experimentele resultaten van SAW vertragingslijnen, SAW transversale filters en SAW resonator filters worden gegeven. Toepassing van siliciumgeintegreerde SAW filters in een FM upconversie radio-ontvanger (op één enkele 'chip') wordt besproken.

Hoofdstuk 1. Een kort overzicht van de propagatie en transductie eigenschappen van akoestische oppervlaktegolven op homogene substraten wordt gegeven en de twee basis SAW filtertypen, te weten het SAW transversaal filter en het SAW resonator filter, worden geintroduceerd. Silicium-geintegreerde SAW filters zijn devices met een lage ruis en een hoog intermodulatie-vrij dynamisch bereik. Ze zijn daarom uitstekend geschikt om 'on-chip' frequentie-selectiviteit in een elektronisch systeem te verkrijgen. Het ontwerp van SAW filters in ZnO-SiO_2-Si gelaagde structuren wordt in twee delen gesplitst. Het eerste deel omvat de bepaling van de laagdikten en de plaats van de interdigitale transducent. In het tweede deel wordt het ontwerp van het metalen interdigitale patroon bepaald. Dit laatste deel van het ontwerp wordt in dit proefschrift niet in detail behandeld omdat alleen eerste-orde modellen voor het SAW filterontwerp zijn gebruikt. Deze modellen zijn reeds goed bekend en identiek aan de modellen die voor SAW filterontwerp op monokristallijne piezoelektrische

substraten worden gebruikt.

Hoofdstuk 2. De gelaagde structuur voor silicium-geintegreerde SAW filters wordt met betrekking tot akoestische golfpropagatie en -transductie onderzocht. Er wordt aangetoond dat een monokristallijne benadering van de gesputterde ZnO laag resulteert in waarden van de fasesnelheid die tot 10% te hoog kunnen zijn en waarden voor de piezoelektrische koppeling die tot 20% te hoog kunnen zijn. Voor ZnO en AlN worden de fase- en groepssnelheid en de piezoelektrische koppeling gegeven als functie van ωh, met ω de radiale frequentie en h de laagdikte. De numerieke resultaten worden verkregen bij een constante verhouding van de piezoelektrische en dielektrische laagdikten. De figuren kunnen daarom gebruikt worden om de dispersie in akoestische golfpropagatie in de gelaagde structuur te bepalen. Bovendien wordt de invloed op de fasesnelheid van laagdiktevariatie in de piezoelektrische laag (als gevolg van fabricagetoleranties) gegeven. In vergelijking met de ZnO-SiO$_2$-Si gelaagde structuur heeft de AlN-SiO$_2$-Si gelaagde structuur meer dispersie, een lagere piezoelektrische koppeling, een hogere fase- en groepssnelheid en de ligging van de centrale frequentie is gevoeliger voor laagdiktevariatie van de piezoelektrische laag. Het enige voordeel van AlN is de mogelijke afwezigheid van hogere-orde Rayleigh-golf modi.

Hoofdstuk 3. Het akoestische oppervlaktegolf versterkingsmechanisme wordt, om toegepast te kunnen worden in SAW filters en SAW oscillatoren, bestudeerd. Versterking is mogelijk door de interactie tussen de akoestische golf en de driftende ladingsdragers in het silicium substraat. Op deze wijze kan er niet alleen versterking worden verkregen, maar tevens een onderdrukking van 'triple transit' echo's, hogere-orde Rayleigh-golf modi en volumegolven. Allereerst wordt een ééndimensionaal model gegeven om het SAW versterkingsmechanisme te begrijpen, vervolgens wordt een perturbatie methode, gebaseerd op de continuiteit van de effectieve permittiviteit op het ZnO-SiO$_2$ grensvlak, besproken. Een nieuwe benadering voor de effectieve permittiviteit van een piezoelektrische laag wordt gegeven en de fasesnelheden en versterking/verzwakking worden berekend met fouten, respectievelijk kleiner dan 0.1% en 0.5%. De numerieke resultaten tonen de invloed van de frequentie, de geleidingen van het silicium substraat en van de epitaxiale laag, de driftsnelheid van de ladingsdragers (ten opzichte van de SAW fasesnelheid), de genormaliseerde laagdikten (van de ZnO, SiO$_2$ en epitaxiale laag), de mate van depletie van de epitaxiale laag en de diffusie van de ladingspakketjes.

Hoofdstuk 4. De technologie om silicium-geintegreerde SAW devices te maken wordt besproken. Een inventarisatie van interdigitaal patroonfabricage wordt gegeven. Een hoge-resolutie aluminium etstechnologie gebaseerd op elektronenstraal lithografie, droog etsen van het dubbellaags resistmasker in een lagedruk O$_2$-plasma en het etsen van de aluminium laag in een SiCl$_4$-plasma zijn ontwikkeld om de elektrodebreedte en -vorm precies in de hand te hebben. Elektrodebreedtes tot 200 nm zijn gefabriceerd. Bovendien is er een monolithische integratie van elektronische schakelingen en SAW devices op één 'chip' gerealiseerd in een gewijzigde versie van het Delftse BIFET proces. Aandacht wordt besteed aan ZnO-depositie (door DC magnetron sputteren) en -passivatie.

Hoofdstuk 5. Experimentele resultaten van SAW vertragingslijnen, SAW transversale filters en SAW resonator filters worden in dit hoofdstuk gegeven. Een nieuwe configuratie om de elektromagnetische overspraak in silicium-geintegreerde SAW devices te onderdrukken wordt gepresenteerd. Een 10–15 dB extra onderdrukking wordt met deze methode experimenteel behaald. Voor een optimale signaaloverdracht moeten de ingangs- en uitgangstransducenten kortgesloten zijn voor het signaal. Daarom moet het device worden gestuurd met een spanningsbron en belast met een kortsluiting. De kortsluitstroom is het uitgangssignaal en de overdrachtsfunctie is dan in wezen een transconductantie. Ruis- en intermodulatiemetingen tonen een uitstekende prestatie vergeleken met die van de elektronische schakelingen.

Hoofdstuk 6. De prestatie van silicium-geintegreerde SAW filters wordt samengevat en mogelijke toepassingen van deze filters worden besproken. Als een voorbeeld van het gebruik van silicium-geintegreerde SAW filters wordt de FM upconversie radio-ontvanger met 'on-chip' SAW filters in meer detail besproken. Het SAW device bepaalt in grote mate de totale oppervlakte van de 'chip' voor deze ontvanger. De prestatie wordt hoofdzakelijk beperkt door de versterker aan de ingang.

ABOUT THE AUTHOR

Jacobus Hendrik Visser was born in Hillegom, The Netherlands, on July 22, 1961. After finishing primary education at the "Boaz-school" in Hillegom, he moved with his family to Ouddorp. He graduated from high school (Atheneum B) "Rijksscholengemeenschap Goeree Overflakkee" in Middelharnis in 1979. He then moved to Delft to start his study at Delft University of Technology. On November 21, 1985 he received (cum laude) his Master's degree (the Ingenieurs' degree) from the Department of Electrical Engineering, Delft University of Technology, Delft, The Netherlands. In addition, a qualification to teach mathematics to senior high school students was obtained. Towards the end of his studies he worked for two months as a trainee with Omron Tateisi Electronics Co. in Minakuchi and Kyoto, Japan. The training involved the manufacturing and testing of LEDs, photo diodes/transistors, pressure and humidity sensors.

In January 1986 Jaco Visser started his Ph.D. research in surface acoustic wave (SAW) filters in ZnO-SiO_2-Si layered structures, carried out in the Microacoustics Group of the Laboratory of Electronic Instrumentation, Department of Electrical Engineering at Delft University of Technology. The project, funded by the Netherlands Technology Foundation (Stichting voor Technische Wetenschappen – STW), involved the realization of an FM upconversion radio receiver with on-chip SAW filters and was carried out in close cooperation with the Laboratory of Electronics and the Delft Institute for MicroElectronics and Submicron Technology (DIMES). His research resulted in a number of papers, a patent, this Ph.D. Thesis and in presentations at (international) conferences and in industrial presentations. During his Ph.D. research he supervised the Master Thesis' work of three students in the SAW field and taught a laboratory course for graduate students in analog electronic circuitry design and measurement.

LIST OF PUBLICATIONS AND PRESENTATIONS

PUBLICATIONS

J. H. Visser and A. Venema, "A computational technique to determine the amplification of Rayleigh-wave modes in multilayered structures," *Proc. IEEE 1986 Ultrasonics Symp.*, pp. 463–468.

J. H. Visser and A. Venema, "Silicon SAW devices and electromagnetic feedthrough," *Proc. IEEE 1988 Ultrasonics Symp.*, pp. 297–301.

J. H. Visser, P. T. M. van Zeijl, and L. K. Nanver, "On-chip SAW filters in integrated radio systems," *Digest of Technical Papers IEEE 1989 International Conference on Consumer Electronics*, pp. 90–91.

P. T. M. van Zeijl, J. H. Visser, and L. K. Nanver, "FM radio receiver front-end circuitry with on-chip SAW filters," *IEEE Trans. on Consumer Electronics*, vol. CE-35, pp. 512–519, 1989.

B. M. Blok, J. H. Visser, E. van der Drift, J. Romijn, and A. Venema, "High resolution technology for silicon-integrated surface acoustic wave devices," accepted for publication in *J. Vac. Sci. and Technol. B.*, Dec. 1989.

A. J. M. van der Harg, J. H. Visser, E. van der Drift, and J. Romijn, "High resolution technology for surface acoustic wave devices, monolithically integrated with electronic circuitry," accepted for publication in *Microcircuit Engineering 89: Proc. International Conference on Microlithography.*

J. H. Visser, M. J. Vellekoop, A. Venema, E. van der Drift, P. J. M. Rek, A. J. Nederlof, and M. S. Nieuwenhuizen, "Surface acoustic wave filters in ZnO-SiO_2-Si layered structures," accepted for publication in *Proc. IEEE 1989 Ultrasonics Symp.*

J. H. Visser, J. C. Haartsen, and A. Venema, "SAW propagation, transduction and amplification in ZnO-SiO_2-Si layered structures," in preparation.

PATENT

J. H. Visser, "Akoestische-oppervlaktegolfinrichting in meerlaagse structuur met reductie van elektromagnetische overspraak," Dutch Patent Appl. 8801765, July 12, 1988 (STW). "Surface acoustic wave device having multilayer structure with reduction in electromagnetic feedthrough," patent pending in Europe, USA and Japan.

PRESENTATIONS

Oral presentation: "A computational technique to determine the amplification of Rayleigh-wave modes in multilayered structures" at the *IEEE Ultrasonics Symposium*, Williamsburg (VA), USA, November 19, 1986.

Poster presentation: "Development of a fully silicon-integrated upconversion FM receiver (I)" at the *FOM/STW Scientific Meeting Semiconductor Study Group*, Veldhoven, The Netherlands, December 16–17, 1986.

Oral presentation: "Design aspects of SAW filters and SAW amplification devices." *Scientific Visit Siemens (Microacoustics R & D)* to Delft University of Technology, Delft, The Netherlands, September 29, 1987.

Poster presentation: "Development of a fully silicon-integrated upconversion FM receiver (II)" at the *FOM/STW Scientific Meeting Semiconductor Study Group*, Veldhoven, The Netherlands, December 2–3, 1987.

Oral presentation: "Silicon SAW devices and electromagnetic feedthrough" at the *IEEE Ultrasonics Symposium*, Chicago (IL), USA, October 5, 1988.

Poster presentation: "On-chip combination of SAW filter and electronic circuitry" at the *FOM/STW Scientific Meeting Semiconductor Study Group*, Veldhoven, The Netherlands, November 23–24, 1988.

Oral presentation: "The design and realization of SAW transversal filters and resonators in silicon." *Scientific Visit Technische Universität Wien* to Delft University of Technology, Delft, The Netherlands, March 30, 1989.

Oral presentation: "The amplification of surface acoustic waves in silicon." *Scientific Visit Technische Universität Wien* to Delft University of Technology, Delft, The Netherlands, March 31, 1989.

Oral presentation: "Silicon-integrated SAW filters and amplifiers" at *Hewlett-Packard, Microwave Technology Division*, Santa Rosa (CA), USA, May 30, 1989.

Poster presentation: "High resolution technology for silicon-integrated surface acoustic wave devices" at the *33rd International Symposium on Electron, Ion and Photon Beams*, Monterey (CA), USA, June 1, 1989.

Oral presentation: "Surface acoustic wave filters in silicon" at *IC Sensors*, Milpitas (CA), USA, June 2, 1989.

Oral presentation: "On-chip SAW filters in integrated radio systems" at the *IEEE International Conference on Consumer Electronics*, Chicago (IL), USA, June 8, 1989.

Oral presentation: "Silicon-integrated surface acoustic wave filters" at *Siemens (Microacoustics R & D)*, München, Germany (BRD), August 11, 1989.

Oral presentation: "Surface acoustic wave filters in ZnO-SiO_2-Si layered structures" at the *IEEE Ultrasonics Symposium*, Montréal, Canada, October 4, 1989.

Oral presentation: "Surface acoustic wave filters and amplifiers in ZnO-SiO_2-Si layered structures" at *Ford Motor Company*, Dearborn (MI), USA, October 9, 1989.

Oral presentation: "Surface acoustic wave filters in ZnO-SiO_2-Si layered structures" at *IBM Thomas J. Watson Research Center, Eastview Research Lab.*, Yorktown Heights (NY), USA, October 11, 1989.

Oral presentation: "Surface acoustic wave filters in ZnO-SiO_2-Si layered structures" at *IBM Almaden Research Center*, San Jose (CA), USA, October 13, 1989.